Ultimate Shear Behavior of Post-Tensioned Deep Transfer Girders

Auteur : Ozkan, Muhammed
Promoteur(s) : Mihaylov, Boyan; 3832
Faculté : Faculté des Sciences appliquées
Diplôme : Master en ingénieur civil des constructions, à finalité spécialisée en "civil engineering"
Année académique : 2017-2018
URI/URL : http://hdl.handle.net/2268.2/4588

University of Liège – Faculty of Applied Sciences

Ultimate Shear Strength of Post-Tensioned Deep Transfer Girders

Graduation studies conducted for obtaining a master's degree in civil engineering

Author: Muhammed Furkan Ozkan

Promoter: Boyan Mihaylov
Jury Members: Almila Uzel – Frédéric Collin – Jean-Marc Franssen

Academic year 2017-2018

Abstract

Ultimate Shear Behaviour of Post-Tensioned Deep Transfer Girders

University of Liège – Faculty of Applied Sciences

Muhammed Furkan Ozkan – Master student in Civil Engineering

Academic Year – 2017-2018

Promoter – Boyan Mihaylov

Deep beams are typically used as transfer girders in tall buildings, cap beams in bridges, in foundations and offshore structures. They are characterized by high shear resistance due to their small shear-span-to-effective-depth ratio a/d that does not exceed about 2.5. Due to the large loads they carry, the design of such members is very important in order to avoid partial or complete collapse of the structure. As opposed to slender beams, deep beams cannot be designed based on the simple but powerful hypothesis that plane sections remain plane. Experimental studies on deep beams have shown that the use of prestressing improves the shear resistance.

The aim of this thesis is to study a Two-Parameter-Kinematic-Theory (2PKT) developed by Mihaylov et al. (2013) for reinforced concrete deep beams and to extend the theory to prestressed deep beams. The original theory is able to predict the ultimate shear strength of reinforced concrete deep beams using only two kinematic parameters. In order to cover the case of prestressed deep beams, an extended model is proposed. This extended model captures the effect of prestressing in three ways: 1) increase of the shear force derived from flexural equilibrium; 2) effect of the prestressing on the geometry and strength of the critical loading zone (CLZ); and 3) dowel action of the prestressing reinforcement. The extended model is validated against a collected database of tests conducted on rectangular deep beams without openings and with straight prestressing tendons. The extended theory is also compared to the original 2PKT approach. It is shown that the ultimate shear strengths predicted by the extended model agree very well with the experimental results. Compared to the results from the original model, the predictions are significantly improved.

In order to further validate the extended theory, non-linear finite element modelling is also performed. It is shown that the 2PKT method that uses only two degrees of freedom produces very similar (or even better) results that the complex numerical models with thousands of degrees of freedom.

Future investigations on this topic can study the effect of curved tendons on the shear resistance of deep beams. Moreover, I-girders can also be studied as they are very common in practice.

Acknowledgements

First and foremost, I would like to thank Professor Boyan Mihaylov for his great guidance throughout the development of this thesis. The door to his office was always open whenever I got into trouble or had a question about my research. All the time he spent for me, his patience, his continuous support, motivation, enthusiasm and specially his great knowledge for concrete structures helped me enormously to achieve this work. I am sincerely grateful to him for his help.

Besides my promoter, I would like to thank all the members of jury and everyone else who will take their time to read this thesis.

Special thanks to my office colleagues Jian Liu, Nikola Tatar and Renaud Franssen. They always answered to my questions and helped me throughout the semester. The working atmosphere was better with them.

Last but not the least, I would like to thank my family and friends who supported me throughout the completion of this work.

Table of contents

List of figures

List of tables

List of annotations

$2PKT$	Two-parameter kinematic theory
$a: M/V$	Shear span
a/d	Shear-span-to-effective-depth
a_g	Maximum aggregate size
a_{ge}	Effective size of coarse aggregate
A_s	Area of longitudinal reinforcement bars
$A_{c,eff}$	Area of concrete providing tension stiffening for bottom reinforcement
b	Width of cross section
C	Compression force in section with maximum moment
CLZ	Critical loading zone
d	Effective depth of section
d_b	Diameter of bottom longitudinal bars
d_{bv}	Diameter of stirrups bar
d_p	Effective depth of section with respect to bottom prestressed reinforcement
d_s	Effective depth of section with respect to bottom non-prestressed reinforcement
DOF	Degree of freedom
E_c	Elastic modulus of concrete
E_s	Elastic modulus of non-prestressed reinforcement
E_p	Elastic modulus of non-prestressed reinforcement
f_{avg}	Average diagonal compressive stress in CLZ
f'_c	Concrete cylinder strength
f_{py}	Yielding stress of prestressed reinforcement
f_{ye}	Effective yield strength of bottom longitudinal bars
f_{yv}	Yield strength of stirrups
FEM	Finite element model
F_p	Tension force in prestressed reinforcement
F_s	Tension force in non-prestressed reinforcement
h	Height of the section
k	Crack shape coefficient
l_0	Length of heavily cracked zone at bottom of critical diagonal crack
l_{b1}	Width of loading plate
l_{b1e}	Effective width of loading plate
l_{b2}	Width of support plate
l_k	Length of dowels provided by bottom longitudinal reinforcement
M_{max}	Maximum bending moment in beam corresponding to measured shear strength
n_b	Number of bottom longitudinal bars
P	Applied concentrated load
RC	Reinforced concrete
T	Tensile force in bottom reinforcement
V	Shear force
V_{ci}	Shear resisted by aggregate interlock
V_{CLZ}	Shear carried by critical loading zone
V_d	Shear resisted by dowel action
$V_{exp.}$	Experimental shear strength
V_{pred}	Predicted shear force

V_s Shear resisted by stirrups
V/P Ratio of shear force to applied point load ≤1.0
w Width of critical diagonal crack halfway along crack
x Depth of compression zone
α Angle of the line extending from inner edge of support plate to far edge of tributary area of loading plate responsible for shear force V
α_1 Angle of critical diagonal crack
δ_x Displacement along x axis
δ_z Displacement along z axis
Δ_c Transverse displacement of critical loading zone
$\varepsilon_{t,avg}$ Average strain in the bottom longitudinal reinforcement
ε_{top} Strain in the top of the section
ε_v Strain in transverse reinforcement
θ Angle of diagonal cracks in uniform stress field
ρ_h Ratio of horizontal web reinforcement
ρ_l Ratio of bottom longitudinal reinforcement
ρ_v Ratio of transverse reinforcement
σ_p Stress in prestressed reinforcement
σ_s Stress in non-prestressed reinforcement

1. Introduction

1.1 General Information

Deep beams are those members whose shear-span-to-depth ratio does not exceed approximatively 2.5 (Fig. 1.1). Such beams behave like a tied arch and the tension in the bottom longitudinal reinforcement is almost constant from support to support. Today, these beams have many applications as transfer girders in tall buildings, cap beams in bridges, in offshore structures and foundations. In particular, deep beams are commonly used at the lower levels of high-rise buildings to open large usable space for commercial and other purposes (Fig. 1.1). Because of their very low a/d ratios, the classical assumption that supposes a linear distribution of strains over the height of the section is no longer valid for deep beams. For that reason, code provisions that are already developed for slender beams cannot be used for deep beams. Moreover, because of the relatively high shear forces in deep beams, they develop large shear deformations and are susceptible to shear failures. As shear failures are by nature very brittle, the design of deep beams is very important to avoid partial or complete collapse of the structure without prior warning.

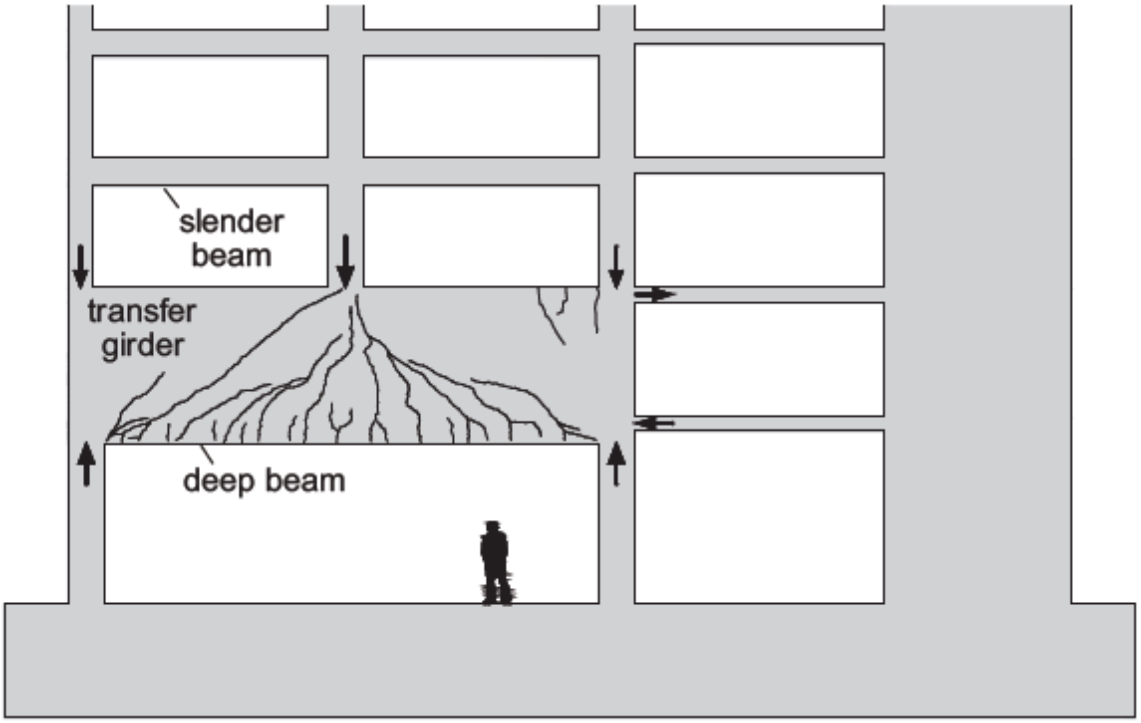

Figure 1.1 - Illustration of deep and slender beams in buildings (Mihaylov et al. 2013)

A significant portion of the shear force in deep beams is carried by strut action, where compressive stresses flow directly from the load to the support (Mihaylov et al., 2013). For that reason, the use of strut-and-tie models (STM) for the design of deep beams is very common. However, as there are many parameters that have an effect on the shear behaviour of deep beams, the STMs can sometimes produce very conservative results. Mihaylov et al. (2013) proposed a kinematic model for deep beams that takes into account the main parameters on the shear behaviour. This approach is called a Two-Parameter-Kinematic-Theory (2PKT) and captures the deformed shape of deep beams using only two degrees of freedom. Once the deformed shape of the beams is described, the model is completed with equilibrium equations and stress-strain relationships to predict the shear failure of deep beams. This 2PKT method was extended later to a five-spring model for deep beams in order to predict the complete pre- and post-peak shear behaviour of the beam. Four of

the springs of the model correspond to the shear resistance components of the beam (shear resisted in the critical loading zone, by aggregate interlock, by stirrups and by dowel action), while the fifth spring models the flexural behaviour. Both models have been validated against a large number of test results producing excellent predictions.

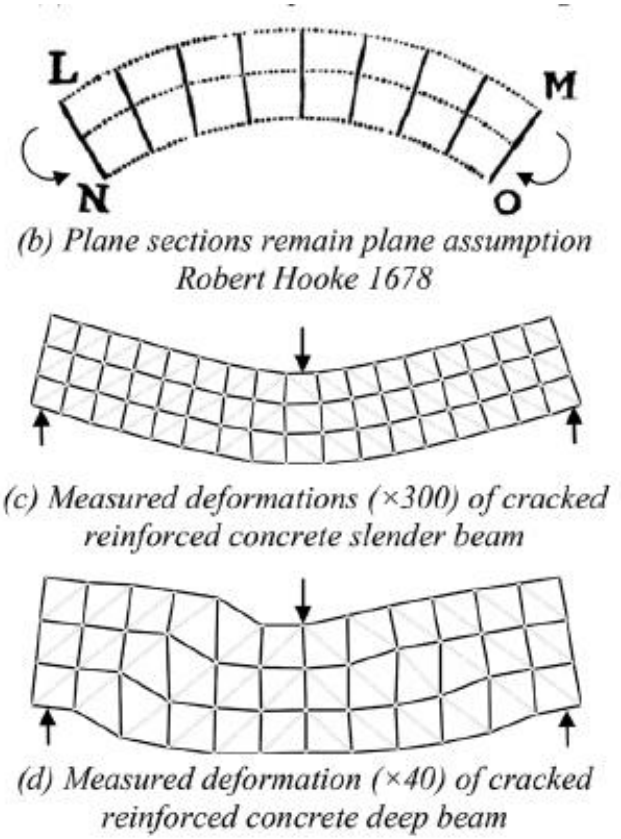

Figure 1.2 – Deformation patterns of deep and slender beams (Mihaylov et al. 2013)

To improve the behaviour of reinforced concrete, prestressed concrete is used since the beginning of the 20th century. One of the biggest advantages of prestressed concrete is that for a given deformation, the load that can be supported is higher than in reinforced concrete. In particular, it is possible to design members which work without cracks under service loads as compared to reinforced concrete which necessarily works with cracks. In slender beams, where the simple but powerful hypothesis that plane sections remain plane is used, the prestressing has a positive impact on the strength by decreasing the crack widths, and therefore increasing the aggregate interlock resistance across the shear cracks. In the case of deep beams, experimental studies have showed again that the shear resistance is improved with the use of prestressing compared to reinforced deep beams. However, while many studies and experiments have been conducted for the behaviour of reinforced concrete deep beams, only few experiments exist for prestressed concrete deep beams (Alsheiger and Ramirez 1992, Tan and Mansur 1992, Teng, Kong and Poh 1998, Tan et al. 1999, Tan and Tong 1999, Arthur 1965). As a result, there are not sufficiently accurate and universally accepted models for such members.

1.2 Objective of the thesis

This thesis is a continuation of the development of the 2PKT and five-spring model proposed by Mihaylov et al. (2013 and 2015). These two models are capable to predict both the strength as well as the complete pre- and post-peak shear behaviour of reinforced concrete deep beams.

As discussed above, some experiments showed that the use of prestressing in deep beams improves the shear resistance and stiffness of deep beams. However, the current 2PKT and five-spring model do not take into account the effects of the prestressing. The goal of this thesis therefore consists of extending the 2PKT approach to take into account the effects of prestressing, and therefore to provide accurate results for the shear strength of pre- and post-tensioned deep beams.

The first step in the thesis is to search the literature and collect as many experiments on prestressed deep beams as possible. Then, the existing model is applied to the experiments and an analysis of the results is performed to evaluate the parameters that influence the shear behaviour when prestressing is used. After that, the modifications brought to the model are explained. The predictions of the modified model are then compared to the experiments and non-linear finite element simulations. The thesis is finally concluded with some proposals for future developments.

1.3 Thesis outline

This thesis consists of 6 chapters including the chapter 1 that introduce the thesis and give some general information about the topic.

Chapter 2 describes the experiments used to study the effect of prestressing on deep beams. The analysis of these experiments allowed to bring some modifications to the existing model. Therefore, these experiments are very important and they are all collected from scientific literature.

Chapter 3 describes the modelling approaches of deep beams and specially the two-parameter kinematic theory.

Chapter 4 consists of kinematic modelling of the collected deep beams. First, the original model is applied to the database collected. Then, the modifications on the existing model are described and finally, the results of the extended model are presented and compared with the previous ones.

Chapter 5 consist of finite element modelling. The first point of this chapter is the explanation of the modelling procedure will all the supports, degrees of freedom, restraints etc. Then, the results of the finite element modelling are presented and then compared to both the experiments and the models.

Chapter 6 is the last chapter of this thesis and it consists on a summary of all the work performed. Finally, it is also in this part that future improvements are proposed.

2. Tests on prestressed deep beams

2.1 Introduction

As discussed in the first chapter, the first work of this thesis is the collection of experiments on prestressed deep beams. This work is crucial for the following of this thesis because all the analysis performed are based on the experiments collected. Therefore, a mistake in the experiment or in the data of those has an impact on the results. For that reason, only scientific literature is used. The papers found must provide enough information about the layout of the beam and the properties of the material used. Again, as discussed in the first chapter some authors worked on prestressed deep beams but the amount of experimental work performed is still scarce today.

2.2 Selection criteria

The different specimens are collected based on several criteria. Given the small number of experiments on prestressed deep beams, the addition of these criteria led to a limited number of experiments that could be used in this thesis. The selected criteria are listed below:

- Shear-span-to-effective-depth ratio (a/d) ratio less than approximatively 2.5
- Rectangular section
- Straight tendon for prestressing
- Continuous beams without openings

Members with large a/d ratio are dominated by beam action. The tension in the longitudinal reinforcement changes along the length of these beams. However, members with low a/d ratio behave like a tied arch and the longitudinal reinforcement carries an almost constant force. For that reason, selected specimens should have sufficiently low a/d ratio to behave like a deep beam. The transition from one to another occurs at about a/d =2.5.

Due to their parabolic profile, curved tendons are causing an additional vertical force on the concrete as shown in Fig. 2.1. The vertical component of prestress forces can be subtracted from the acting shear force. For that reason, deep beams prestressed with curved tendons do not behave exactly like beams with straight tendons. Therefore, deep beams with curved tendons were excluded from the analysis.

I-girders are commonly used in practice to reduce the self-weight of structural elements. However, the behaviour of those girders is different from the behaviour of rectangular section beams. Therefore, they also have been excluded from this study.

Finally, it has also been shown in the literature that openings in deep beams cause a decreasing in first cracking and ultimate loads. So, all the specimens chosen for this study were continuous and without any openings.

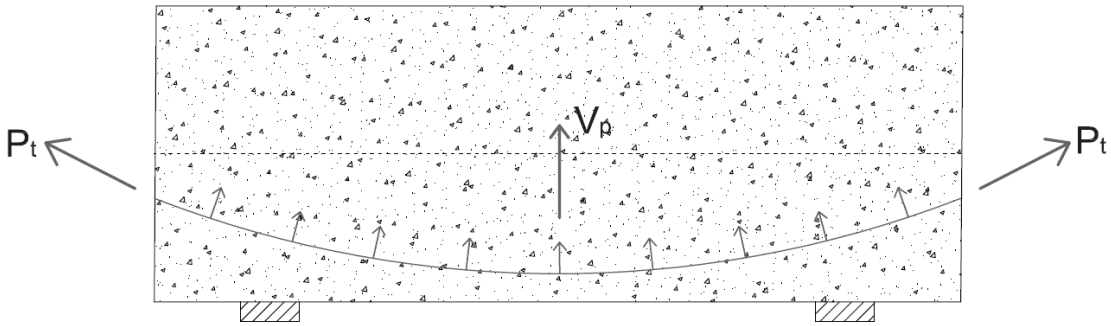

Figure 2.1 – Beneficial effect of curved tendons

2.3 Authors

As discussed before, few experimental results exist on prestressed deep beams (Alsheiger and Ramirez 1992, Tan and Mansur 1992, Teng and Poh 1998, Tan et al. 1999, Tan and Tong 1999, Arthur 1965). Alsheiger and Ramirez (1992) tested three pre-tensioned deep beams to failure and established strut-and-tie models for them. The analysis of struts and ties were performed on a computer programme rather than a visible formula which was apparently unsuitable. The three beams studied had I-sections. Therefore, these specimens could not be studied in this work. Tan and Tong (1999) also carried out an experimental program on six large reinforced and pre-tensioned deep I-girders. Even if the shear-span-to-depth-ratio a/d is very low, this test series is excluded again because of the I-section. Finally, Arthur performed an experimental program on 50 pre-tensioned I-beams without web reinforcement. However, the specimens tested could not be used because of the section geometry. The test found from literature and that are suitable for this project are from Tan and Mansur (1992), Teng and Poh (1998) and Tan et al. (1999). Moreover, thanks to the help of Boyan Mihaylov, a new test setup that has never been published could be found. This test setup was conducted by Simionopoulos at the University of Toronto in 1998.

2.3.1 Tan et al. (1999)

Tan et al. (1999) conducted a study on twelve unbounded prestressed deep beams. The aim of the experiments was to study the size effect in large prestressed beams. The parameters that varied from one specimen to another were the height of the beam ranging from 500 to 1750mm and the shear-span-to-effective-depth ratio a/d ranging from 0.56 to 1.13. All the specimens were simply-supported and were tested under two-point loading with an increasing load until failure. All beams had the same cylinder strength of about 40 MPa and the maximum aggregates size used was 10mm. The experimental setup is shown in Fig. 2.2.

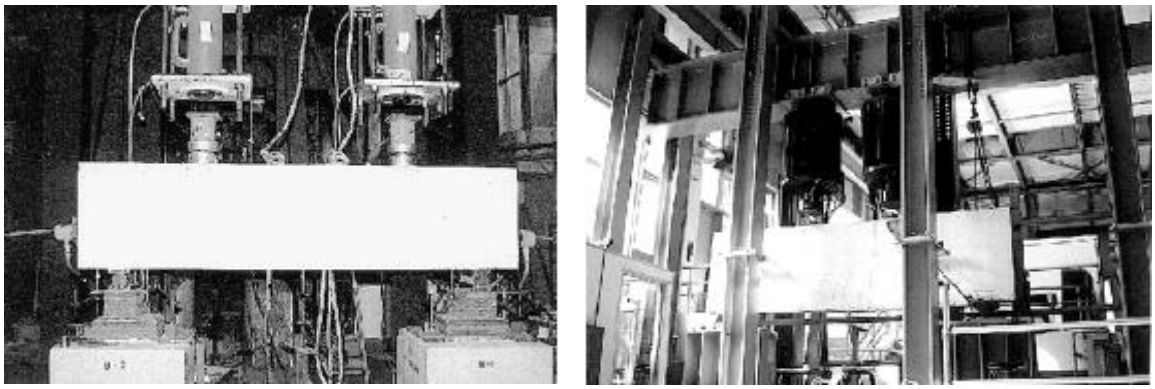
(a) (b)

Figure 2.2 – Experimental setup for (a) small and (b) large deep beams by Tan et al. (1999)

Straight strands of 15.2mm diameter were used for all specimens and the combined main-steel-and-strand ratio was kept between 2.3 and 2.5% for all beams. This high ratio was needed to prevent flexural failure to occur. The prestressing force applied was around 80% of breaking load. The strands had an average yield stress of 1708 MPa and an ultimate stress of 1834 MPa. To measure the force in each strand during the post-tensioning, a load cell was used. A low amount of stirrups was used in the test in order to study the effect of beam size on concrete shear strength. These stirrups represent only 0.1% and therefore, they do not have a significant influence on the ultimate strength. The beams were divided into four groups based on their height h= 500, 1000, 1400 and 1750mm. In each height group, three different beams were tested by varying the shear span. In order to maintain the same fracture energy, the width of the specimens were kept constant at 140mm. Moreover, in order to prevent premature crushing or bearing failure from taking place, local reinforcements were added at loading and support points.

In all specimens, flexural cracks appeared first near the section of maximum moment. Then, with increasing loads, the cracks propagated towards the loading point. Among the twelve beams tested, three of them failed by web crushing. Two of them failed by bearing failure and the rest in shear-compression or diagonal splitting. When the failure mode is studied with the size of the beam, the conclusion is that for larger prestressed beams (h=1400 and 1750mm), bearing failures occurred while typical diagonal splitting failures were expected. The reason for this failure mode may be the high location in the section of the prestressing strands that may delay and inhibit the diagonal crack. Failure modes are then dependent on the height of the section, the shear-span-to-height ratio, and the position of the prestressing strands. To prevent bearing failures, it is therefore recommended by the authors to use some reinforcing cages in loading zones.

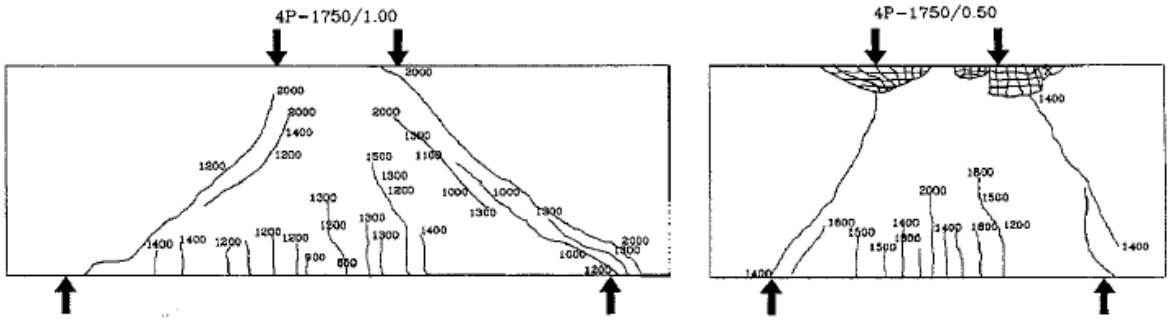

(a) (b)

Figure 2.3 – Typical cracking pattern at failure in (a) diagonal splitting and (b) by bearing failure by Tan et al. (1999)

Based on the results, it is noticeable that as the beam becomes more rigid with decreasing the a/d ratio, the lower the a/d ratio, the steeper the deflection curve. Therefore, for geometrically similar beams, brittleness is increased by increasing the height of the section. Also, an increased height leads to more extensive crack patterns at the same shear stress.

Compared to reinforced concrete deep beams, prestressing improved the diagonal cracking and serviceability strengths. The ultimate stress was also improved with prestressing. A pronounced size effect was also observed in this test series. Figure 2.4 presents the variation of ultimate shear stress with h and a/h. For a given a/h ratio, when the height is increased, a loss in the ultimate shear stress is captured. It is noted by the authors that the critical height beyond which no significant size effect is observed is comprised between 1400 and 1750mm in this test series while it was between 500 and 1000mm for the same beams without prestressing. However, while the size effect is evident for the height of the section, it seems relatively independent of the a/h ratio.

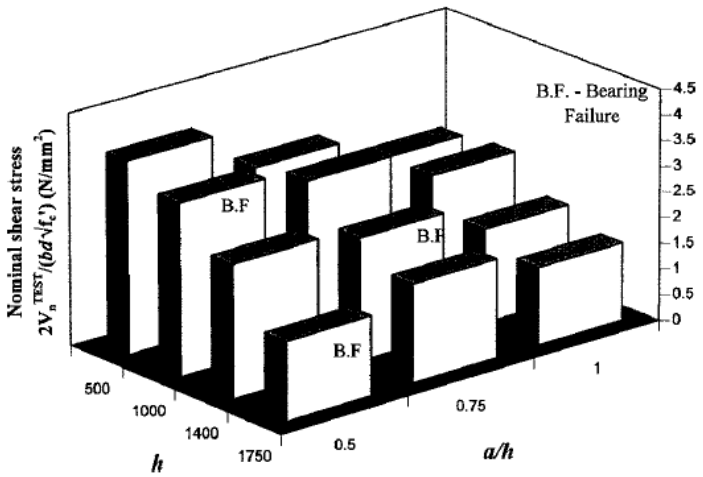

Figure 2.4 – Variation of ultimate shear stress with h and a/h by Tan et al. (1999)

2.3.1 Tan and Mansur (1992)

Tan and Mansur (1992) conducted a study on 8 bounded pre-tensioned deep beams. The aim of their tests was to study the effects of partial prestressing on the behaviour and strength of deep beams. The main parameters that varied in this test are the degree of prestress, the shear-span-to-effective-depth ratio a/d and the concrete strength f'_c. All the beams were simply supported and tested under one-point loading with an increasing load until failure. The deep beams were all 400mm height. An extra length of 200 mm was added at each end in order to provide the transmission length required for the transfer of prestress to the concrete. The width of the section was equal to 150mm for all specimens. Four of the specimens were tested with a shear span of 525mm while for the four others the shear span equals 700mm. Detail about the section and the setup of the experiment is shown in Fig. 2.5.

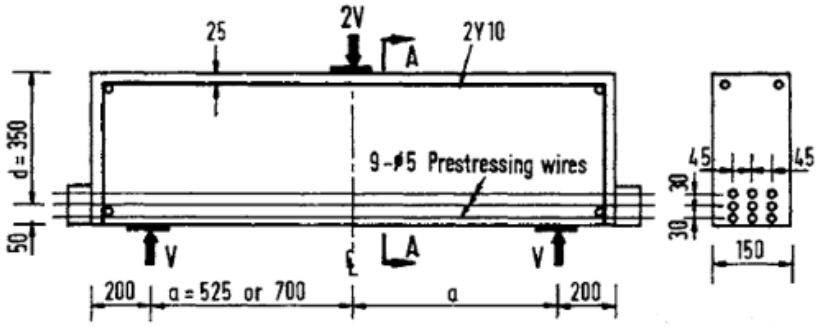

Figure 2.5 – Details of test specimens and experimental setup by Tan and Mansur (1992)

Nine prestressing wires of 5mm diameter were used as primary reinforcement. These wires were placed symmetrically compared to the vertical axis of the section. The specimens were divided into 2 groups depending on their a/d ratio (1.5 or 2). In each of these groups, the partial prestressing ratio (PPR) was varied by prestressing none, three (the middle column), six (the outer columns) or all of the wires. As a result, the corresponding values for the PPR were 0, 0.33, 0.67 and 1. Based on this arrangement, the effective depths with regard to prestressed bars and non-prestressed bars were kept identical. Moreover, the properties of prestressed and non-prestressed bars were also the same. The wires used had an average yield stress of 1480 MPa and an ultimate stress of 1623 MPa. No stirrups were used in the specimens and the maximum aggregates size was 20mm. The properties of the specimens in terms of the varying parameters are presented in Fig. 2.6.

Type	Specimen	a/d	PPR, Eq. (1)	Degree of Prestress, Eq. (2)	f_{cu}, MPa
Deep beam	S13	1.5	0	0	68.8
	S23		0.33	0.211	83.8
	S33		0.67	0.483	73.2
	S43		1.00	0.601	38.3
	S14	2.0	0	0	38.3
	S24		0.33	0.220	87.4
	S34		0.67	0.483	65.1
	S44		1.00	0.685	68.8

Figure 2.6 – Properties of test specimens by Tan and Mansur

All the specimens were completed with some instruments to measure the strains in the reinforcements and the mid-span deflection. A transducer (LVDT) and electrical resistance strain gages were used to measure the deflection and strains respectively.
In all specimens, flexural cracks appeared first near the section of maximum moment. Then, with increasing loads, the cracks propagated towards the loading point. Among the eight beams tested, five of them failed in shear-compression while three beams failed in flexure. The specimens failed in flexure when the partial prestressing ratio (PPR) was high and in shear when it was low. Figure 2.7 shows one typical beam failing in shear-compression and another failing in flexure.

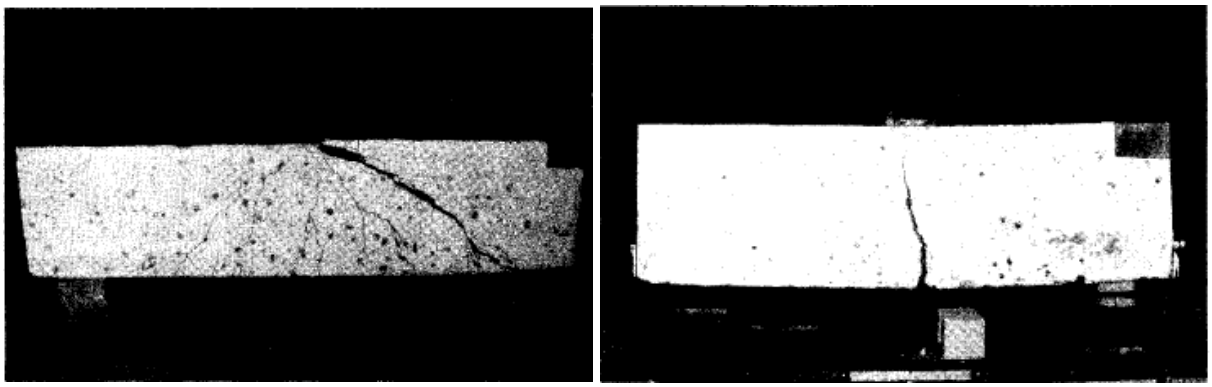

(a) (b)

Figure 2.7 – Typical cracking pattern at failure (a) in shear compression and (b) in flexure (b) by Tan and Mansur (1992)

Results showed that stiffness and cracking moment increased with the partial prestressing ratio (PPR). The ultimate shear strength of the specimens was increased when decreasing the a/d ratio, increasing the degree of prestress and increasing the concrete strength.

2.3.3 Teng, Kong and Poh (1998)

In order to study the effect of various tendon profiles and different degrees of prestressing, Teng, Kong and Poh (1998) tested 34 unbounded deep beams where 13 of them were reinforced while 21 were prestressed. Of the remaining 21 beams, 15 were prestressed with straight tendons while six were prestressed with tendons having various profiles and eccentricities. Based on our selection criteria, only the specimens with straight tendons are studied. Among these selected beams, the main parameters that varied in this test were the initial prestressing force and the vertical and horizontal reinforcement ratio. Some beams were provided with some vertical reinforcement, some were provided with both vertical and horizontal reinforcement while the others did not have any vertical and horizontal reinforcement ratio. All the deep beams were simply supported and tested

under one-point loading with an increasing load until failure of the specimens. The depth of all specimens equals 600mm. An extra length of 200 mm was added at each end in order to provide the transmission length required for the transfer of prestress to the concrete.

Straight strands of 15.2mm diameter were used for all specimens. The prestressing force applied was varied from 113 to 266kN. The strands had an average yield stress of 1725 MPa. Four kinds of unstressed steel were used: R8, R10, T10 and T22. The letters R and T denote round bars and deformed bars respectively. Load cells were used to measure the force in the tendon during the test. The experimental setup is shown in Fig. 2.8.

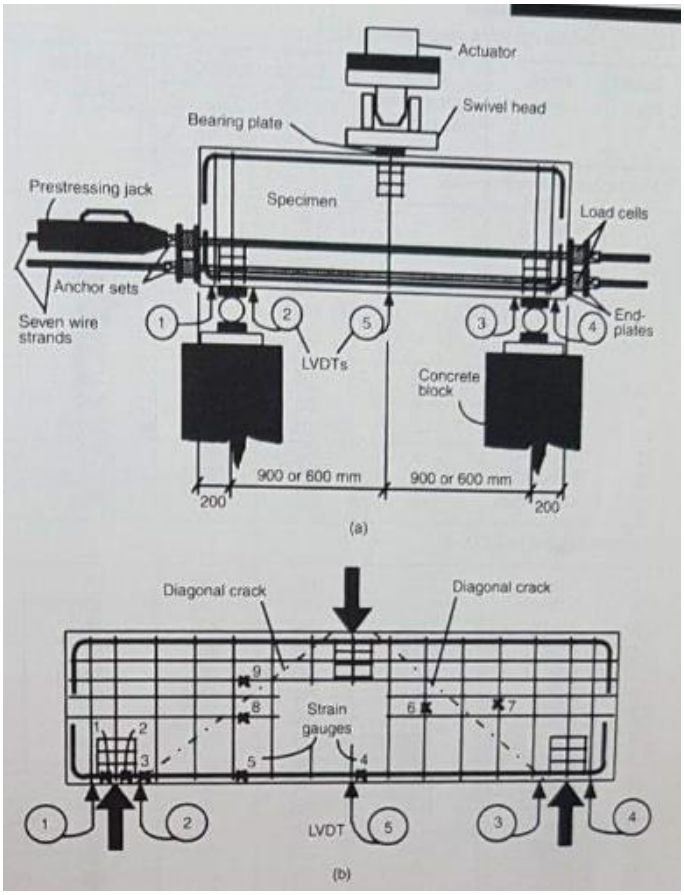

Figure 2.8 – Experimental setup by Teng, Kong and Poh (1998)

In all tested specimens, flexural cracks appeared first near the section of maximum moment. The load corresponding to first flexural crack was about 35% of the ultimate failure loads. Then, with increasing loads, the cracks propagated towards the loading point. At 50% of the failure load, the first major diagonal crack appeared. This crack started to form at about one third of the beam depth from the beam soffit. Then, it propagated quickly through the depth of the beam. It is also observed that the first diagonal cracking load was increased by the use of prestressing but not by the use of vertical or orthogonal reinforcement. Among the 15 selected beams, two of them failed in flexure while the rest failed in shear.

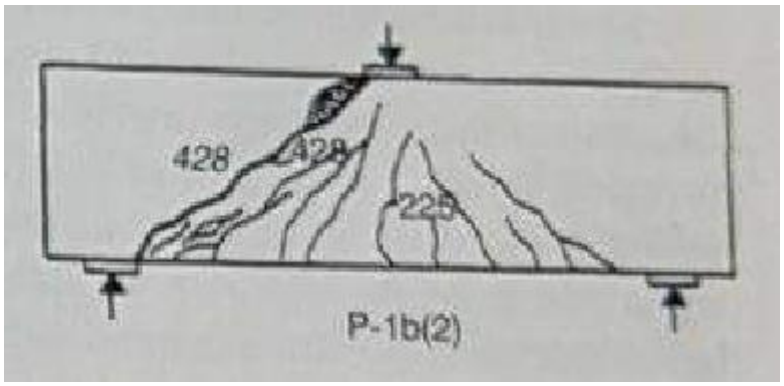

Figure 2.9 – Typical cracking pattern at failure in shear for tests by Teng, Kong and Poh (1998)

The effect of prestressing enhanced the shear strength. It is noted that the contribution of prestressing was most effective in beams with minimum or no web reinforcement and became less effective in beams with heavy orthogonal reinforcement.

2.3.4 Simionopoulos (1998)

This test series has been conducted by Simionopoulos at Mark Huggins Structural Laboratory at the University of Toronto in 1998. However, it has never been published because the results were not expected and they could not be understood. Thanks to the help of Professor Boyan Mihaylov, the data for this experiment could be collected. The aim of this study was to compare the predictions of the new general shear design method developed in University of Toronto and of the traditional ACI shear design procedures. For that purpose a large-scale experimental program was initiated. Eight prestressed deep beams with horizontal tendon profile were tested and two others with draped tendon profile. The two specimens having draped tendon profile are excluded from our study. The main parameters that varied in the test were the height of the beam and the position of the prestressing tendon. The beams were separated into four groups based on their height h=125, 250, 500, 1000mm. In each height group, one beam was tested with the tendon in the centre of the section while another beam was provided with a tendon having a certain eccentricity. Various kind of deformed reinforcing bars were used during the test. These bars and their properties are listed in Fig. 2.10.

Bar Number	Heat	Nominal Diameter [mm]	Area [mm^2]	Yield Stress [MPa]	Ultimate Stress [MPa]	Theoretical Modulus of Elasticity, E [MPa]
10	Z0001	11.3	100	458*	692	200000
15	K3997	16.0	200	437	643	200000
20	K12365	19.5	300	483	667	200000
30	C1167	29.9	700	550	n/a	200000

Figure 2.10 – Properties of reinforcing bars used by Simionopoulos (1998)

The prestress force in all specimens was induced by post-tensioning. 13mm diameter seven-wire strands were used for all beams and the ultimate tensile strength of these strands equals 1950 MPa. The number of strands used per beam varied from one to eight. All beams had the same cylinder strength of about 43 MPa. The specimens were all simply supported and tested under one-point loading as shown in Fig. 2.11.

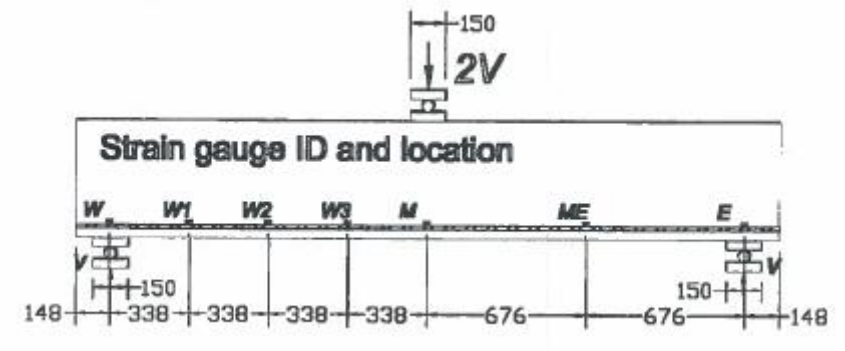

Figure 2.11 – Experimental setup by Simionopoulos (1998)

As the experiment has never been published, no information/study about the results is available except the ultimate failure loads.

2.3.5 Test database of deep prestressed beams

The complete database for the four tests described in this chapter is shown from Table 2.1 to 2.4. Values highlighted in blue correspond to the values that are not referenced by the authors and that were guessed for this study.

Authors	*Beam name*	*a/d*	*b (mm)*	*h (mm)*	*a = M/V (mm)*	l_{b1} *(mm)*	l_{b2} *(mm)*	*V/P*	ρ_l *(%)*	*# of RC bars*	d_s *(mm)*	*RC bar diam. (mm)*	f_y *(MPa)*	*Es (MPa)*	a_g *(mm)*
Tan and Mansur - 1992	S13	1,5	150	400	525	100	100	0,5	0,34	9	350	5	1480	193500	20
	S23	1,5	150	400	525	100	100	0,5	0,34	6	350	5	1480	193500	20
	S33	1,5	150	400	525	100	100	0,5	0,34	3	350	5	1480	193500	20
	S43	1,5	150	400	525	100	100	0,5	0,34	0	350	5	1480	193500	20
	S14	2	150	400	700	100	100	0,5	0,34	9	350	5	1480	193500	20
	S24	2	150	400	700	100	100	0,5	0,34	6	350	5	1480	193500	20
	S34	2	150	400	700	100	100	0,5	0,34	3	350	5	1480	193500	20
	S44	2	150	400	700	100	100	0,5	0,34	0	350	5	1480	193500	20
Tan et al. - 1999	1P-500/0,50	0,56	140	500	250	250	250	1	2,30	4	425	20	510	200000	10
	1P-500/0,75	0,84	140	500	375	250	250	1	2,30	4	425	20	510	200000	10
	1P-500/1,00	1,13	140	500	500	250	250	1	2,30	4	425	20	510	200000	10
	2P-1000/0,50	0,56	140	1000	500	250	250	1	2,30	6	915	25	510	200000	10
	2P-1000/0,75	0,84	140	1000	740	250	250	1	2,30	6	915	25	510	200000	10
	2P-1000/1,00	1,13	140	1000	1000	250	250	1	2,30	6	915	25	510	200000	10
	3P-1400/0,50	0,56	140	1400	705	250	250	1	2,50	8	1275	25	510	200000	10
	3P-1400/0,75	0,84	140	1400	1050	250	250	1	2,50	8	1275	25	510	200000	10
	3P-1400/1,00	1,13	140	1400	1420	250	250	1	2,50	8	1275	25	510	200000	10
	4P-1750/0,50	0,56	140	1750	880	250	250	1	2,50	10	1535	25	510	200000	10
	4P-1750/0,75	0,84	140	1750	1320	250	250	1	2,50	10	1535	25	510	200000	10
	4P-1750/1,00	1,13	140	1750	1760	250	250	1	2,50	10	1535	25	510	200000	10

Table 2.1 – Collected database of prestressed deep beams

Authors	*Beam name*	*a/d*	*b (mm)*	*h (mm)*	*a = M/V (mm)*	l_{b1} *(mm)*	l_{b2} *(mm)*	*V/P*	ρ_l *(%)*	*# of RC bars*	d_s *(mm)*	*RC bar diam. (mm)*	f_y *(MPa)*	E_s *(MPa)*	a_g *(mm)*
Teng, Kong and Poh - 1998	P-1c	1,64	150	600	900	150	150	0,5	1,09	2	550	22	754	200000	10
	P-1a	1,64	150	600	900	150	150	0,5	1,09	2	550	22	754	200000	10
	P-1b	1,64	150	600	900	150	150	0,5	1,09	2	550	22	754	200000	10
	P-2a	1,64	150	600	900	150	150	0,5	1,09	2	550	22	754	200000	10
	P-2b	1,64	150	600	900	150	150	0,5	1,09	2	550	22	754	200000	10
	P-3a	1,64	150	600	900	150	150	0,5	1,09	2	550	22	754	200000	10
	P-3b	1,64	150	600	900	150	150	0,5	1,09	2	550	22	754	200000	10
	P-1b(2)	1,64	160	600	900	150	150	0,5	1,02	2	550	22	478	200000	10
	P-1c(2)	1,64	160	600	900	150	150	0,5	1,02	2	550	22	478	200000	10
	P-1-1,5-WO	1,64	160	600	900	150	150	0,5	1,18	2	550	22	478	200000	10
	P-1-1,5-WV	1,64	160	600	900	150	150	0,5	1,18	2	550	22	478	200000	10
	P-1-1,5-WVH	1,64	160	600	900	150	150	0,5	1,18	2	550	22	478	200000	10
	P-1-1,0-WO	1,09	160	600	600	150	150	0,5	1,18	2	550	22	478	200000	10
	P-1-1,0-WV	1,09	160	600	600	150	150	0,5	1,18	2	550	22	478	200000	10
	P-1-1,0-WVH	1,09	160	600	600	150	150	0,5	1,18	2	550	22	478	200000	10
Simiono poulos - 1998	BP100	2,92	300	1000	2700	150	150	0,5	1,04	3	925	29,9	550	200000	10
	BP100E	2,92	300	1000	2700	150	150	0,5	1,04	3	925	29,9	550	200000	10
	BP50	3,00	300	500	1350	150	150	0,5	1,04	5	450	16	437	200000	10
	BP50E	3,00	300	500	1350	150	150	0,5	1,04	5	450	16	437	200000	10
	BP25	3,00	300	250	675	60	60	0,5	1,19	3	225	16	437	200000	10
	BP25E	3,00	300	250	675	60	60	0,5	1,19	3	225	16	437	200000	10

Table 2.2 – Collected database of prestressed deep beams (continued)

Authors	*Beam name*	f'_c *(MPa)*	ρ_v *(%)*	d_{bv} *(mm)*	f_{yv} *(MPa)*	ρ_h *(%)*	# of prestr. bars	*Prestr. bar diameter (mm)*	d_p *(mm)*	*P (kN)*	f_{py} *(MPa)*	E_p *(MPa)*	*Failure mode*	$V_{exp.}$ *(kN)*
Tan and Mansur - 1992	S13	58,5	0	10	508	0	0	5	350	0,0	1480	193500	Shear	159
	S23	71,2	0	10	508	0	3	5	350	55,2	1480	193500	Flexure	198
	S33	62,2	0	10	508	0	6	5	350	126,3	1480	193500	Flexure	202
	S43	32,6	0	10	508	0	9	5	350	157,2	1480	193500	Shear	144
	S14	32,5	0	10	508	0	0	5	350	0,0	1480	193500	Shear	62
	S24	74,3	0	10	508	0	3	5	350	57,5	1480	193500	Flexure	156
	S34	55,3	0	10	508	0	6	5	350	126,3	1480	193500	Shear	115
	S44	58,5	0	10	508	0	9	5	350	179,2	1480	193500	Shear	144
Tan et al. - 1999	1P-500/0,50	46,6	0	6	510	0	1	15,2	380	126,8	1709	200000	Shear	815
	1P-500/0,75	42,7	0	6	510	0	1	15,2	380	133,9	1709	200000	Shear	590
	1P-500/1,00	39,3	0	6	510	0	1	15,2	380	138,9	1709	200000	Shear	450
	2P-1000/0,50	43,5	0,12	6	510	0,12	2	15,2	760	301,2	1709	200000	Bear. Fail.	1350
	2P-1000/0,75	40,6	0,12	6	510	0,12	2	15,2	760	301,9	1709	200000	Shear	1200
	2P-1000/1,00	35,8	0,12	6	510	0,12	2	15,2	760	336,9	1709	200000	Shear	900
	3P-1400/0,50	34,8	0,12	6	510	0,12	3	15,2	1080	450,0	1709	200000	Shear	1300
	3P-1400/0,75	33,5	0,12	6	510	0,12	3	15,2	1080	472,2	1709	200000	Bear. Fail.	1250
	3P-1400/1,00	39,5	0,12	6	510	0,12	3	15,2	1080	450,0	1709	200000	Shear	950
	4P-1750/0,50	38	0,12	6	510	0,12	4	15,2	1200	589,5	1709	200000	Bear. Fail.	1100
	4P-1750/0,75	38,3	0,12	6	510	0,12	4	15,2	1200	604,9	1709	200000	Shear	1325
	4P-1750/1,00	40,9	0,12	6	510	0,12	4	15,2	1200	662,3	1709	200000	Shear	1100

Table 2.3 – Collected database of prestressed deep beams (continued)

Authors	*Beam name*	f'_c *(MPa)*	ρ_v *(%)*	d_{bv} *(mm)*	f_{yv} *(MPa)*	ρ_h *(%)*	# of prestr. bars	*Prestr. bar diameter (mm)*	d_p *(mm)*	*P (kN)*	f_{py} *(MPa)*	E_p *(MPa)*	*Failure mode*	$V_{exp.}$ *(kN)*
Teng, Kong and Poh - 1998	P-1c	38,4	0	0		0	1	15,2	300	129,1	1725	200000	Shear	275
	P-1a	38,4	0	0		0	1	15,2	475	132,1	1725	200000	Shear	290
	P-1b	38,3	0	0		0	1	15,2	475	186,0	1725	200000	Shear	200
	P-2a	38,4	0,70	10	406	0	1	15,2	475	141,8	1725	200000	Shear	412,5
	P-2b	38,3	0,70	10	406	0	1	15,2	475	160,4	1725	200000	Flexure	425
	P-3a	38,5	0,70	10	406	1,23	1	15,2	475	130,6	1725	200000	Flexure	437,5
	P-3b	38,4	0,70	10	406	1,23	1	15,2	475	179,5	1725	200000	Shear	460
	P-1b(2)	40,1	0	0		0	1	15,2	475	112,8	1734	200000	Shear	214
	P-1c(2)	40,1	0	0		0	1	15,2	300	134,1	1734	200000	Shear	287,5
	P-1-1,5-WO	43,4	0	0		0	2	15,2	450	266,4	1734	200000	Shear	370
	P-1-1,5-WV	43,5	0,42	8	412	0	2	15,2	450	265,4	1734	200000	Shear	437,5
	P-1-1,5-WVH	43,5	0,42	8	412	0,84	2	15,2	450	266,1	1734	200000	Shear	400
	P-1-1,0-WO	43,2	0	0		0	2	15,2	450	219,2	1734	200000	Shear	417,5
	P-1-1,0-WV	43,3	0,65	10	348	0	2	15,2	450	211,5	1734	200000	Shear	537,5
	P-1-1,0-WVH	43,3	0,65	10	495	1,31	2	15,2	450	225,4	1734	200000	Shear	560
Simiono poulos - 1998	BP100	42,6	0	0	0	0	8	12,9	500	1038,0	1755	195000	Shear	464
	BP100E	42,6	0	0	0	0	8	12,9	667	1036,0	1755	195000	Shear	561
	BP50	42,6	0	0	0	0	4	12,9	250	495,0	1755	195000	Shear	224
	BP50E	43	0	0	0	0	4	12,9	333	496,0	1755	195000	Shear	299
	BP25	43	0	0	0	0	2	12,9	125	247,0	1755	195000	Shear	142,4
	BP25E	43	0	0	0	0	2	12,9	167	250,0	1755	195000	Shear	164
	BP12	43,5	0	0	0	0	1	12,9	62,5	114,0	1755	195000	Shear	73,5
	BP12E	43,5	0	0	0	0	1	12,9	83,5	113,0	1755	195000	Shear	60,4

Table 2.4 – Collected database of prestressed deep beams (continued)

3. Modelling approaches for prestressed deep beams

3.1 Strut-and-tie models

Strut-and-tie models (STM) are a very effective engineering approach that transforms complex stress patterns into simple flow of tensile (ties) and compressive (struts) forces. They are commonly used to design shear critical structures and more generally, disturbed regions in concrete beams (Eurocode2). They are very easy to use and can be adopted to many different concrete structures as well as to deep beams. When a deep beam is idealized with a strut-and-tie model, the prestressing and the main flexural reinforcement are represented by a tie, the force path between loading zones and support zones as an inclined strut, and when the beam is subjected to two-point loading, the path between both loading points is represented as an horizontal strut (Fig. 3.1).
Alsheiger and Ramirez (1992) proposed detailed strut and tie models for three pre-tensioned deep beams with I-sections. However, analyses with these models were performed with a computer program rather than a simple formula. For this reason, these analyses were unsuitable for every-day design. To address this issue, Tan et al. (2001) proposed a strut-and-tie model for simply supported prestressed concrete deep beams and developed a relevant formula (Fig. 3.1). A linear failure criterion modified from the Mohr-Coulomb theory was used to take into account the concrete softening effect in the struts.

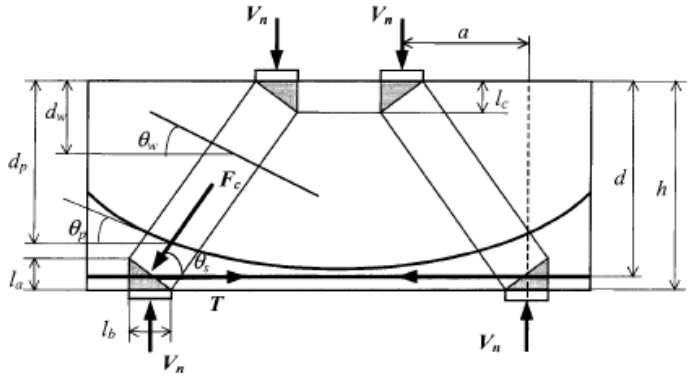

Figure 3.1 – Strut and tie model proposed by Tan et al. (2001)

Finally, Wang and Meng (2008) developed a modified strut and tie model for simply supported prestressed concrete deep beams (Fig. 3.2). Equivalent external loads were used to take into account the effects of prestressing.

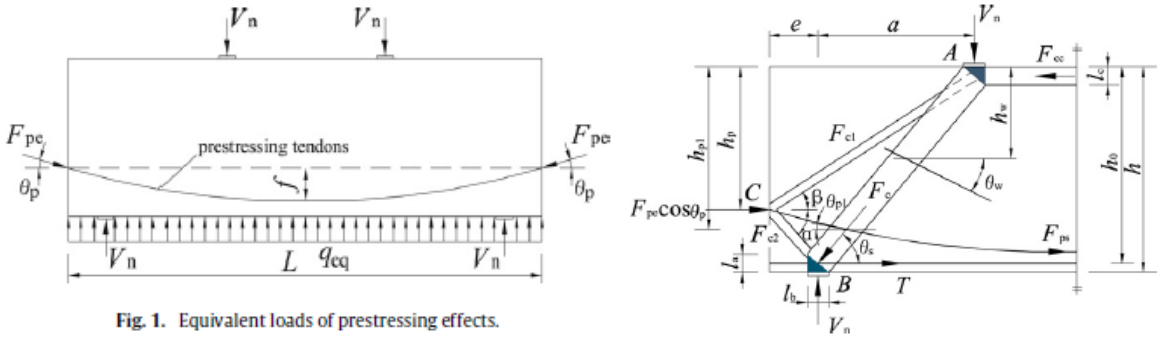

Figure 3.2 – Equivalent loads of prestressing effects and modified strut and tie model proposed by Wang and Meng (2008)

The model proposed by Wang and Meng (2008) as well as the one of Tan et al. (2001) were compared to 56 prestressed deep beams resulting in conservative shear strength predictions as shown in Fig. 3.3.

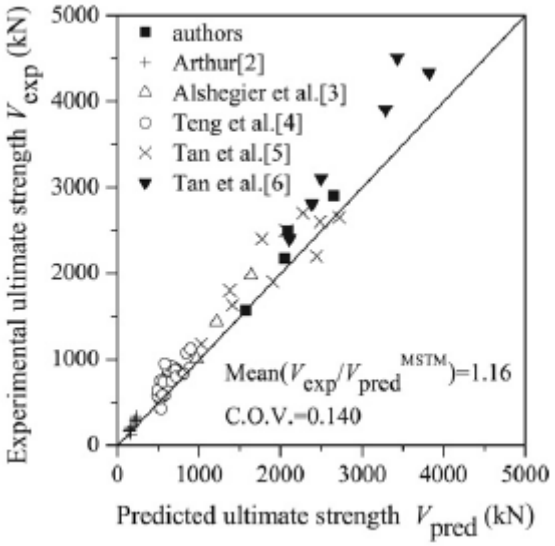

Figure 3.3 – Shear strength predictions by Wang and Meng (2008)

However, even if strut and tie models are very easy to use and very powerful, they are not always able to produce adequate results for the ultimate failure strength of deep beams because of the large number of parameters that influence the shear behaviour of those beams. Furthermore, as strut-and-tie models are based on the flow of forces in the member, they are not well suited for predicting deformations.

3.2 Finite element models

Non-linear finite element models (FEM) are a numerical approach used to solve complex engineering problems. The method divides a continuous domain into multiple finite elements with deformation patterns. Due to material and geometrical nonlinearities, FE models are solved iteratively until the conditions for equilibrium between internal and external forces are satisfied. Sophisticated FEMs tend to be generally more accurate than strut-and-tie models. However, this method requires long time for modelling and computations as well as significant expertise to be used safely.

The FEM software used in this thesis is called VecTor2. It has been developed at the University of Toronto since the 1980s. It is based on the Modified compression Field Theory (Vecchio and Collins 1986) and Disturbed Stress Field Model (Vecchio 2000). The software implements a 2D plane-stress formulation and is able to model both monotonic and cyclic loading. The prestressing can be easily implemented in the model by means of prestrains in the prestressing reinforcement. Second order effects are also incorporated into the program's analysis algorithms. Moreover, multiples behaviour models for cracked concrete are available to use.

The finite elements implemented in VecTor2 are linear, triangular, rectangular, and quadrilateral. The reinforcements can be represented in the model either by linear elements or as smeared reinforcement in the concrete elements.

3.3 Two-parameter kinematic Theory

The two-parameter kinematic theory (2PKT) has been developed by Mihaylov et al. in 2013. The model is able to describe the deformed shape of deep beams using just two kinematic parameters (degrees of freedom, DOF). This model is combined with equilibrium equations and stress-strain relationships to predict the shear strength and deformation patterns of deep beams at shear failure. More recently, the 2PKT method was extended to a five-spring model to predict the complete pre- and post-peak shear behaviour of deep beams (Mihaylov 2015). This new model keeps the same philosophy as the 2PKT but calculations are repeated at every load stage and not only at ultimate. This thesis however focuses on extending the original 2PKT to prestressed deep beams.

The 2PKT was developed based on an experimental study conducted by Mihaylov et al. (2010). Ten large reinforced concrete deep beams were tested to failure under cyclic or monotonic and reversed-cyclic loading. The results indicated that cyclic loading does not have a significant effect on the ultimate shear strength. Figure 3.4 shows one of the specimens after failure, including its measured crack and deformation patterns. The figure illustrates a shear failure with a critical crack extending between the loading and support zones. The crack diagram as well as the deformations diagram indicate that the concrete zone above the critical crack deforms relatively little and the shear deformations are concentrated around the crack.

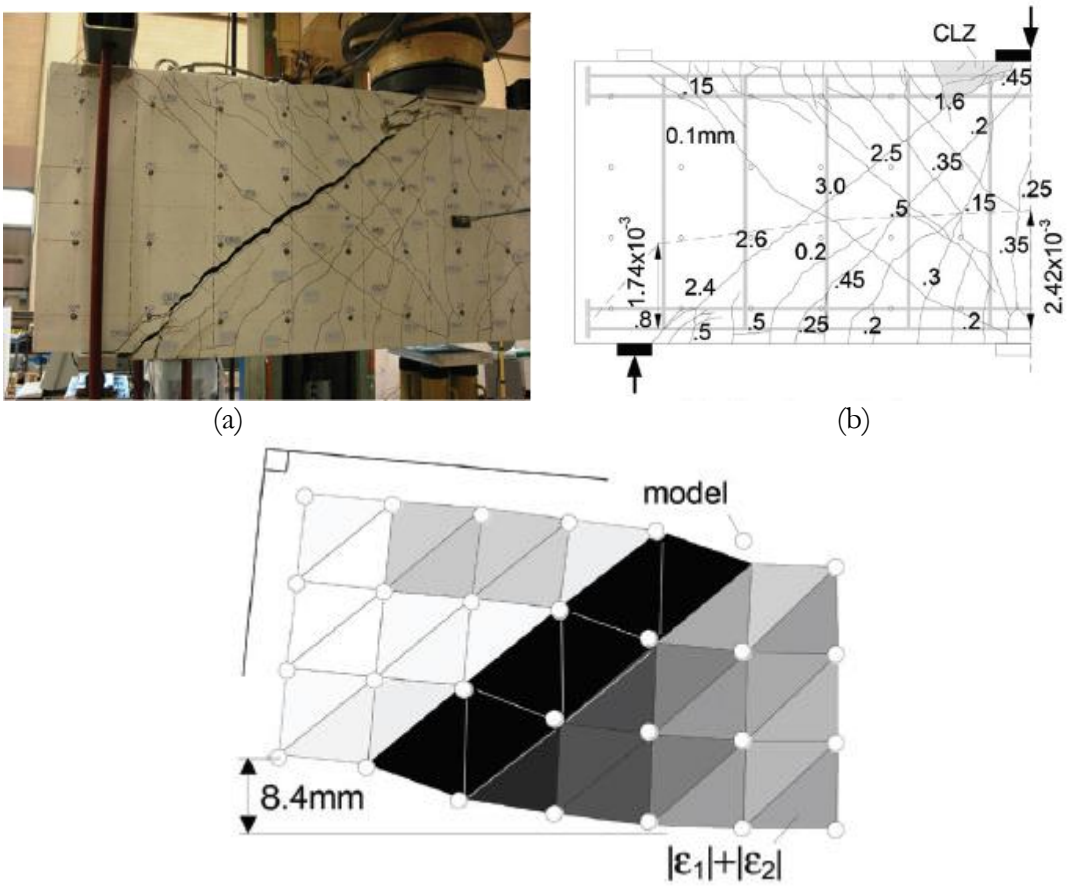

Figure 3.4 – (a) Photo of specimen S1C after failure, (b) Cracks width at failure, (c) Deformations at failure X30 (Mihaylov et al., 2013)

Based on these observations, it is assumed in the 2PKT that the critical shear crack of deep beams develop along a straight line that extends from the inner edge of the support to the far edge of the

loading plate. The concrete zone above the critical crack is modelled as a rigid block while the concrete under the crack is represented by a series of rigid radial struts ("fan" of struts) that connect the loading point to the bottom longitudinal reinforcement. These two zones are connected by the critical loading zone (CLZ) where the concrete crushes, the stirrups and the bottom longitudinal reinforcement.

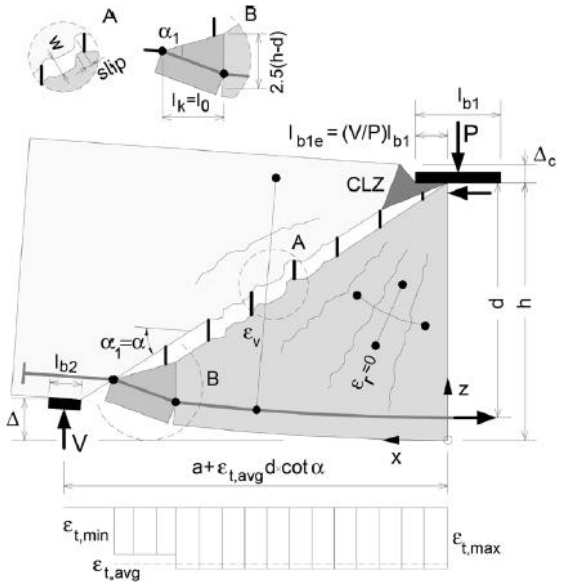

Figure 3.5 – Details of 2PKT (Mihaylov et al. 2013)

The main assumption of the model is that the motion of the concrete block above the critical crack consists of a rotation about the top of the crack and a vertical translation with respect to the fan of struts. The rotation is proportional to the average strain in the bottom reinforcement $\varepsilon_{t,avg}$ while the vertical translation equals the displacement Δ_c that develops in the critical loading zone (Mihaylov et al.,2013). Therefore, $\varepsilon_{t,avg}$ and Δ_c are the two degrees of freedom of the model. Strain $\varepsilon_{t,avg}$ is associated with widening of the critical crack while displacement Δ_c in the critical loading zone causes both widening and slip displacement in the crack. Finally, the angle of the critical crack, α_1 is assumed equal to the angle of the diagonal of the shear span α, but should not be taken smaller than 35° to represent the transition from deep to slender beams.

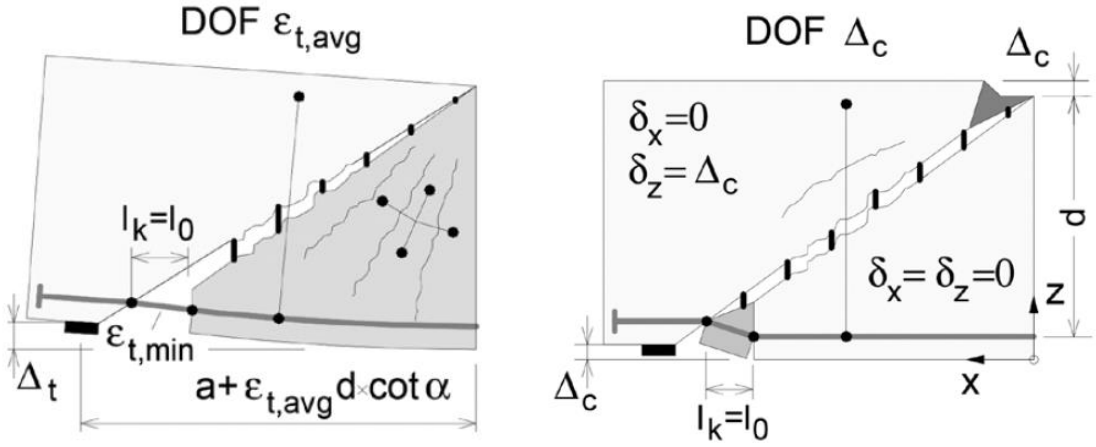

(a) (b)

Figure 3.6 – Degrees of freedom of 2PKT (Mihaylov et al. 2013)

Based on these assumptions, the displacements of all points above and below the critical crack can be derived in terms of the two degrees of freedom:

- For points below the critical crack:

$$\delta_x(x,z) = \varepsilon_{t,avg} x \tag{3.1}$$

$$\delta_z(x,z) = \frac{\varepsilon_{t,avg} x^2}{h-z} \tag{3.2}$$

- For points above the critical crack:

$$\delta_x(x,z) = \varepsilon_{t,avg}(h-z)\cot\alpha \tag{3.3}$$

$$\delta_z(x,z) = \varepsilon_{t,avg} x \cot\alpha + \Delta_c \tag{3.4}$$

It can be seen from Eq. 3.1 that the strain for point below the critical crack remains constant along the depth of the section. Therefore, no matter the position of prestressing tendon, the strain in it will be the same as the strain in the bottom non-prestressed reinforcement. Using this displacement field, the width of the critical diagonal crack at mid-depth is expressed as:

$$w = \Delta_c \cos\alpha_1 + \frac{\varepsilon_{t,avg} l_k}{2\sin\alpha_1} \tag{3.5}$$

where the two terms of this equation are associated with the two degrees of freedom. Length l_k is shown in Fig. 3.6 and is estimated as:

$$l_k = l_0 + d(\cot\alpha - \cot\alpha_1) \tag{3.6}$$

$$l_0 = 1.5(h-d)\cot\alpha_1 \geq s_{max} \tag{3.7}$$

$$s_{max} = \frac{0.28\, d_b}{\rho_l} \frac{2.5(h-d)}{d} \tag{3.8}$$

where s_{max} is the spacing of the cracks along the bottom reinforcement, d_b is the diameter of the bottom bars, ρ_l is the flexural reinforcement ratio and l_0 is the length of heavily cracked zone at bottom of critical diagonal crack.
In addition to deformations, the 2PKT also models the mechanisms of shear resistance across the critical diagonal crack. A big portion of the shear is carried by the critical loading zone, while the other mechanisms are the aggregate interlock along the crack, the tension in the transverse reinforcement (stirrups) as well as the dowel action of the bottom reinforcement. Therefore, the shear strength of a deep beam is expressed as:

$$V = V_{CLZ} + V_{ci} + V_s + V_d \tag{3.9}$$

Where subscripts "CLZ", "ci", "s" and "d" stand for critical loading zone, crack interface (aggregate interlock), stirrups, and dowel action respectively. In order to calculate the shear strength of a given member, the four components of the equation above should be expressed in terms of the two degrees of freedom defined.
The shear resisted by aggregate interlock is given by:

$$V_{ci} = \frac{0.18\sqrt{f'_c}}{0.31 + \frac{24w}{a_{ge} + 16}}\ bd \tag{3.10}$$

where f'_c is the concrete cylinder strength, b is the cross section width and where the effective aggregate size a_{ge} equals the maximum aggregate size a_g for concrete strengths less than 60 MPa and zero for strengths larger than 70 MPa. A linear interpolation is used for intermediate concrete strengths.
The shear resisted by the stirrups is given by:

$$V_s = \rho_v b(d\ cot\ \alpha_1 - l_0 - 1.5l_{b1e})f_v\ \geq 0 \tag{3.11}$$

where ρ_v is the ratio of transverse reinforcement and where l_{b1e} is the effective width of the loading plate and is expressed as:

$$l_{b1e} = (\frac{V}{P})\ l_{b1} \geq 3\ a_g \tag{3.12}$$

where $\frac{V}{P}$ is the ratio of shear force to applied point load and l_{b1} is the longitudinal length of the loading plate. The stress in the stirrups f_v is calculated by assuming an elastic-perfectly plastic behaviour of the steel:

$$f_v\ =\ E_s\ \varepsilon_v\ \leq f_{yv} \tag{3.13}$$

where E_s is the elastic modulus of steel and where the transverse strain ε_v halfway along the critical crack is derived from the kinematic model as:

$$\varepsilon_v\ =\ \frac{1}{0.9d}(\Delta_c + 0.25\varepsilon_{t,avg} d\ cot^2\ \alpha_1) \approx\ \frac{1.5\Delta_c}{0.9d} \tag{3.14}$$

The expression for the shear resisted by dowel action of the bottom reinforcement is derived based on the assumption that the dowels of length l_k work in double curvature with plastic hinges forming at each end:

$$V_d\ =\ n_b f_{ye} \frac{d_b^3}{3l_k} \tag{3.15}$$

where n_b represents the number of bars and d_b the bar diameter. The effective yield strength of the steel in the plastic hinges is given by:

$$f_{ye} = f_y \left[1 - \left(\frac{T}{f_y A_s}\right)^2\right] \leq 500MPa \tag{3.16}$$

and accounts for the tension T in bar-dowels :

$$T = E_s\ \varepsilon_{t,avg}\ A_s \tag{3.17}$$

The last component of the shear force is the shear carried in the critical loading zone. This zone is a key component of the two-parameter kinematic theory and is illustrated in Fig. 3.7.

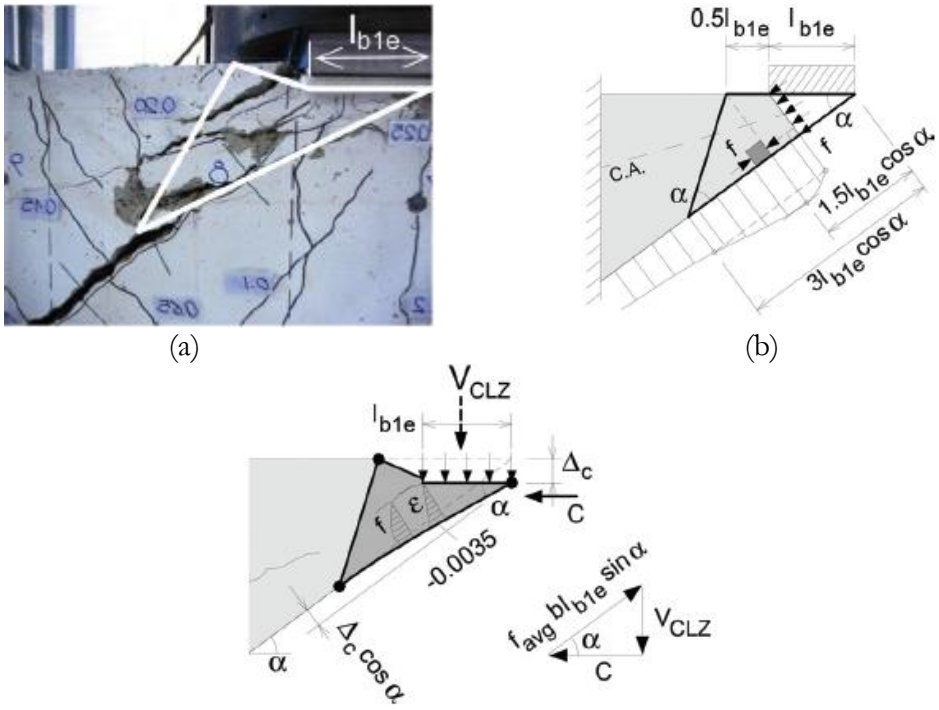

(a) (b)

(c)

Figure 3.7 – (a) CLZ after failure, (b) dimensions of CLZ, (c) deformations and shear capacity of CLZ (Mihaylov et al., 2013)

A simple linear stress analysis was used to determine the dimensions of the critical loading zone. The concrete above the critical crack was modelled as a variable depth elastic cantilever fixed on the left side and loaded with diagonal compressive stresses on the opposite side. Based on the analysis, it can be seen that the compressive stress along the bottom edge of the cantilever reaches the maximum value at a distance $1.5l_{b1e}\,cos\,\alpha$ from the tip section and returns to the applied stress at a distance of $3l_{b1e}\,cos\,\alpha$ from the same section. A triangular critical loading zone could be defined based on this result as illustrated in Fig. 3.7b. It is however noted that the effective width of the loading l_{b1e} should not be taken less than three times the maximum size of coarse aggregate a_g as it is shown in equation 3.12.
Moreover, knowing the geometry of the critical loading zone, the analysis showed that the vertical displacement of the critical loading zone at failure is given from:

$$\Delta_c = 0.0105 l_{b1e}\,cot\,\alpha \tag{3.18}$$

Therefore, the conclusion is that the vertical displacement is not anymore an unknown at failure. The only unknown DOF that remains is the strain in the bottom reinforcement $\varepsilon_{t,avg}$. Based on the vertical displacement, the shear resisted by the critical loading zone can be expressed as:

$$V_{CLZ} = k f_{avg}\, b l_{b1e} sin^2\alpha \tag{3.19}$$

Where k is a crack shape coefficient that is equal to 1 for beams having $cot\,\alpha < 2$ and 0 for beams with $cot\,\alpha > 2.5$. A linear transition for intermediate values of $cot\,\alpha$ is supposed for the value of k. The average compressive stress is calculated by:

$$f_{avg} = 1.43 f'^{0.8}_c \tag{3.20}$$

As mentioned before, the ultimate shear strength is given by the sum of the shear four mechanisms accounted for in the 2PKT. However, the strain in the bottom reinforcement $\varepsilon_{t,avg}$ should be found at failure. So far, the shear behaviour of the beam is presented. In order to find the ultimate shear strength, the flexural behaviour will be studied as well. From moment equilibrium of the shear span about the point of application of the compression force C in the section with maximum moment, the shear force can be expressed as:

$$V = \frac{T(0.9d)}{a} \tag{3.21}$$

Where T is the tension force in the bottom reinforcement.
The equilibrium of forces written below can then be solved to find the value of DOF $\varepsilon_{t,avg}$.

$$V = \frac{T(0.9d)}{a} = V_{CLZ} + V_{ci} + V_s + V_d \tag{3.22}$$

Once the strain $\varepsilon_{t,avg}$ is found, all the shear mechanisms that contribute to the shear resistance can be calculated and the sum of all these mechanisms give the predicted shear strength of the member.

4. Kinematic Modelling of Prestressed Deep Beams

4.1 Application of the original 2PKT to tests database

The first step in the kinematic modelling of prestressed deep beams is to apply the 2PKT method without modifications to the tests discussed in Chapter 2. In this way it will be identified whether the original 2PKT provides reasonable accuracy and whether it requires significant improvement. In this context, as the original model does not take into account the prestressing, the prestressed reinforcement will be treated as non-prestressed. The total amount of flexural reinforcement in the section is then given by:

$$A^*_s = A_s + A_p \tag{4.1}$$

and the effective depth of this reinforcement is given from:

$$d^* = \frac{A_s d_s + A_p d_p}{A_s + A_p} \tag{4.2}$$

To study the specimens and their shear strength at failure, it is also important to compare the maximum shear strength at shear failure to the shear strength of the same specimen at flexural failure. In order to calculate the maximum bending moment resisted by the specimens, all of them were modelled on the software Response 2000 which is a computer program capable of predicting the full load-deformation response of reinforced and prestressed concrete members. The program is based on the modified compression field theory and was developed at the University of Toronto by Evan Bentz under the supervision of Professor Michael P. Collins. Once the maximum bending moment was found by Response 2000, as all the specimens were tested under one or two-point loading, the shear force at flexural failure was computed from:

$$V\ at\ flexural\ failure = \frac{M_{max}}{a} \tag{4.3}$$

Where a is the shear span of the specimens.

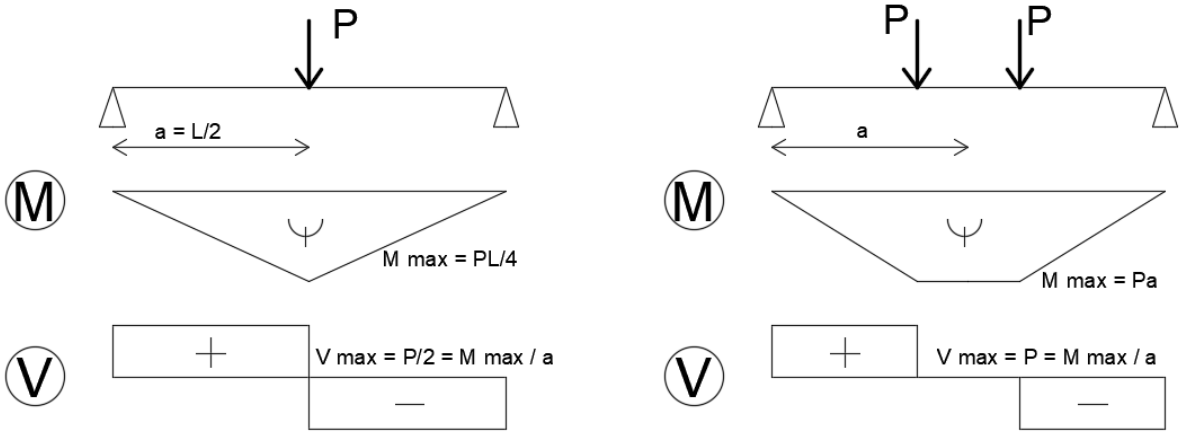

Figure 4.1 – Bending moment and shear diagram under one-point loading and two-point loading

In addition to calculation of the shear strength based on the 2PKT and the flexural strength based on the classical plane-sections-remain plane approach, it is also needed to account for potential bearing failures due to high stresses under the point loads. Assuming that such failures occur when the stresses under the loading plates reach f'_c, the shear corresponding to bearing failure is:

$$V_{max}\ by\ bearing\ failure = \frac{V}{P} b l_{b1e} f'_c \quad (4.4)$$

The final shear strength prediction at failure is given by:

$$V_{max} = Min\ \{V\ at\ flexural\ failure;\ V_{max}\ by\ 2PKT;\ V_{max}\ by\ bearing\ failure\} \quad (4.5)$$

4.1.1 Tests by Tan et al. (1999)

Tan et al. (1999) tested twelve unbounded prestressed deep beams. The objective of their experiment was to study the size effect in prestressed deep beams. For that reason, the main parameters that varied in this experiment are the shear-span-to-effective-depth ratio a/d and the height of the beams. The specimens were divided into four height groups (h=500, 1000, 1400 and 1750mm). Then, in each group, the shear span was varied in order to have 3 different shear-span-to-effective-depth ratio (a/d=0,56; 0,84; 1,13).

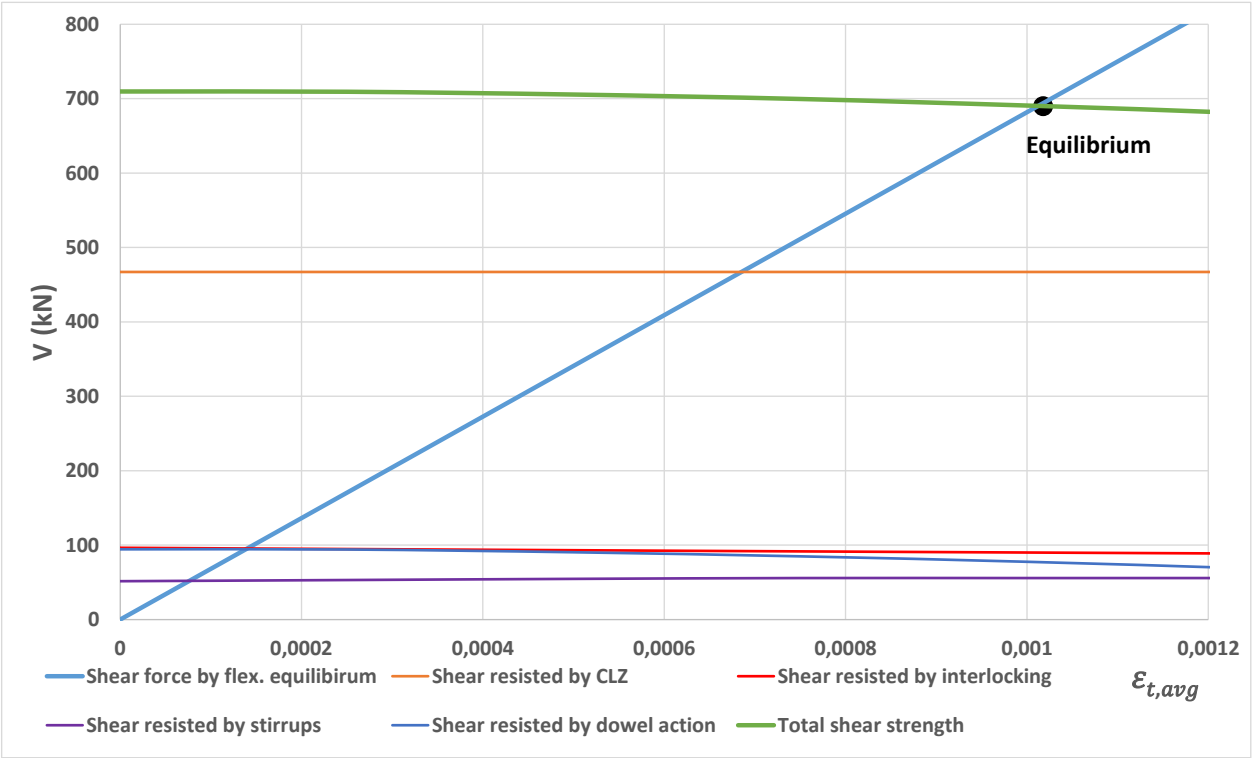

Figure 4.2 – Contribution to shear strength of the different shear mechanisms for specimen 3P-1400/1.0 from tests by Tan et al. (1999)

To illustrate how the 2PKT method works, it is first applied to specimen 3P-1400/1.00. The solution of the 2PKT equations is shown graphically in Fig. 4.2. On the horizontal axis of the plot is the unknown DOF $\varepsilon_{t,avg}$ while on the vertical axis are the shear forces. The solution begins with calculating the geometry of the kinematic model and DOF Δ_c (Eq. 3.18). Then, with the obtained Δ_c and for each value of DOF $\varepsilon_{t,avg}$ on the horizontal axis, the shear strength components V_{CLZ}, V_{ci}, V_s and V_d are calculated from Eq. 3.10, 3.11, 3.15 and 3.19. Therefore, the sum of the shear components equals the shear resistance of the beam which is plotted with a thick green line. To ensure equilibrium of the shear forces, the shear resistance must be equal to the shear force obtained from the moment equilibrium of the beam (Eq. 3.22). This shear force is plotted with a thick blue line and increases linearly with $\varepsilon_{t,avg}$ due to the elastic behaviour of the flexural reinforcement. Therefore, the solution of the 2PKT equations lies at the intersection of

the thick green and blue lines which can be viewed as shear capacity and shear demand lines, respectively. The abscissa of the intersection point is the predicted DOF $\varepsilon_{t,avg}$ while the ordinate is the predicted shear strength. For beam 3P-1400/1.0, the predicted shear strength is 693 kN while the experimentally obtained value is 950 kN. This results in a shear-strength experimental-to-predicted ratio of 1.371. Flexural and bearing failures were not governing as they corresponded to higher shear forces (1765 and 1383 kN, respectively).
It can also be seen from Fig. 4.2 that a big portion of the shear strength is provided by the critical loading zone. Indeed, at failure, shear component V_{CLZ} represents 67% of the total shear strength while the interlocking, the dowel action and the stirrups represents respectively 13%, 8% and 12%. It is also important to note that, as evident from the figure, the shear strength provided by the critical loading zone is independent of the strain in the bottom reinforcement while the interlocking strength decreases with the increase of the strain and the opening of cracks. It will therefore be a key issue to study how the critical loading zone behave with the variation of strain in the longitudinal reinforcement for prestressed deep beams.

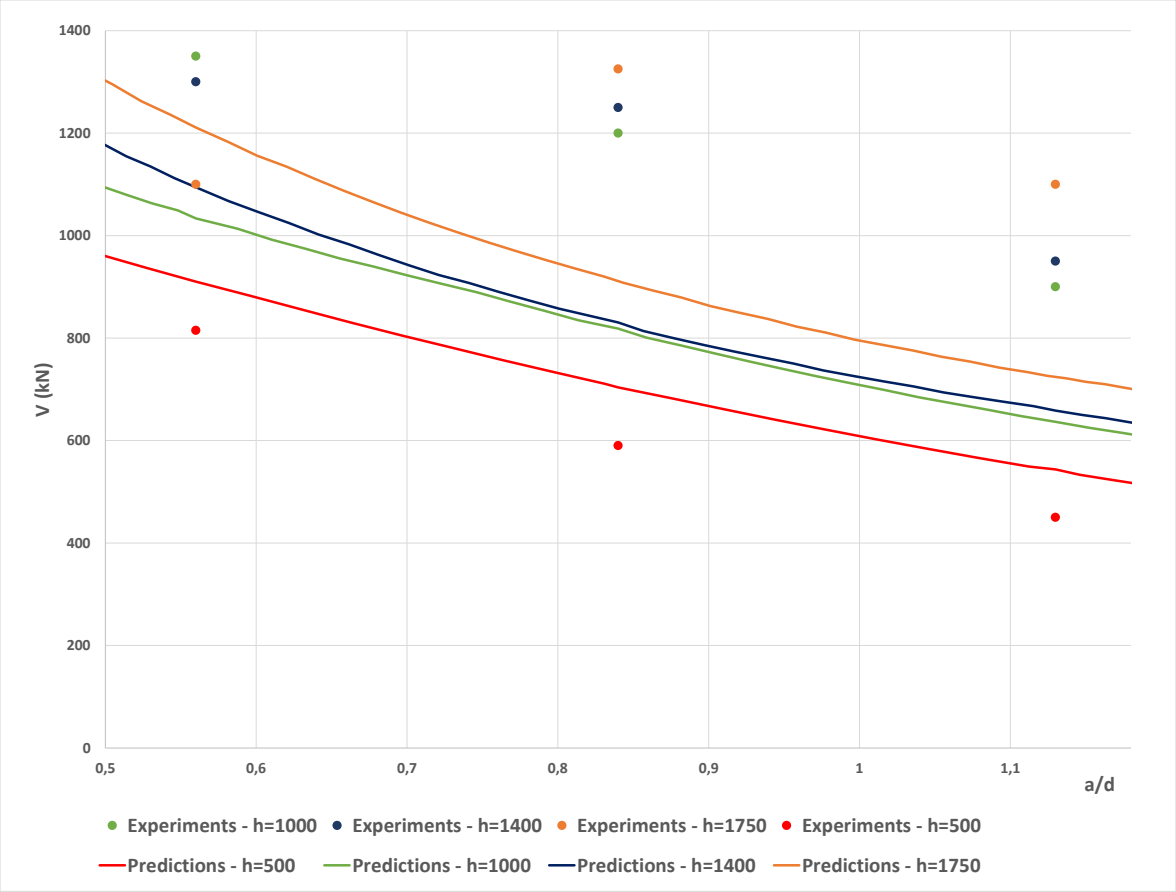

Figure 4.3 – Comparison experiments/predictions of the original 2PKT for tests by Tan et al. (1999)

Similar calculations were performed with all 12 beams tested by Tan et al. (1999) and the results are shown in Fig. 4.3. On the horizontal axis is the main variable in the tests, namely the ratio between the yield force of the prestressed reinforcement to that of the total flexural reinforcement. The predicted shear strengths are plotted with continuous lines while the measured strengths are presented with discrete points. It can be seen that the results predicted by the original 2PKT are inaccurate. All the predictions are conservative except for beams of 500mm height. The trend of the prediction curve seems to follow the experiments. However, the predictions are too low compared to the experimental failure loads. For specimen 4P-1750/0,50 that has a height of 1750 mm and an a/d ratio of 0.56, a bearing failure occurred. For that reason, this specimen has an

experimental failure load that is already under the prediction curve. This specimen will be therefore excluded from the analysis.

Surprisingly, it is also shown that the height of the specimens does not influence a lot the prediction curve. Indeed, the prediction curves for specimens of height 1000mm and 1400mm are nearly one on top of the other. This result is due to the fact that the shear strength is mainly governed by the shear resisted by the critical loading zone. However, as the length of the loading plates are the same for all specimens, and as the concrete compressive strength is relatively constant, there are not significant differences in the shear resisted by the critical loading zone for different height of specimens. The small increase of the shear strength for higher specimens that is shown in Fig. 4.3 comes from the increase of interlocking with the height of the beam.

Finally, Table 4.1 presents the experimental results and corresponding predictions for the tests by Tan et al. (1999). As shown at the bottom of the table, the average value of the ratio between the experimental results and the predictions equals 1.23 and the coefficient of variation is equal to 22,2%. These values show that the model should be improved.

Beam Name	**V exp. (kN)**	**V by flexure (kN)**	**V by 2PKT (kN)**	**V by bearing failure (kN)**	**V pred. (kN)**	**V exp./V pred.**
1P-500/0,50	815	1248	963	1631	963	0,84
1P-500/0,75	590	816	702	1495	702	0,84
1P-500/1,00	450	597	514	1376	514	0,87
2P-1000/0,50	1350	2606	1093	1523	1093	1,23
2P-1000/0,75	1200	1737	823	1421	823	1,45
2P-1000/1,00	900	1237	595	1253	595	1,51
3P-1400/0,50	1300	3381	1067	1218	1067	1,21
3P-1400/0,75	1250	2234	798	1173	798	1,56
3P-1400/1,00	950	1765	693	1383	693	1,37
4P-1750/0,50	1100	4293	1187	1330	1187	0,92
4P-1750/0,75	1325	2875	899	1341	899	1,47
4P-1750/1,00	1100	2224	746	1432	746	1,47
					Average	**1,23**
					Coefficient of variation	**22,2%**

Table 4.1 – Summary of predictions of the original 2PKT for tests by Tan et al. (1999)

4.1.2 Tests by Tan and Mansur (1992)

As mentioned in chapter 2, Tan and Mansur (1992) conducted a study on 8 pretensioned deep beams. The goal of their experiment was to study the effect of partial prestressing on the strength of deep beams. The specimens were divided into two groups based on their shear-span-to-effective-depth ratio (a/d = 1.5 or 2). In each group, the degree of prestress was varied from one specimen to another. Figure 4.4 shows the predictions of the original 2PKT model compared to the experimental results.

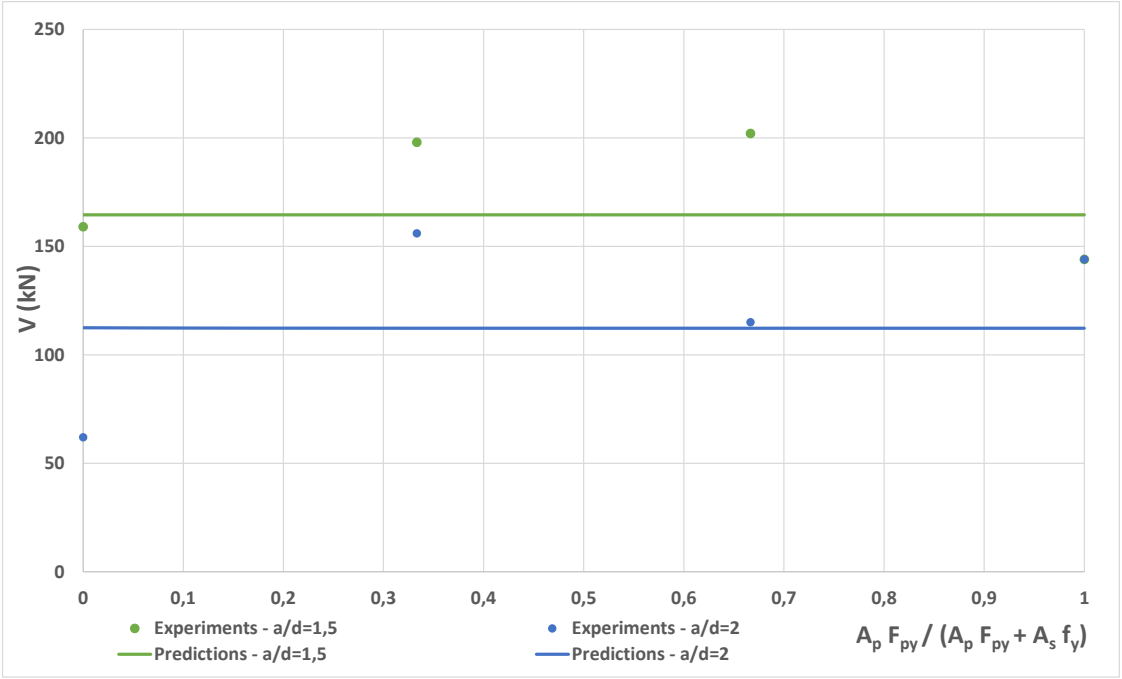

Figure 4.4 – Comparison experiments/predictions of the original 2PKT for tests by Tan and Mansur (1992)

It can be seen that the results predicted by the original 2PKT are reasonable. For beams having a/d ratio of 1.5 the predictions are conservative except for the first beam which was not prestressed. This observation is also repeated for the second group where the a/d ratio equals 2. This result seems surprising because the 2PKT was developed for non-prestressed beams. It should also be noted that the experimental results show a very significant scatter, which accounts in part for the unconservative predictions obtained for the non-prestressed beam with a/d of 2.0.

Finally, Table 4.2 summarizes the experimental results and corresponding predictions for the tests by Tan and Mansur (1992). As shown at the bottom of the table, the average value of the ratio between the experimental results and the predictions is equal to 1.09 which is already a reasonable value. The coefficient of variation equals 16,8%.

Beam Name	**V exp. (kN)**	**V by flexure (kN)**	**V by 2PKT (kN)**	**V by bearing failure (kN)**	**V pred. (kN)**	**V exp./V pred.**
S13	159	179,6	168,7	412	168,7	0,94
S23	198	184,0	172,2	502	172,2	1,15
S33	202	188,8	185,2	439	185,2	1,09
S43	144	188,8	119,9	229	119,9	1,20
S14	62	127,1	84,3	229	84,3	0,74
S24	156	136,9	113,3	524	113,3	1,38
S34	115	136,9	112,5	391	112,5	1,02
S44	144	139,6	116,1	412	116,1	1,24
					Average	**1,09**
					Coefficient of variation	**16,8%**

Table 4.2 – Summary of predictions of the original 2PKT for tests by Tan and Mansur (1992)

4.1.3 Tests by Teng, Kong and Poh (1998)

Teng, Kong and Poh (1998) tested 15 prestressed deep beams with straight tendons. The objective of their experiment was to study the effect of curved tendons on deep beams. However, the specimens tested differ from several parameters. Therefore, for this test series it is really complicated to show clear experiments/predictions curves for all specimens. The ratio experiment/predictions was therefore studied for each specimen. However, Fig. 4.5 shows comparison between experiments and predictions for some similar specimens:

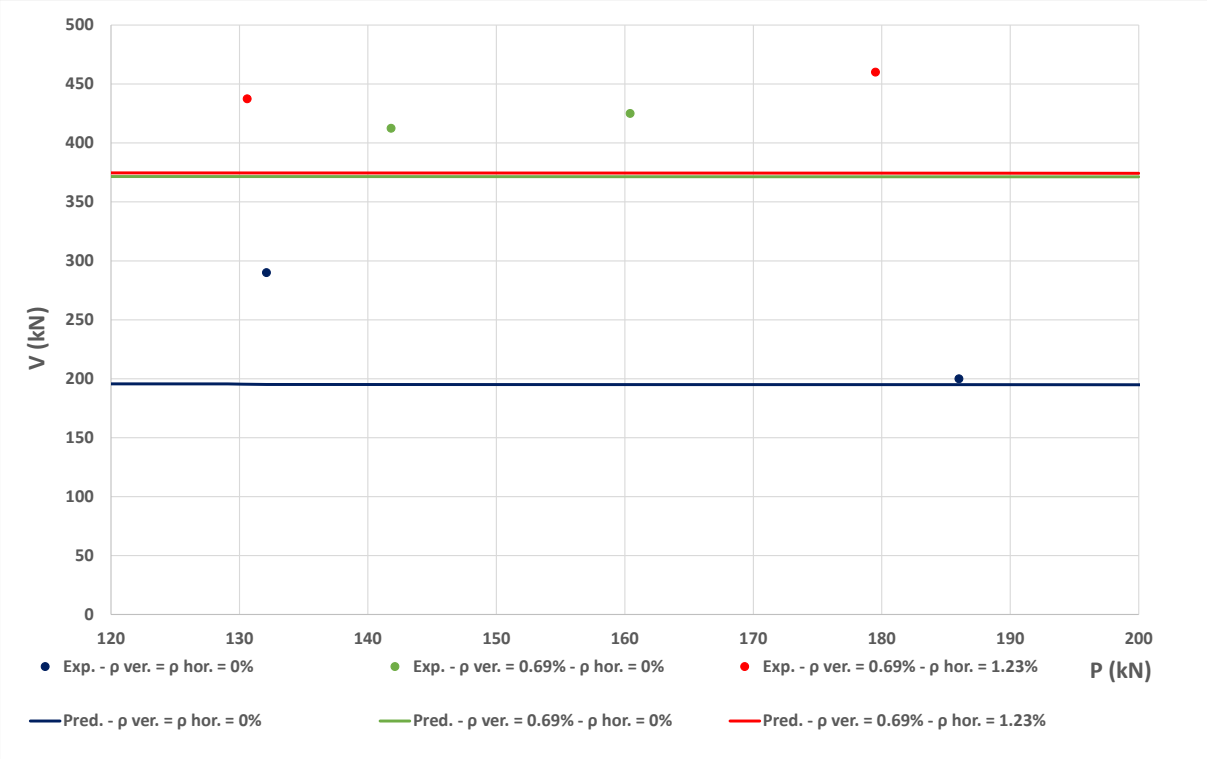

Figure 4.5 – Comparison experiments/predictions of the original 2PKT for tests by Teng, Kong and Poh (1998)

It can be seen again based on these plots that the original 2PKT does not take into account the prestressing. All the predictions are conservative for this test. However, the predictions are far from the experimental results except for one specimen. It can also be seen that the model does not take into account the presence of horizontal web reinforcement.

The other specimens that are not represented in Fig. 4.5 are quiet different from each other. For that reason, the ratio between the experimental failure force and the predicted failure force was studied for each specimen thanks to Fig. 4.6. It can be seen that the ratios between the experimental results and the predictions range between 1 and 2. The predictions should be increased to improve the results.

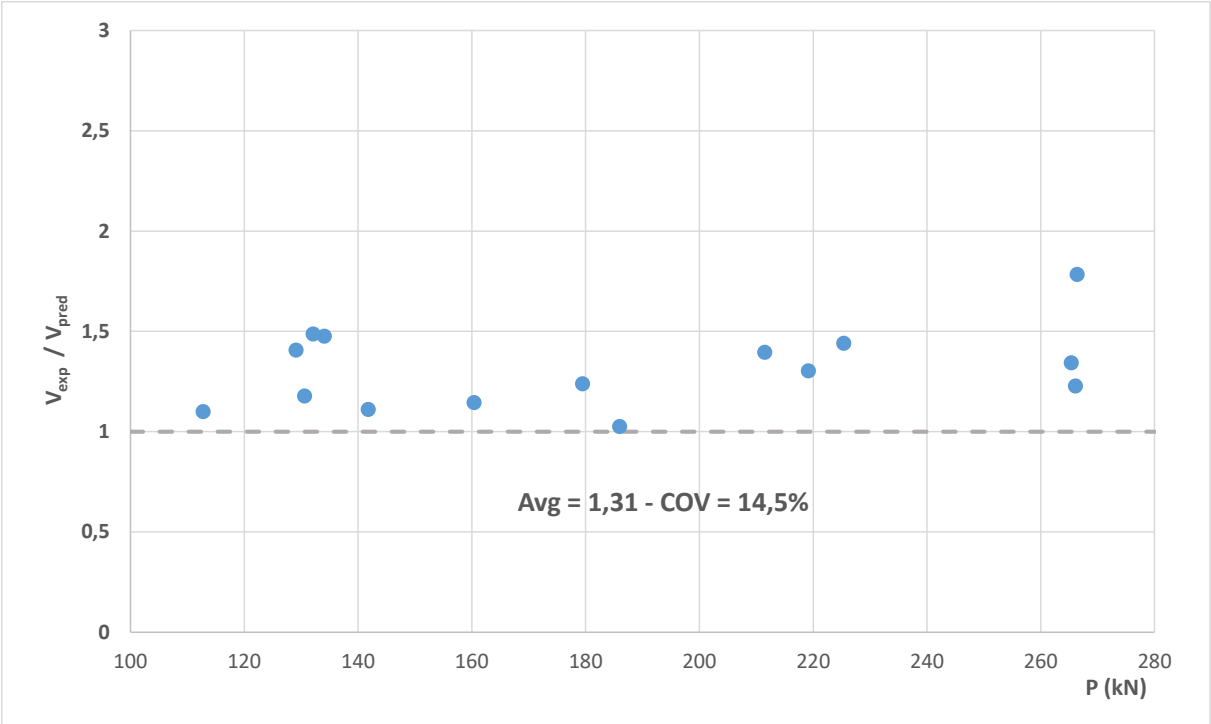

Figure 4.6 – Experiment/predictions ratios of the original 2PKT for tests by Teng, Kong and Poh (1998)

Finally, Table 4.3 summarizes the different shear strengths and predictions for all the specimens in this test. The average value of the ratio between the experimental results and the predictions equals 1.31 and the coefficient of variation equals 14.4 %. These values show again that the model could be improved.

Beam Name	V exp. (kN)	V by flexure (kN)	V by 2PKT (kN)	V by bearing failure (kN)	V pred. (kN)	V exp./V pred.
P-1c	275	397	196	432	196	1,40
P-1a	290	466	196	432	196	1,48
P-1b	200	464	195	431	195	1,02
P-2a	413	451	371	431	371	1,11
P-2b	425	444	371	431	371	1,14
P-3a	438	481	372	432	372	1,17
P-3b	460	481	371	431	371	1,23
P-1b(2)	214	362	195	480	195	1,09
P-1c(2)	288	288	195	481	195	1,47
P-1-1,5-WO	370	420	208	520	208	1,78
P-1-1,5-WV	438	420	326	521	326	1,34
P-1-1,5-WVH	400	444	326	522	326	1,22
P-1-1,0-WO	418	631	320	518	320	1,30
P-1-1,0-WV	538	631	385	519	385	1,39
P-1-1,0-WVH	560	667	389	519	389	1,43
					Average	**1,31**
					Coefficient of variation	**14,4%**

Table 4.3 – Summary of predictions of the original 2PKT for tests by Teng, Kong and Poh. (1998)

4.1.4 Tests by Simionopoulos (1998)

In order to compare the new general shear design method developed at the University of Toronto (1998) with the traditional ACI shear design procedures, eight deep beams prestressed with straight tendons were tested under one-point loading. The specimens were separated into four groups based on their height h=125, 250, 500, 1000mm. In each height group, one beam was tested with the tendon in the centre of the section while another beam was provided with an eccentric tendon. The smallest specimens (h=125mm) are excluded from our analysis due to a lack of information. Figure 4.7 shows the predictions of the original 2PKT model compared to the experimental results.

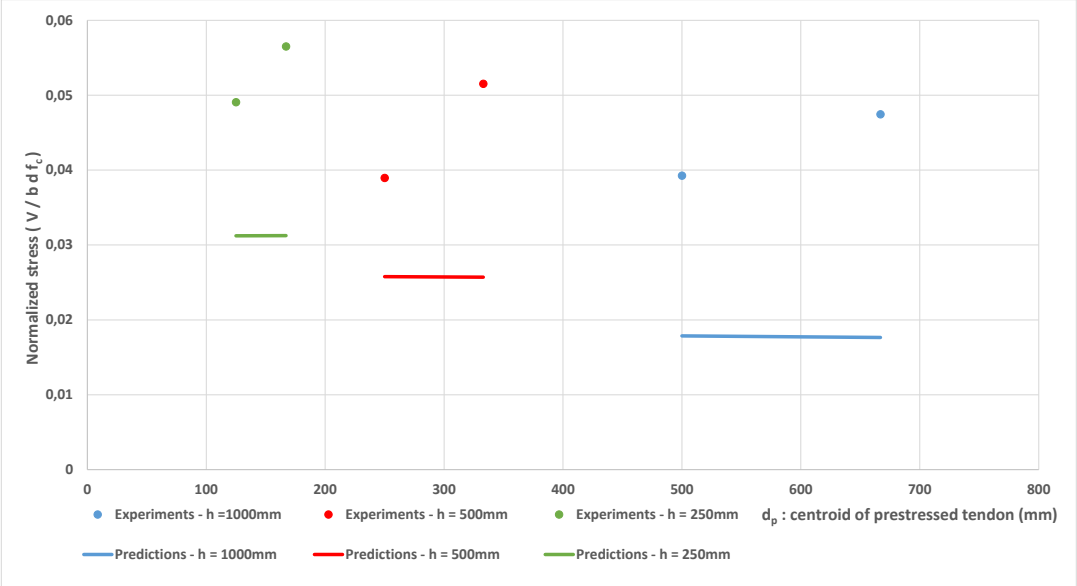

Figure 4.7 – Comparison experiments/predictions of the original 2PKT for tests by Simionopoulos (1998)

It can be seen based on these plots that the position of the tendon does not have an influence on the predictions of the model while the experiment shows that deeper tendons increase the shear strength. However, the size effect is well presented by the predictions. Indeed, the normalized failure stress tend to decrease when the height of the section is increased.

Table 4.4 summarizes the different shear strengths and predictions for all specimens in this test. The average value of the ratio between the experimental results and the predictions equals 1.93 and the coefficient of variation equals 20.4 %. Compared to previous tests, these results are inaccurate. The main reason for these values is that the specimens have a/d ratio of 2.9 and they are out of the range of deep beams. However, as they behaved like a tied arch, they are still studied in our analysis.

Beam Name	V exp. (kN)	V by 2PKT (kN)	V by bearing failure (kN)	V pred. (kN)	V exp./V pred.
BP100	464	211	959	211	2,19
BP100E	561	209	959	209	2,68
BP50	224	148	959	148	1,51
BP50E	299	149	968	149	2,00
BP25	142,4	90,6	387	90,6	1,57
BP25E	164	90,7	387	90,7	1,80
				Average	**1,93**
				Coefficient of variation	**20,4%**

Table 4.4 – Summary of predictions of the original 2PKT for Tests by Simionopoulos (1998)

4.2. Modifications to the 2PKT

As evident from the results presented in Section 4.1, the original 2PKT requires certain modifications to take into account the effects of prestressing. This section describes the modifications which concern three different aspects: the shear force obtained from flexural equilibrium, the geometry of the CLZ and the dowel action contribution of the prestressing reinforcement.

4.2.1 Shear force from flexural equilibrium

The first modification on the existing model concerns the shear force obtained from flexural equilibrium. So far, the shear force from flexural equilibrium was calculated from Eq. 3.21 which does not account for the prestrain applied to the prestressing tendons in the section. Indeed, when no external loads act on the member, there is still a significant tension force in the tendon. Therefore, the contribution to shear force of the prestressed and non-prestressed reinforcement should be separated as follows:

$$V = \frac{E_s\, \varepsilon_{t,avg}\ A_s\, (0.9\, d_s)}{a} + \frac{E_p\, A_p\, (\varepsilon_{t,avg} + \Delta\varepsilon_p)\, (0.9\, d_p)}{a} \tag{4.6}$$

where d_p and d_s are respectively the effective depths of prestressed and non-prestressed reinforcement and $\Delta\varepsilon_p$ is the prestrain applied to the tendon (i.e. the difference between the strain in the tendon and the strain in the surrounding concrete).

Figure 4.8 illustrates the contribution to the shear force of both prestressed and non-prestressed reinforcement. The shear force from flexural equilibrium (blue line) corresponds to the sum of the contribution of both contributions. Therefore, as the intersection of the shear force from flexural equilibrium and the total strength of the beam is at a higher location, the effect of prestressing on the shear derived from flexural equilibrium increase the ultimate shear strength. However, as the total strength curve (green curve) is quite flat, the increase of the shear strength is relatively low. In particular, for beams where the amount of non-prestressed reinforcement is much bigger than the amount of prestressed reinforcement, the effect of prestressing on the shear derived from flexural equilibrium tend to be insignificant.

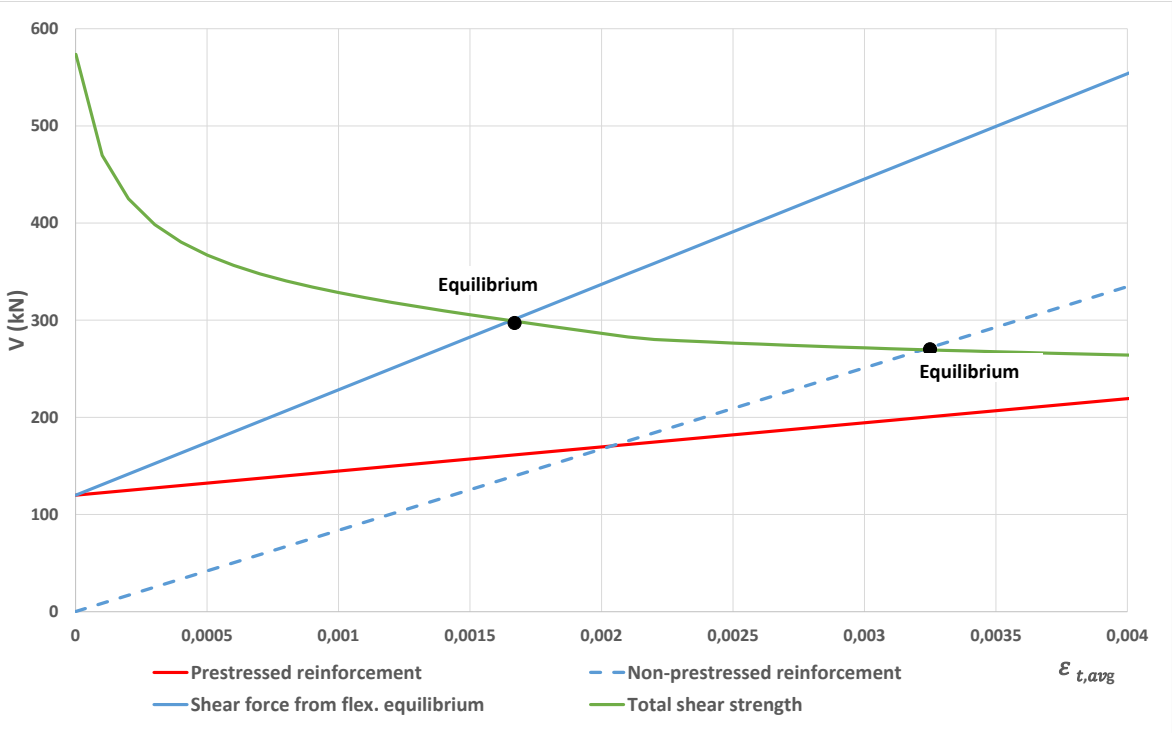

Figure 4.8 – Effect of prestressing on the shear derived from flexural equilibrium

4.2.2 Geometry of CLZ

As mentioned before, the critical loading zone is a key component of the 2PKT because it typically represents the mechanism that carries the biggest portion of the shear force. It is expected, based on the intermediate results presented in Section 4.1, that the prestressing force on the member should influence the geometry of the CLZ and therefore its strength. Also, it can be supposed that the size of the CLZ depends on the depth of the flexural compression zone. The deeper is the compression zone, the larger is the critical loading zone. Therefore, as a first step, it is needed to express the depth of the compression zone x as a function of DOF $\varepsilon_{t,avg}$.

The depth of the compression zone is derived based on assumptions illustrated in Fig. 4.9 for a rectangular section with both prestressed and non-prestressed reinforcement. To derive the formula for the depth of the compression zone, the strain distribution along the height of section is needed. Based on Eq. 3.1, it is known that the strain remains constant along the height of the section and equals $\varepsilon_{t,avg}$. However, in order to be able to derive an expression for the depth of the compression zone, a linear distribution of the strain is supposed from the position of the tendon to the top of the section, while under the prestressing tendon the strain is assumed to be constant and equal to $\varepsilon_{t,avg}$. In addition, it is assumed that both the bottom reinforcement and the concrete in the compression zone are in the linear elastic range. This will allow for the derivation of a closed-form expression for x.

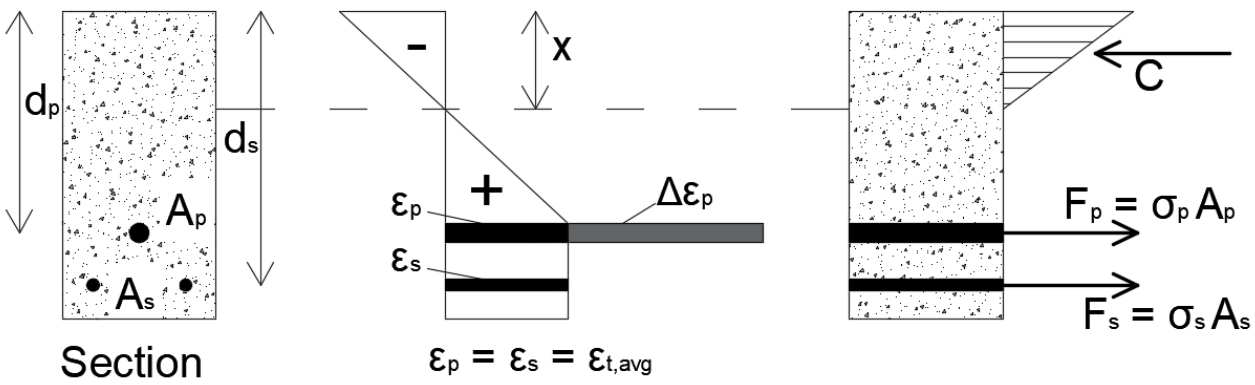

Figure 4.9 – Strain distribution supposed to derive the depth of compression zone

Based on this strain distribution, the strain in the top of the section is given by:

$$\varepsilon_{top} = \frac{-\varepsilon_p}{(-1 + \frac{1}{x}\, d_p)} \tag{4.7}$$

Then, assuming a linear elastic behaviour, the stresses in the reinforcements and the concrete can be expressed as follows:

$$\sigma_{top} = \varepsilon_{top}\, E_c \tag{4.8}$$

$$\sigma_p = E_p(\varepsilon_p + \Delta\varepsilon_p) \tag{4.9}$$

$$\sigma_s = E_s\, \varepsilon_s \tag{4.10}$$

where $\varepsilon_p = \varepsilon_s = \varepsilon_{t,avg}$. The forces acting on the section are then given from:

$$C = \frac{\sigma_{top} x\, b}{2} \tag{4.11}$$

$$F_p = \sigma_p\, A_p \tag{4.12}$$

$$F_s = \sigma_s\, A_s \tag{4.13}$$

To ensure horizontal equilibrium, the following equation must be satisfied:

$$\sum F_x = 0 \rightarrow C + F_p + F_s = 0 \tag{4.14}$$

Replacing the three terms in the right hand side of the equation above, one obtains:

$$\frac{\sigma_{top}\, x\, b}{2} + \sigma_p\, A_p + \sigma_s\, A_s = 0 \tag{4.15}$$

After rearranging the different terms, a quadratic equation for x is obtained:

$$\frac{-\,\varepsilon_{t,avg}\, E_c\, b\, x^2}{2} - x\left(\sigma_p\, A_p + \sigma_s\, A_s\right) + \left(\sigma_p\, A_p + \sigma_s\, A_s\right) d_p = 0 \tag{4.16}$$

This equation has two solutions as follows:

$$x = \frac{\left(\sigma_p A_p + \sigma_s A_s\right) \pm \sqrt{\left(\sigma_p A_p + \sigma_s A_s\right)^2 + 2\,\varepsilon_{t,avg}\,E_c\,b\left(\sigma_p A_p + \sigma_s A_s\right) d_p}}{-\,\varepsilon_{t,avg}\,E_c\,b} \qquad (4.17)$$

The solution with the positive sign does not have physical meaning because it gives negative values for the depth of compression zone. Therefore, the required solution is obtained by using the negative sign in Eq. (4.17).

Now that the depth of the compression zone is derived, the geometry of the critical loading zone should be expressed as a function of it. The geometry of this critical zone is given by two parameters α and l_{b1e} that represent the angle of the critical diagonal crack and the effective width of the loading plate, respectively. As the angle α is computed from the geometry of the specimens, the parameter that has to be determined is only l_{b1e}. So far, this parameter depended only on the width of the loading plate and the maximum aggregate size as shown in Eq. 3.12. To link the effective width of the loading plate to the depth of the compression zone, the crack patterns of collected specimens were studied. Based on this study, three different methods were identified and tested. Figure 4.10 illustrates the new geometry of the critical loading zone as well as the relation between the effective width of the loading plate and the depth of the compression zone for each method.

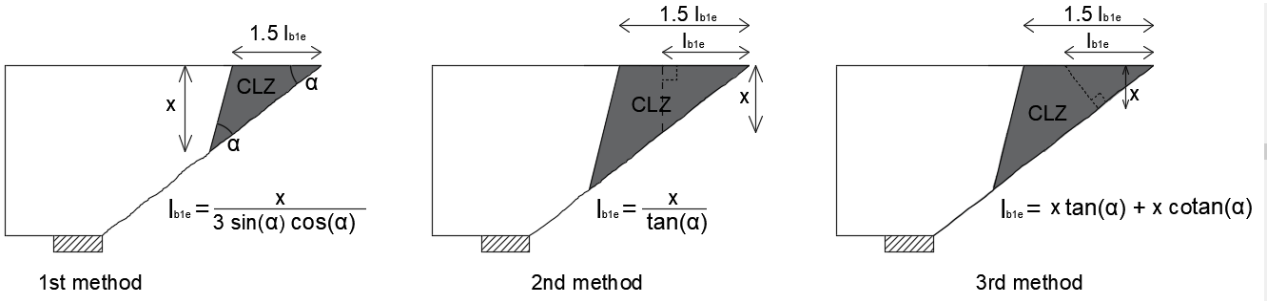

Figure 4.10 – Tested methods to establish the link between the depth of the compression zone x and the effective width of the loading plate l_{b1e}.

Among these three methods, the first one produced the best results when it was implemented in the 2PKT and the shear strength predictions were compared with experimental results. The main assumption of this method is that the critical diagonal crack extends above the flexural crack as shown in Fig. 4.11 that represents the crack pattern of one specimen (specimen BP100E) from the tests by Simionopoulos (1998).

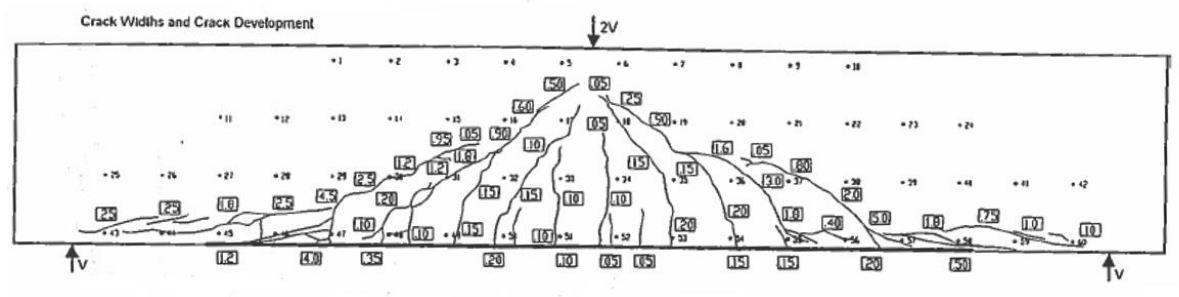

Figure 4.11 – Crack pattern of specimen BP100E from tests by Simionopoulos (1998).

Mihaylov et al. (2013) showed in the original 2PKT that the length of the critical loading zone along the critical diagonal crack is $3l_{b1e}\cos\alpha$ (Fig. 4.12). Based on this result, the horizontal length at which the depth of the compression zone is reached is $3l_{b1e}\cos^2\alpha$. Therefore, the effective width of the loading plate can be expressed from:

$$tan\,\alpha = \frac{x}{3l_{b1e}\,cos^2\,\alpha} \rightarrow\ l_{b1e} = \frac{x}{3\,tan\,\alpha\,cos^2\,\alpha} = \frac{x}{3\,sin\,\alpha\,cos\,\alpha} \tag{4.18}$$

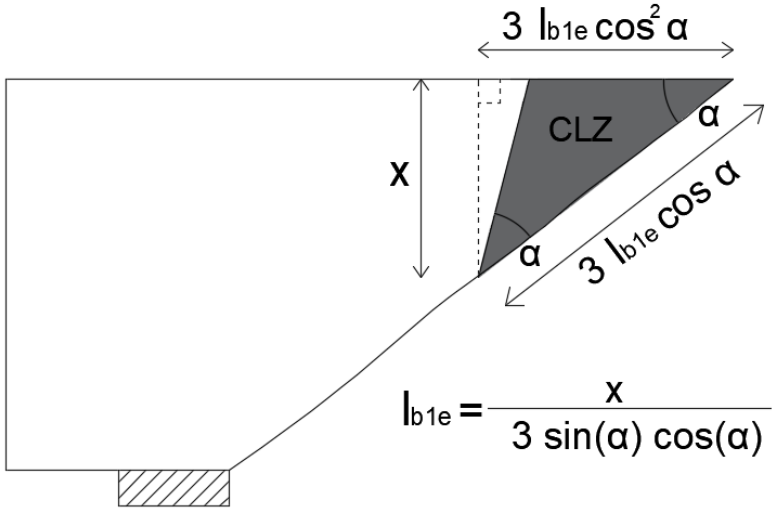

Figure 4.12 – Proposed geometry of the critical loading zone in prestressed beams

Finally, it is also clear that the effective width of the loading plate should be at least equal to the real width of the loading plate. For that reason, the final expression for the effective width is given by:

$$l_{b1e} = max\left\{\frac{x}{3\,sin\,\alpha\,cos\,\alpha};\ \frac{V}{P}l_{b1}\right\} \tag{4.19}$$

After these modifications of the effective width, the shear strength of the critical loading zone becomes also a function of the depth of the compression x, and therefore of the strain $\varepsilon_{t,avg}$ in the bottom reinforcement. Moreover, now that the effective width is a function of the strain in the bottom reinforcement, the vertical shear displacement of the critical loading zone Δ_c becomes also a function of the strain $\varepsilon_{t,avg}$. In the original model, this displacement was computed as a constant value depending only on the width of the loading plate.

4.2.3 Dowel action contribution of prestressing reinforcement

Finally, the last modification on the model is to add the contribution of the prestressing reinforcement to the shear carried by dowel action. The shear carried by dowel action of the prestressing reinforcement is then expressed as follows:

$$V_d\ =\ n_b f_{ye}\frac{d_b^3}{3l_k} \tag{4.20}$$

where n_b represents the number of prestressing bars and where the effective yielding stress is computed from:

$$f_{ye} = f_y\left[1 - \left(\frac{T}{f_y A_s}\right)^2\right] \tag{4.21}$$

The tension force in the prestressing tendon is calculated with the tension stiffening effect as follow:

$$T = E_p A_p\left(\varepsilon_{t,avg} + \Delta\varepsilon_p\right) \tag{4.22}$$

4.3 Validation of the modified 2PKT

4.3.1 Tests by Tan et al. (1999)

The solution of the extended 2PKT equations is shown graphically in Fig. 4.13.

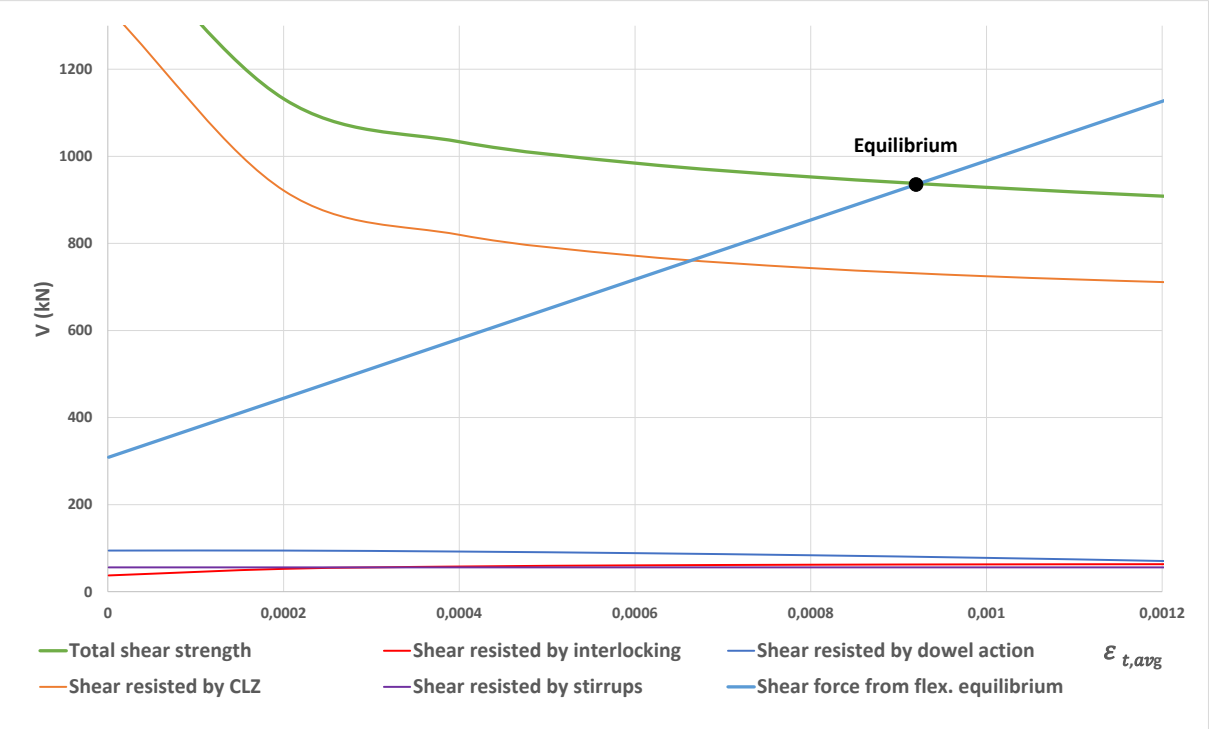

Figure 4.13 - Contribution to shear strength of the different shear mechanisms for specimen 3P-1400/1.0 from tests by Tan et al. (1999)

For beam 3P-1400/1.0, the predicted shear strength is 939 kN while the experimentally obtained value is 950 kN. This results in a shear-strength experimental-to-predicted ratio of 1.01. Flexural and bearing failures were not governing as they corresponded to higher shear forces (1765 kN and 1383 kN, respectively). Again, the shear resisted by the critical loading zone governs the total shear strength. However, compared to Fig. 4.2 where the solutions of the original 2PKT were shown, it is important to note that the shear strength provided by the critical loading zone is now dependent on the strain in the bottom reinforcement and decreases with the increase of the strain. This result is due to the fact that the size of CLZ is now dependent on the depth of the compression zone (Eq. 4.19) which is itself dependent on the strain in the bottom reinforcement (Eq. 4.17)

Moreover, the shear strength provided by the CLZ increased significantly compared to the original model. At failure, the shear resisted by the different shear mechanisms for the original and the extended model are compared in Table 4.5. It can be seen that the contribution of the critical loading zone increased thanks to the modification of its geometry with the effect of prestressing. However, based on the results, it can be seen that the strength given by interlocking reduces in the extended 2PKT. This is due to the fact that the shear displacement Δ_c of the critical loading zone increases because it is now a function of the strain in the bottom reinforcement. Therefore, as the crack width w depends on the displacement of the critical loading zone, it increases as well and the interlocking is reduced.

	Original 2PKT	Extended 2PKT
Critical loading zone	67%	77%
Aggregate interlock	13%	7%
Stirrups	8%	6%
Dowel action	12%	9%

Table 4.5 - Contribution to the shear strength at failure of the different mechanism for the original and extended 2PKT for specimen 3P-1400/1.00 from Tan et al. (1999)

The predictions of the extended two-parameter-kinematic-theory are presented from Fig. 4.14 to 4.17.

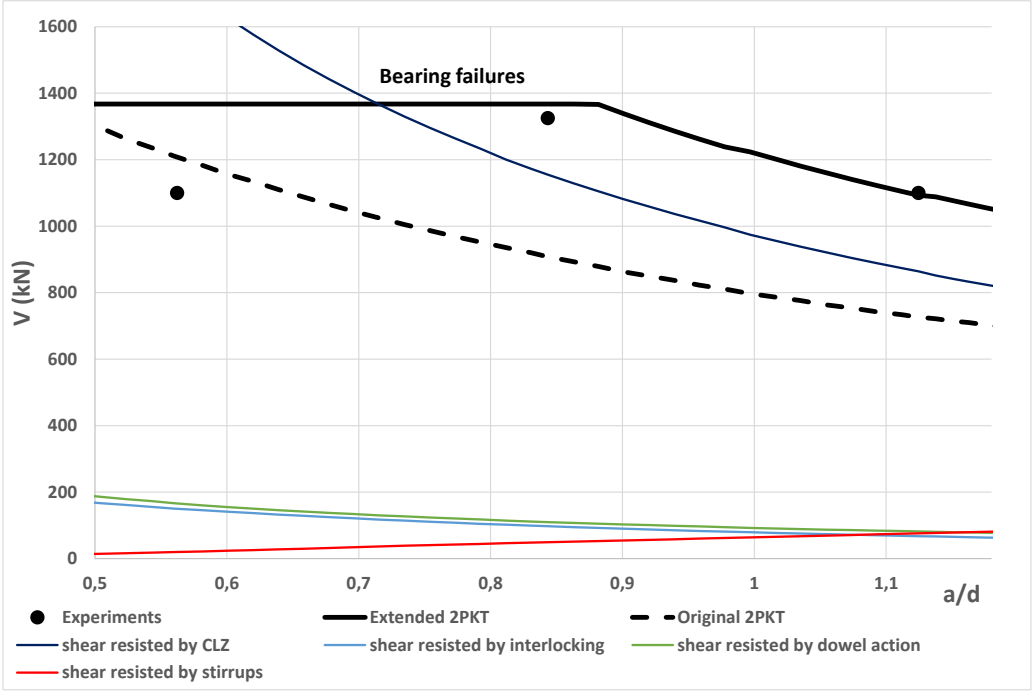

Figure 4.14 – Comparison experiments/predictions of the extended 2PKT for specimens of h= 1750mm from Tan et al. (1999)

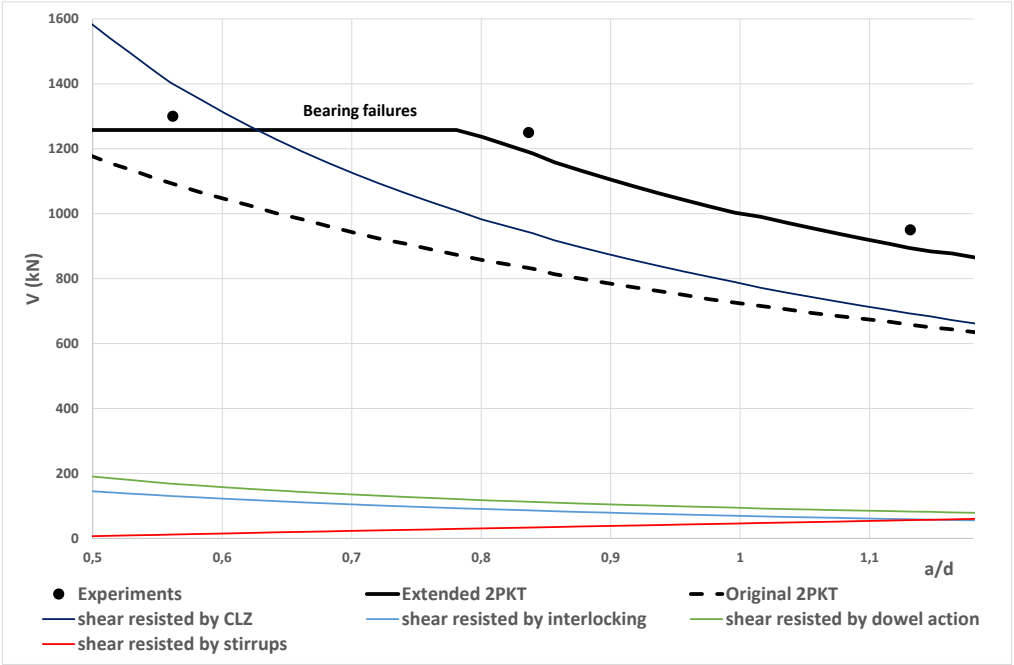

Figure 4.15 – Comparison experiments/predictions of the extended 2PKT for specimens of h= 1400mm from Tan et al. (1999)

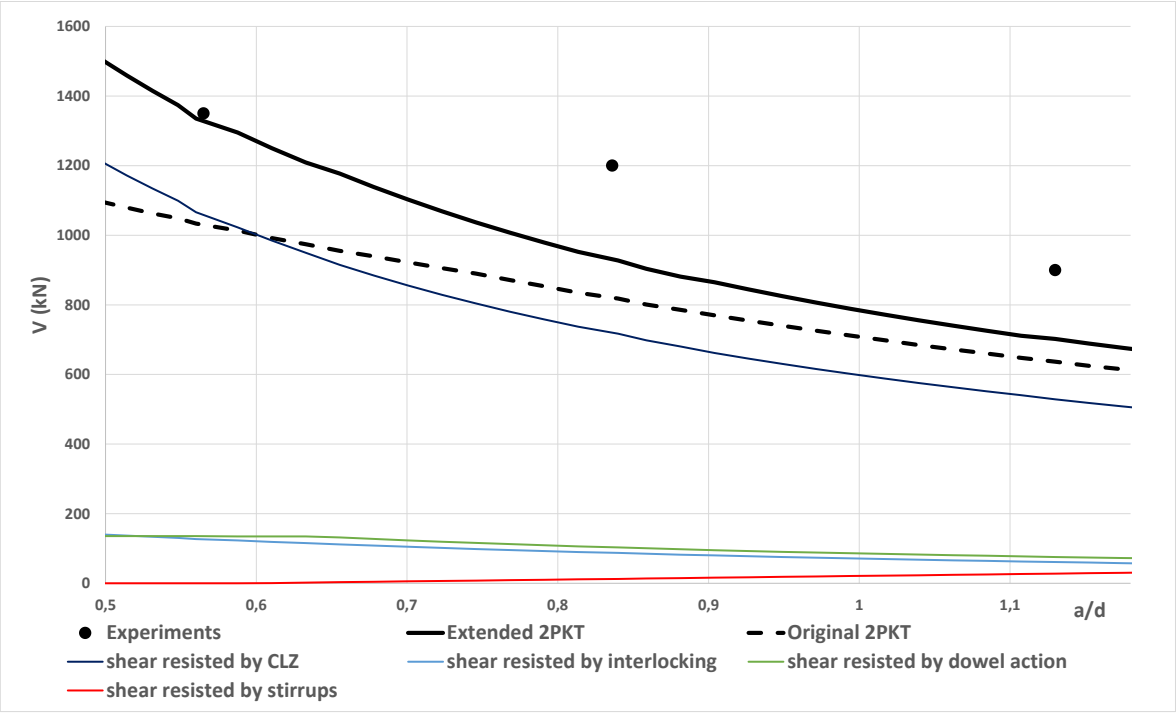

Figure 4.16 – Comparison experiments/predictions of the extended 2PKT for specimens of h= 1000mm from Tan et al. (1999)

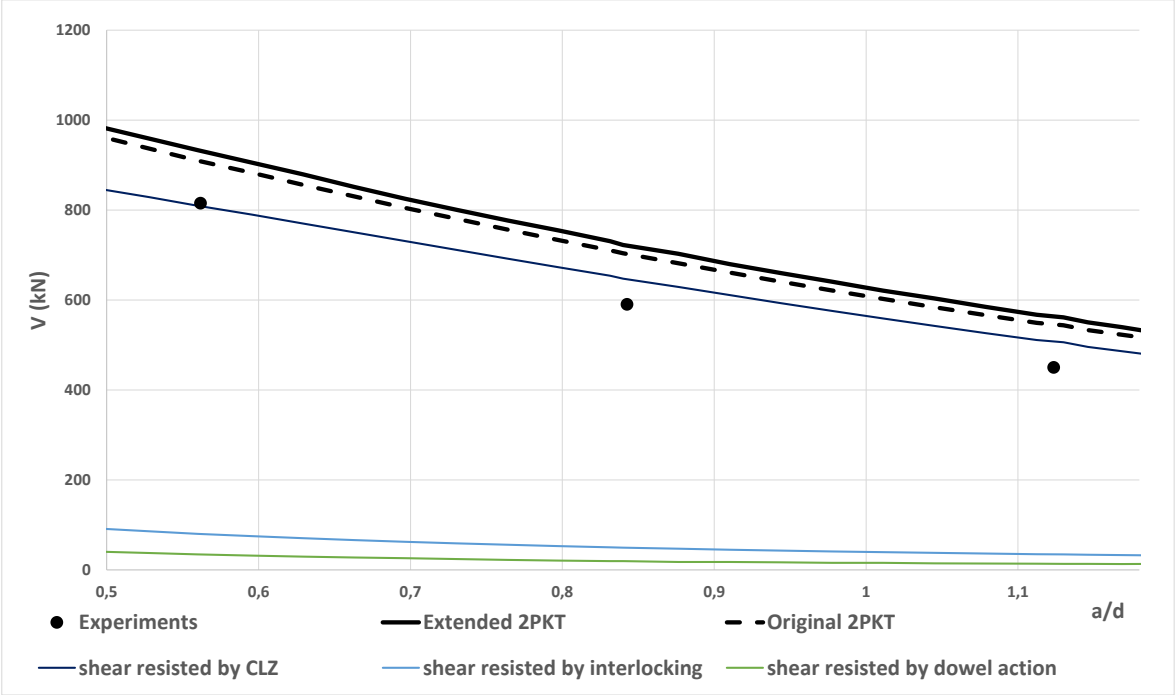

Figure 4.17 – Comparison experiments/predictions of the extended 2PKT for specimens of h= 500mm from Tan et al. (1999)

The predictions of the extended model are plotted with continuous and thick black lines while the predictions of the original model are shown with thick dashed lines. Thin and coloured lines correspond to the shear strength provided by the different shear mechanisms. Finally, the results of the experiments are plotted with discrete black points. It can be seen from the figures above that the extended model improves considerably the predictions.

For the specimens with a depth of 1750 mm, the new model is very close to the experiment except for the specimen that has a/d ratio of 0.56 for which a bearing failure occurred. For a shear span to effective depth ratio between 0.5 and 0.88, the model predicted some bearing failures. These failures are the reason for the flat parts of the curves.

For specimens of 1400 mm height, the model is very accurate across the entire range of a/d ratios. The prediction curve follows really well the trend given by the experimental results. Compared to the original 2PKT, the predictions are increased considerably.

For specimens of 1000 mm height, the prediction curve follows relatively well the experiments and the predictions are increased compared to the original model. However, for the experimental points at a/d equal to 0.83 and 1.13, the experimental shear strengths are still about 30% higher than the predicted values.

Finally, for the smaller specimens of 500 mm height where web-crushing failures occurred, the original model was already predicting non-conservative results. The extended model ranges just a little higher than the previous results and the trend of the predictions is still reasonable because it follows well the trend of the experiments.

Figure 4.18 shows the effect of the height h and of the shear-span-to-depth ratio a/h on the nominal predicted shear stress at failure. As it was the case for the experiments (Fig. 2.4), a pronounced size effect is observed. For a given a/h ratio, a significant decrease in the nominal shear stress can be seen with increasing heights. However, this decrease tend to reduce beyond a certain critical height that is comprised between 1400 and 1750mm. The size effect seems to be less dependent on the a/h ratio. It can be seen that a loss in the nominal shear stress occurs when the shear span is increased and the height is kept constant. However, this effect is mainly evident for smaller specimens (h=500 and 1000mm). Indeed, for bigger specimens, the size effect do not depend on the a/h ratio. These observations can be repeated for the experimental results as shown in Fig. 2.4. It can be concluded then that the extended 2PKT captures well the size effect. Moreover, as the size effect is mainly due to the interlocking, it is important to note that the critical crack width is therefore adequately estimated by the extended model.

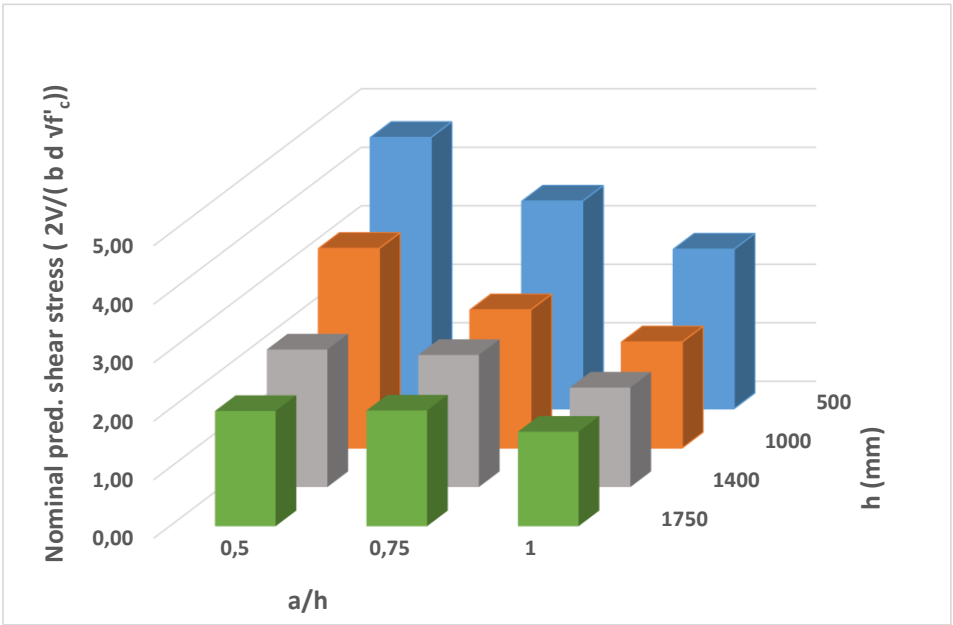

Figure 4.18 – Variation of predicted nominal shear stress with h and a/h for the tests by Tan et al. (1999)

Table 4.6 summarizes the results for the test by Tan et al. (1999). An average value for the ratio between the experimental results and the predictions of 1.0 is obtained and the coefficient of variation equals 16.6%. These values show again that the predictions are adequate. It should be kept in mind that deep beams exhibit a significant scatter in the experimental data, and for this reason the coefficient of variation cannot be improved very significantly. Compared to the original 2PKT, these values are however significantly improved.

Beam Name	V exp. (kN)	V pred. by original 2PKT (kN)	V pred. by extended 2PKT (kN)	V exp./V pred. by original 2PKT	V exp./V pred. by extended 2PKT
1P-500/0,50	815	963	985	0,84	0,82
1P-500/0,75	590	702	722	0,84	0,81
1P-500/1,00	450	514	532	0,87	0,84
2P-1000/0,50	1350	1093	1392	1,23	0,97
2P-1000/0,75	1200	823	931	1,45	1,28
2P-1000/1,00	900	595	670	1,51	1,34
3P-1400/0,50	1300	1067	1703	1,21	1,06
3P-1400/0,75	1250	798	1148	1,56	1,08
3P-1400/1,00	950	693	939	1,37	1,01
4P-1750/0,50	1100	1187	2046	0,92	0,82
4P-1750/0,75	1325	899	1401	1,47	0,98
4P-1750/1,00	1100	746	1131	1,47	0,97
			Average	**1,23**	**1,00**
			Coefficient of variation	**22,2%**	**16,5%**

Table 4.6 – Summary of predictions of original and extended 2PKT for tests by Tan et al. (1999)

Finally, Fig. 4.19 compares the results of the extended 2PKT and of the original 2PKT in terms of the ratio between experimental and predicted shear strengths. It can be seen that the extended 2PKT significantly improves the results compared to the original model. The average ratio is closer to 1 and the variation of the results is reduced.

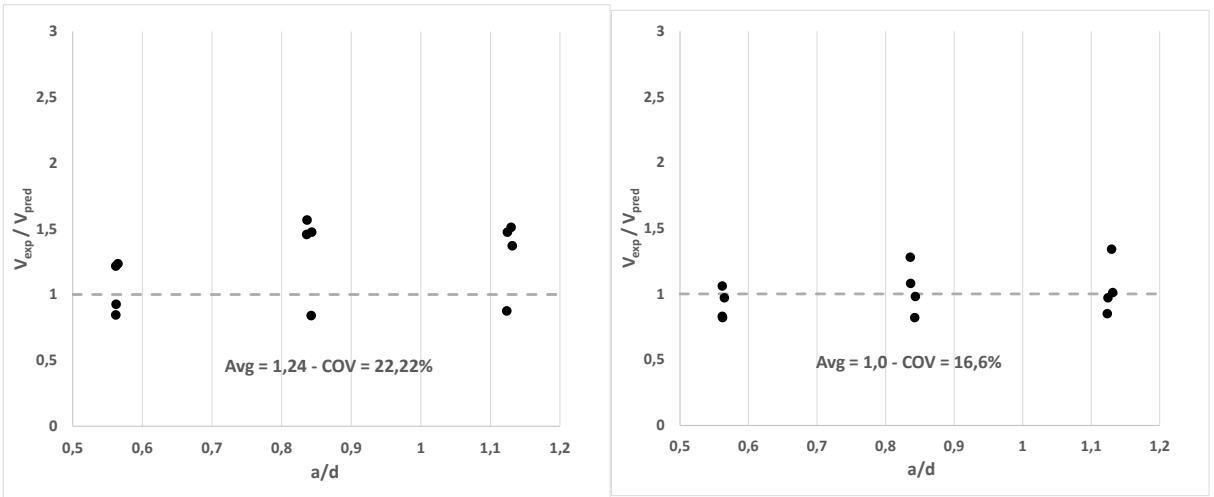

(a) (b)

Figure 4.19 – Comparison between (a) original and (b) extended 2PKT for tests by Tan el al. (1999)

4.3.2 Tests by Tan and Mansur (1992)

The predictions of the extended two-parameter kinematic theory for the tests conducted by Tan and Mansur (1992) are presented in Fig. 4.20:

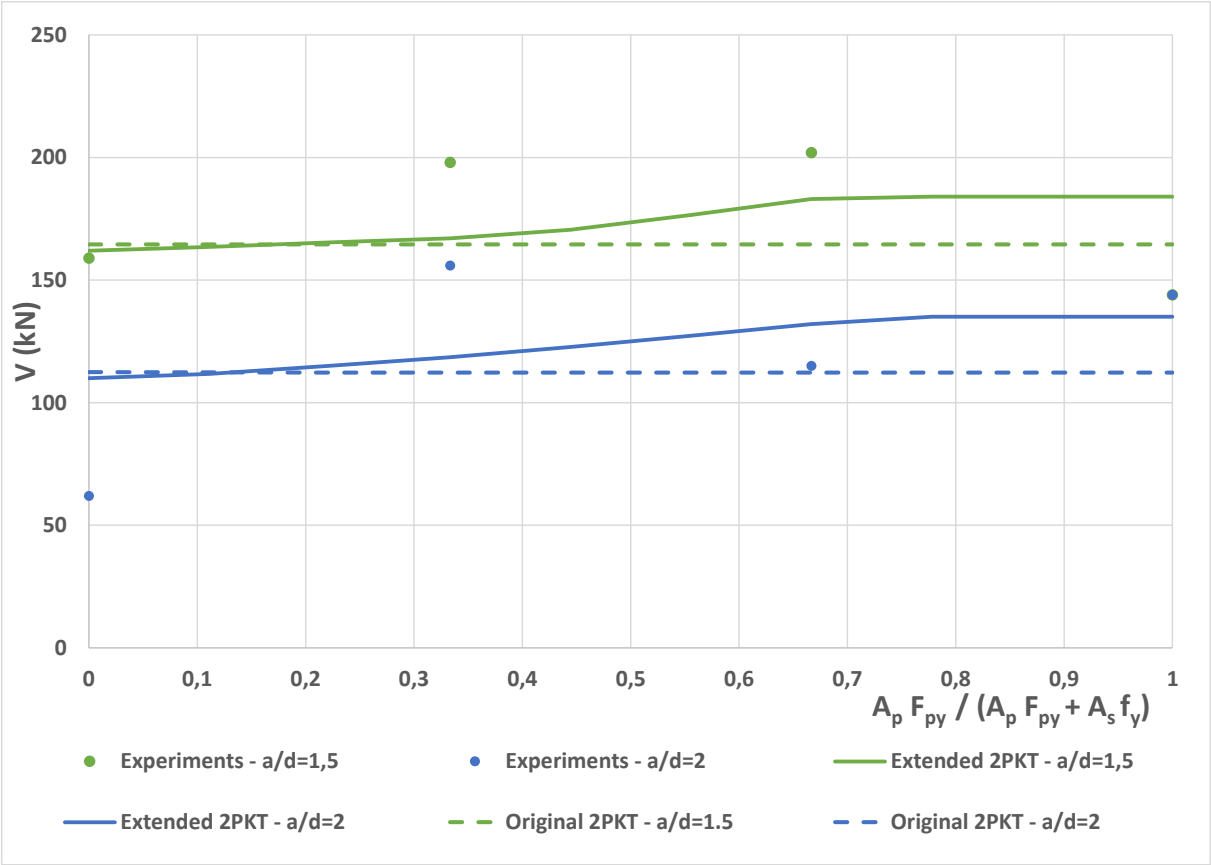

Figure 4.20 – Comparison experiments/predictions of the extended 2PKT for Tan and Mansur (1992)

The predictions of the extended model are plotted in continuous lines while the predictions of the original model are shown with dashed lines. The results of the experiments are plotted with discrete points.

For specimens having a/d ratio of 1.5, the shear strength predicted by the original 2PKT equals 164kN and is the same for all the specimens. This result is due to the fact that all the specimens having a shear span to depth ratio of 1.5 have the same geometry. Therefore, the only difference between those specimens is the amount of prestressed bars. However, as the original model does not take into account the prestressing, there are no differences in the shear strengths predicted. In the extended model, the effect of prestressing is taken into account. The failure is predicted to be by shear for a partial prestressing ratio less 0.65. Then, the flexural failure that occurs at 184kN is predicted by the extended 2PKT. It can be seen for these specimens (a/d=1.5) that the prediction curve (in green continuous lines) follows the experiments. Compared to the original 2PKT, the predictions are nearly all increased and they get closer to the experiments.

The same observations can be repeated for the second batch of specimens where the shear span to effective depth ratio was kept at 2. The predictions are increased with the extended model.

At failure, the shear resisted by the different shear mechanism for the original and the extended model are compared in Table 4.7. It can be seen that there are nearly no differences between both theory for the contribution percentage to the shear strength.

	Original 2PKT	Extended 2PKT
Critical loading zone	66%	65%
Aggregate interlock	34%	35%
Stirrups	0%	0%
Dowel action	0%	0%

Table 4.7 - Contribution to the shear strength at failure of the different mechanism for the original and extended 2PKT for specimen S33 from Tan and Mansur (1992)

Table 4.8 summarizes the different shear strengths and predictions for all the specimens in this test. An average value for the ratio between the experimental results and the predictions of 1.01 is obtained and the coefficient of variation equals 16.8%. Compared to the original 2PKT, these values are significantly improved.

Beam Name	V exp. (kN)	V pred. by original 2PKT (kN)	V pred. by extended 2PKT (kN)	V exp./V pred. by extended 2PKT	V exp./V pred. by original 2PKT
S13	159	168,7	166,0	0,95	0,94
S23	198	172,2	174,2	1,13	1,15
S33	202	174,8	183,8	1,09	1,09
S43	144	119,9	153,3	0,93	1,20
S14	62	84,3	84,1	0,73	0,73
S24	156	113,3	116,8	1,33	1,37
S34	115	112,5	132,2	0,87	1,02
S44	144	116,1	139,6	1,03	1,24
			Average	**1.01**	**1.09**
			Coefficient of variation	**16.8%**	**16.8%**

Table 4.8 – Summary of predictions of original and extended 2PKT for tests by Tan and Mansur (1992)

Finally, Fig. 4.21 compares the results of the extended 2PKT and of the original 2PKT in terms of the ratio between experimental and predicted shear strengths. It can be seen that the extended 2PKT improves the results compared to the original model. However, the difference is not significant as the predictions of the original model were already reasonable.

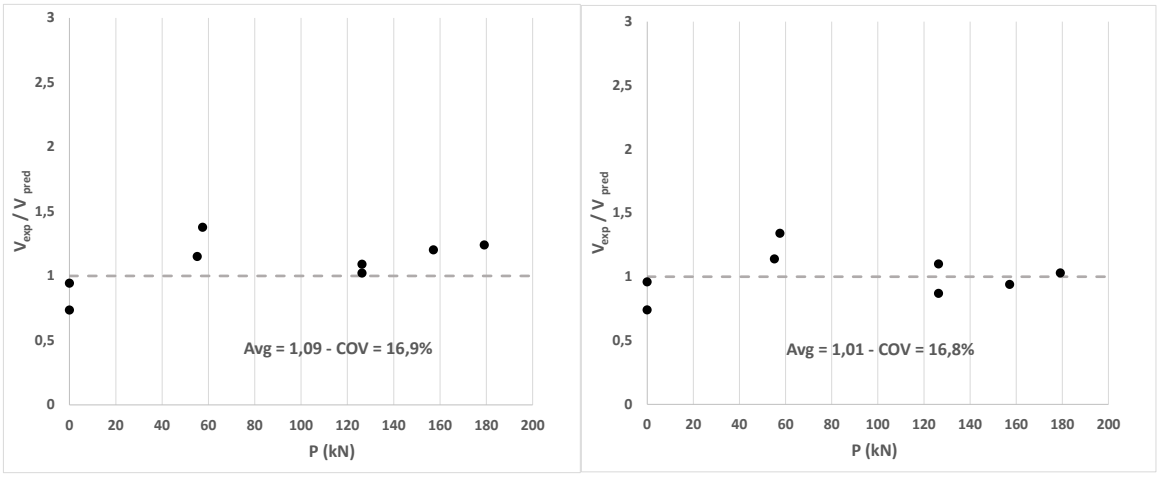

(a) (b)

Figure 4.21 – Comparison between (a) original and (b) extended 2PKT for tests by Tan and Mansur (1992)

4.3.3 Tests by Teng, Kong and Poh (1998)

Some predictions of the extended two-parameter kinematic theory for the tests conducted by Teng, Kong and Poh (1998) are presented in Fig. 4.22:

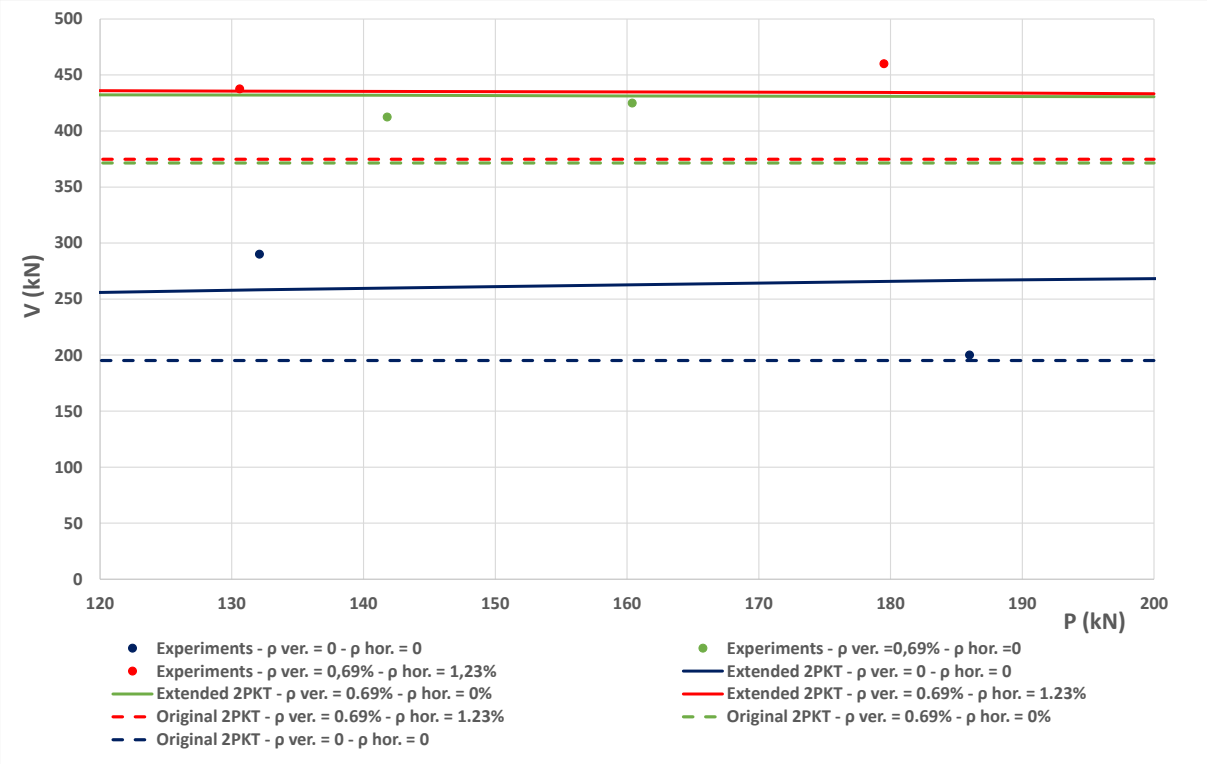

Figure 4.22 – Comparison experiments/predictions of the extended 2PKT for tests by Teng, Kong and Poh (1998)

It can be seen that the extended model improves the predictions and is closer to the experimental values. It also seems that the prestressing force does not show a significant influence on the predictions as well as the experiments. Indeed, for the specimens provided with vertical and/or horizontal web reinforcement, for a difference of 50kN in the prestressing force, the difference on the ultimate shear strength is not significant for both the predictions and the experiments. This observation is mainly due to the fact that the prestrain $\Delta\varepsilon_p$ applied to the tendon shows very small differences in the depth of the compression zone. Therefore, the shear resisted by the critical loading zone remains almost the same.

For the specimens that are not provided with vertical and horizontal web reinforcement, it can be seen that for an increase in the prestressing force, the strength measured experimentally decreases. This result is surprising because the prestressing should normally increase the failure strength, the decrease of strength for this specimen may be due to an experimental mistake or lack of precision. The ratios between the experimental failure force and the predicted failure force for each specimen are presented in Fig. 4.23. It can be seen that the predictions are closer to the experiments for the extended 2PKT. Moreover, a smaller dispersion of the results occurred compared to the original model.

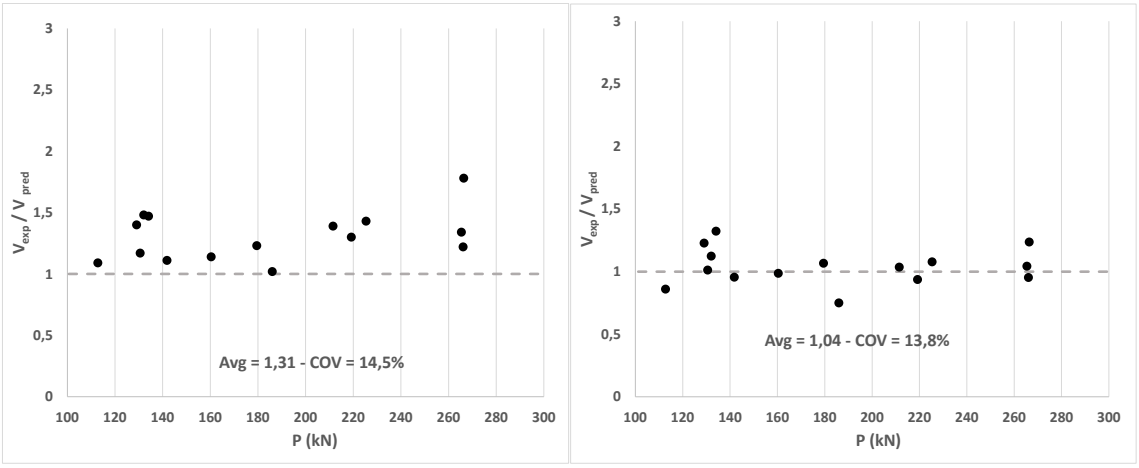

(a) (b)

Figure 4.23 – Experiment/predictions ratios of (a) the original and (b) extended 2PKT for tests by Teng, Kong and Poh (1998)

At failure, the shear resisted by the different shear mechanism for the original and the extended model are compared in Table 4.9. Even if the contribution of the critical loading zone increases in the extended 2PKT, the contribution of the stirrups governs the total strength.

	Original 2PKT	**Extended 2PKT**
Critical loading zone	28%	38%
Aggregate interlock	16%	11%
Stirrups	56%	51%
Dowel action	0%	0%

Table 4.9 - Contribution to the shear strength at failure of the different mechanism for the original and extended 2PKT for specimen P-2a from Teng, Kong and Poh (1998)

Finally, Table 4.10 summarizes the different shear strengths and predictions for all the specimens in this test. An average value for the ratio between the experimental results and the predictions of 1.04 is obtained and the coefficient of variation equals 13.8%. These values shows again that the predictions are accurate. Compared to the original 2PKT, these values are significantly improved.

Beam Name	**V exp. (kN)**	**V pred. by original 2PKT (kN)**	**V pred. by extended 2PKT (kN)**	**V exp./V pred. by extended 2PKT**	**V exp./V pred. by original 2PKT**
P-1c	275	196,5	224	1,22	1,40
P-1a	290	195,6	258	1,12	1,48
P-1b	200	195,2	267	0,75	1,02
P-2a	413	371	432	0,95	1,11
P-2b	425	371	431	0,98	1,14
P-3a	438	372	433	1,01	1,17
P-3b	460	371	431	1,06	1,23
P-1b(2)	214	195	249	0,85	1,09
P-1c(2)	288	195	218	1,32	1,47
P-1-1,5-WO	370	208	299	1,23	1,78
P-1-1,5-WV	438	326	419	1,04	1,34
P-1-1,5-WVH	400	326	420	0,95	1,22
P-1-1,0-WO	418	320	446	0,93	1,30
P-1-1,0-WV	538	385	519	1,03	1,39
P-1-1,0-WVH	560	389	520	1,07	1,44
			Average	**1,04**	**1,31**
			Coefficient of variation	**13,8%**	**14.5%**

Table 4.10 – Summary of predictions original and extended 2PKT for tests by Teng, Kong and Poh (1998)

4.3.4 Tests by Simionopoulos (1998)

The predictions of the extended two-parameter kinematic theory for the tests conducted by Simionopoulos (1998) are presented in Fig. 4.24:

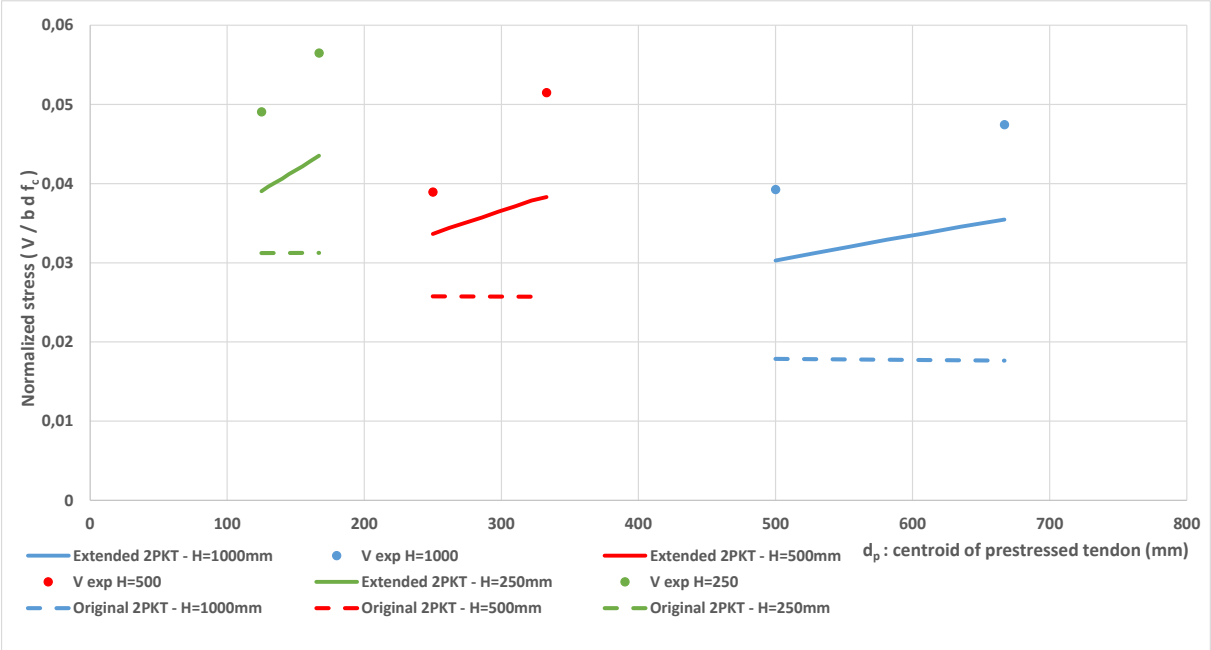

Figure 4.24 – Comparison experiments/predictions of the extended 2PKT for tests by Simionopoulos (1998)

It can be seen from these plots that the extended 2PKT illustrates relatively well the behaviour of these beams. The prediction curves follow the experiments. The position of the tendon in the section affects the ultimate strength. Indeed, the deeper the tendon, the higher the ultimate shear strength. In the original model, however, the position of prestressing strands was not causing significant differences. Moreover, a size effect is also seen based on these plots. A loss in the ultimate strength can be seen for increasing values of the height of the section.

At failure, the shear resisted by the different shear mechanism for the original and the extended model are compared in Table 4.11. It can be seen that the contribution of the critical loading zone increases considerably between both models. Indeed, the contribution of the critical loading zone doubles. Again, the force resisted by interlocking reduces with the extended model because the crack width increases as it is now function of the strain in bottom reinforcement.

	Original 2PKT	**Extended 2PKT**
Critical loading zone	40%	88%
Aggregate interlock	55%	9%
Stirrups	0%	0%
Dowel action	5%	3%

Table 4.11 - Contribution to the shear strength at failure of the different mechanism for the original and extended 2PKT for specimen BP100E from tests by Simionopoulos (1998)

Table 4.12 summarizes the different shear strengths and predictions for all the specimens in this test. As the specimens are not exactly considered deep beams, the results are not as good as the ones for previous test series. However, the results are not uncoherent. An average value for the ratio between the experimental results and the predictions of 1.28 is obtained and the coefficient of variation equals 4.92%. Compared to the original 2PKT, these values are significantly improved.

Beam Name	V exp. (kN)	V pred. by original 2PKT (kN)	V pred. by extended 2PKT (kN)	V exp./V pred. by extended 2PKT	V exp./V pred. by original 2PKT
BP100	464	211	358	1,29	2,20
BP100E	561	209	419	1,33	2,69
BP50	224	148	194	1,15	1,51
BP50E	299	149	222	1,34	2,00
BP25	142,4	91	113	1,25	1,57
BP25E	164	91	126	1,29	1.80
			Average	**1,28**	**1,96**
			Coefficient of variation	**4,92%**	**20,4%**

Table 4.12 – Summary of predictions of original and extended 2PKT for tests by Simionopoulos (1998)

Finally, Figure 4.25 compares the results of the original and extended 2PKT in terms of the ratio between experimental and predicted shear strengths. It can be seen that the predictions of the extended model get closer to the experiments and the dispersion of the results is significantly reduced.

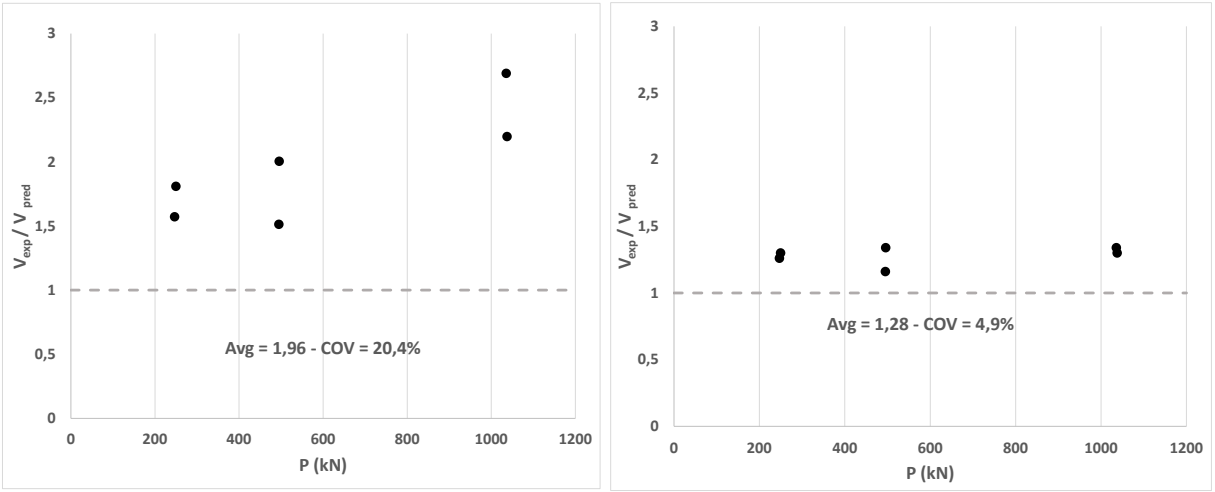

(a) (b)

Figure 4.25 – Comparison between (a) original and (b) extended 2PKT for tests by Simionopoulos (1998)

4.3.5 Global discussion of the results

To conclude with the results of the extended 2PKT, the comparison between the predictions and the experiments was studied only for the beams that failed in shear. For that reason, some specimens were excluded from the analysis for each test series.

For the test series realised by Tan and Mansur (1992), the specimens S23, S33 and S24 failed in flexure. This is why they are excluded from the final analysis.

For the test series conducted by Tan el al. (1999), all the beams that failed in bearing failure were excluded. These beams are 2P-1000-0.5, 3P-1400-0.75 and 4P-1750-0.5.

For the tests conducted by Teng, Kong and Poh (1998), two specimens failed in flexure and they are removed from the final analysis. These specimens are P-2b and P-3a.

Finally, in order to present only the values for prestressed deep beams, the test series conducted at the University of Toronto were not included in the final analysis because the shear-span-to-effective-depth ratio of these beams is not small enough to be considered as deep beams.

The model can therefore be validated for 27 specimens. The results are listed in Table 4.13. The average ratio between the experimental values and the predicted one equals 1.01. The coefficient of variation for this average equals 16.08%. These values are considered adequate for deep beams.

Authors	**Beam Name**	**V exp. (kN)**	**V pred. by original 2PKT (kN)**	**V pred. by extended 2PKT (kN)**	**V exp./V pred. by original 2PKT**	**V exp./V pred. by extended 2PKT**
Tan and Mansur (1992)	S13	159	168,7	166,0	0,94	0,95
	S43	144	119,9	153,3	1,20	0,93
	S14	62	84,3	84,1	0,73	0,73
	S34	115	112,5	132,2	1,02	0,87
	S44	144	116,1	139,6	1,24	1,03
Tan et al. (1999)	1P-500/0,50	815	963	985	0,84	0,82
	1P-500/0,75	590	702	722	0,84	0,81
	1P-500/1,00	450	514	532	0,87	0,84
	2P-1000/0,75	1200	823	931	1,45	1,28
	2P-1000/1,00	900	595	670	1,51	1,34
	3P-1400/0,50	1300	1067	1703	1,21	1,06
	3P-1400/1,00	950	693	939	1,37	1,01
	4P-1750/0,75	1325	899	1401	1,47	0,98
	4P-1750/1,00	1100	746	1131	1,47	0,97
Teng, Kong and Poh (1998)	P-1c	275	196,5	224	1,40	1,22
	P-1a	290	195,6	258	1,48	1,12
	P-1b	200	195,2	267	1,02	0,75
	P-2a	412,5	371	432	1,11	0,95
	P-3b	460	371	431	1,23	1,06
	P-1b(2)	214	195	249	1,09	0,85
	P-1c(2)	287,5	195	218	1,47	1,32
	P-1-1,5-WO	370	208	299	1,78	1,23
	P-1-1,5-WV	437,5	326	419	1,34	1,04
	P-1-1,5-WVH	400	326	420	1,22	0,95
	P-1-1,0-WO	417,5	320	446	1,30	0,93
	P-1-1,0-WV	537,5	385	519	1,39	1,03
	P-1-1,0-WVH	560	389	520	1,44	1,07
				Average	**1.24**	**1,01**
				Coefficient of variation	**20.1%**	**16.1%**

Table 4.13 – Summary of predictions of original and extended 2PKT for all collected specimens failing in shear

5. Finite element modelling (FEM)

This chapter presents the finite element analyses that was carried out for the database. The aim of these analyses is to compare the results predicted by the extended 2PKT model with those from the finite element model. First, the finite element analysis will be presented in terms of the modelling assumptions that were used. Then, for each test series, the results will be presented and compared in terms of the ultimate strength to both the predictions of the extended 2PKT and to the experiments.

5.1 Description of the models and assumptions

As the collected specimens were all known in detail in terms of the geometry, material properties and boundary conditions, they were all modelled accurately in the software. The same assumptions and modelling approaches were used for all specimens. The model for the specimen 4P-1750-1.0 from the tests conducted by Tan et al. (1999) is chosen as an illustration and is presented in Fig. 5.1.

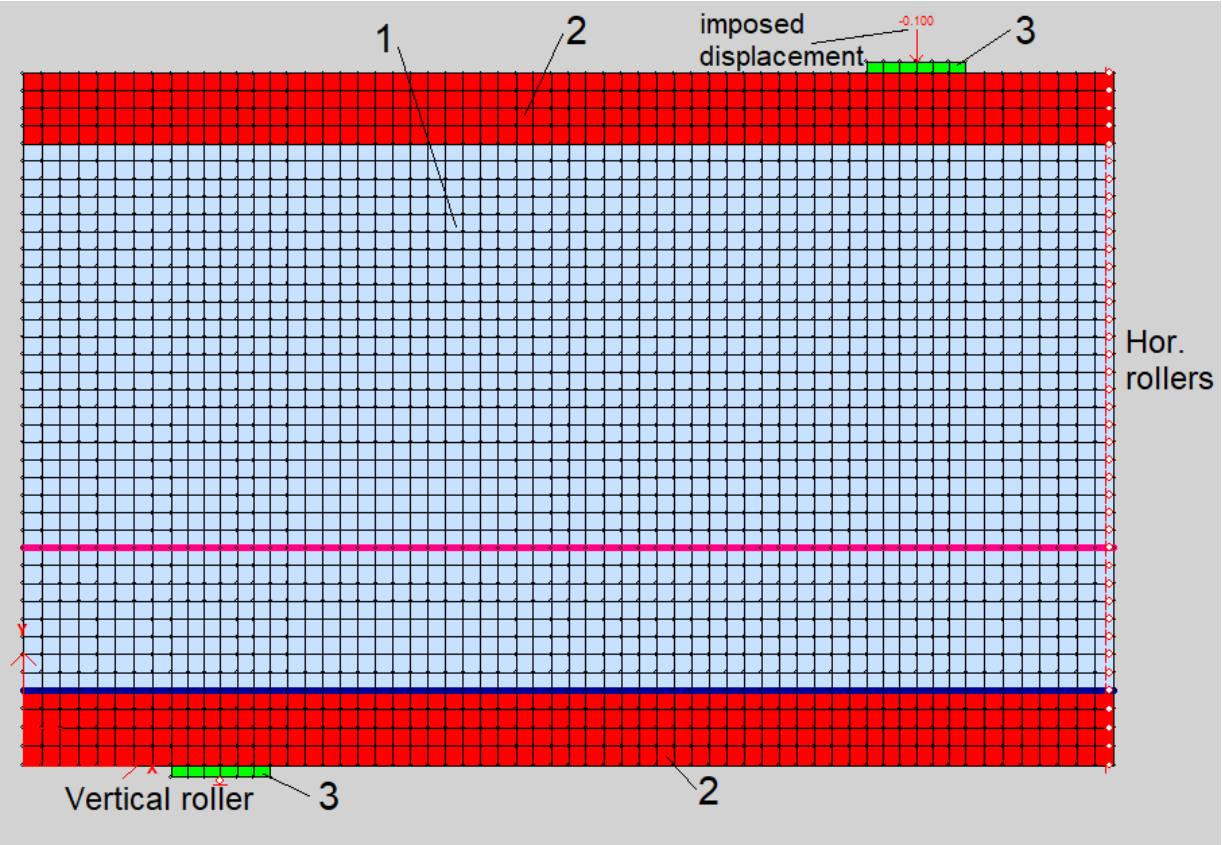

Figure 5.1 - FEM model for specimen 4P-1750-1.0 from tests by Tan et al. (1999)

In order to limit as much as possible the time consumed by the FEM analysis, only one-half was modelled for each specimen since all beams were symmetric. Therefore, this operation reduced the calculation time without any influence on the ultimate shear strength.

It can be seen in Fig. 5.1 that three different materials are used. First, material 1 represents the concrete part of the specimen. Material 2 has the same properties as material 1 except that the latter includes a certain amount of smeared transverse reinforcement while no transverse reinforcement is added in material 1. It is therefore supposed that the top and bottom concrete cover of the beam are not provided with transverse reinforcement. However, while transverse reinforcement was

smeared in the beams, both prestressed and non-prestressed longitudinal reinforcements were modelled as discrete elements as shown in blue and purple in Fig. 5.1. Finally, to model the loading and support plates, material 3 was created and include steel properties.

In terms of support conditions, a vertical roller is used for the support of the beam. Moreover, as only one-half of the beams were modelled, horizontal rollers were added in the axis of symmetry. To get ultimate results at failure, an increasing load was added in the loading zones.

Only linear or rectangular elements were used in the model. The mesh used to model the beam is composed of elements whose size depends on the geometry of the specimens. Indeed, bigger specimens require bigger element size to provide accurate results in a limited time. For that reason, a sensibility analysis was conducted for each specimen and the element size under which no significant difference occur for the failure load was selected.

The compression pre-peak model that was chosen for the concrete is Popovics (NSC) and the post-peak model is Base curve as suggested by VecTor2 users. The rest of the material models were the default options provided in VecTor2 to ensure that the results can be easily reproduced by other researchers.

5.2 Results of finite element modelling

5.2.1 Tests by Tan et al. (1999)

Figure 5.2 shows the crack pattern predicted by finite element modelling and the crack pattern observed in specimen 4P-1750-1.0 from the tests conducted by Tan et al. (1999). Red lines on the picture represents the cracks and wider cracks are represented by thicker lines.

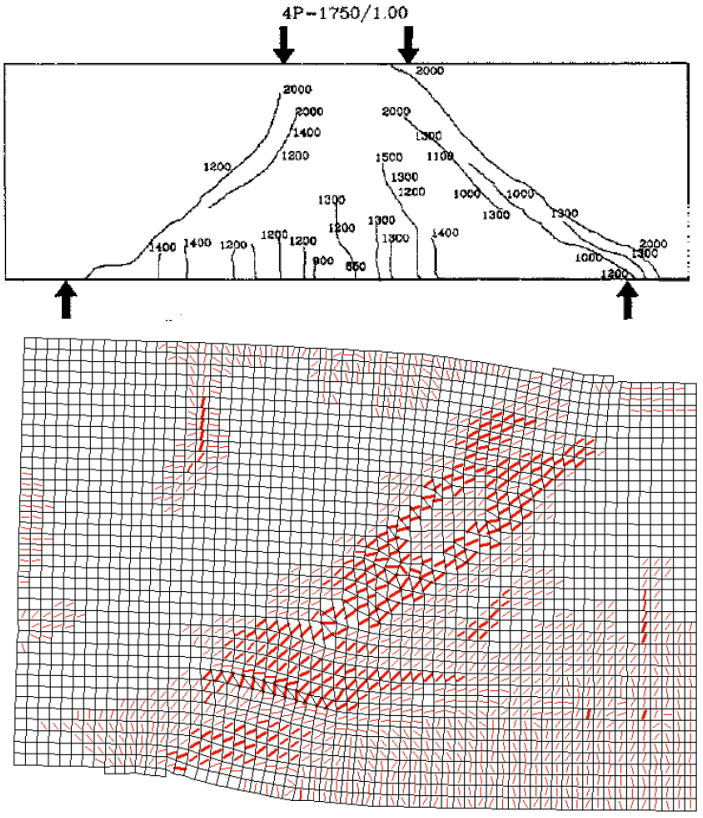

Figure 5.2 – Crack pattern (a) by experiment and (b) by FEM of specimen 4P-1750-1.0

It can be seen that a diagonal shear crack develops in the prediction by FEM. The predicted shear failure modes match well the observed failure mode for most of the beams. For the specimens for which the failure mode does not match with the observed failure mode, some properties of the specimen can be modified to improve the predicted failure mode. However, the modification of the properties lead in general to worst results in terms of ultimate shear strength evaluation. For this reason and to avoid "calibration", even if the predicted failure mode by FEM was not correct, the results of the FEM were taken without any modification of the properties.

Figures 5.3 to 5.6 show the predictions of the finite element modelling and of the extended 2PKT.

It can be seen for the specimens that are 1750 mm high that the predictions of the extended 2PKT are better for all the three experiments. The predictions of the FEM are however close to the extended 2PKT.

For specimens that are 1400 mm high, it can be seen again that the extended 2PKT predictions are closer to the experimental failure strengths except for one specimen where the FEM predicts exactly the failure load.

For the specimens that are 1000 mm high, all the predictions of the extended 2PKT are bigger than the ones of finite element models. Moreover, they are also closer to the experiments.

Finally, for the smaller specimens that are 500mm high, the extended 2PKT predicts higher failure loads again. The experimental failure loads range just between the predictions of both models.

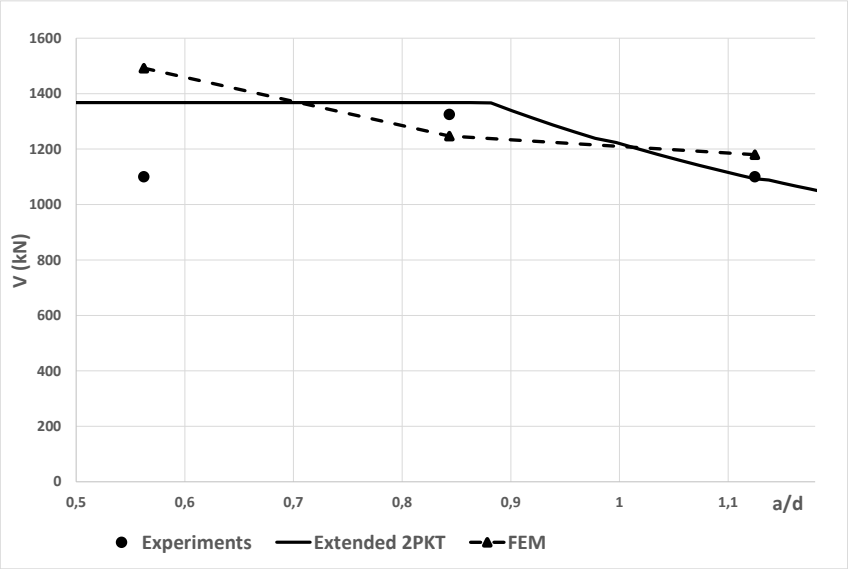

Figure 5.3 – Comparison between FEM and extended 2PKT for h=1750mm for tests by Tan et al. (1999)

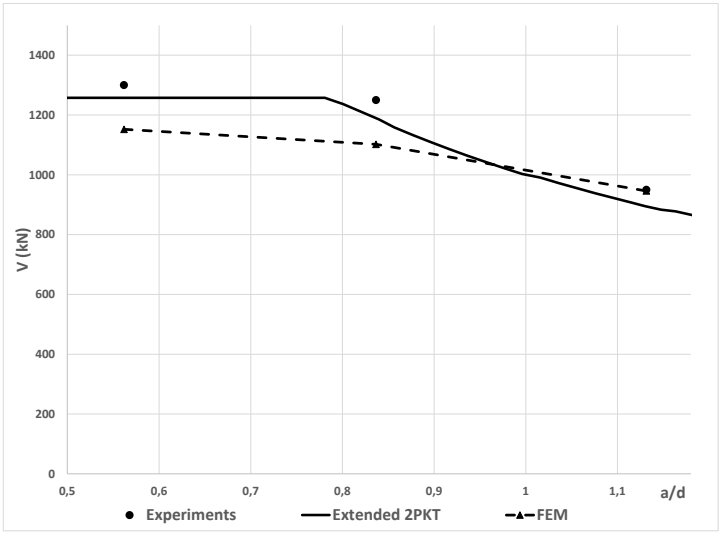

Figure 5.4 – Comparison between FEM and extended 2PKT for h=1400mm for tests by Tan et al. (1999)

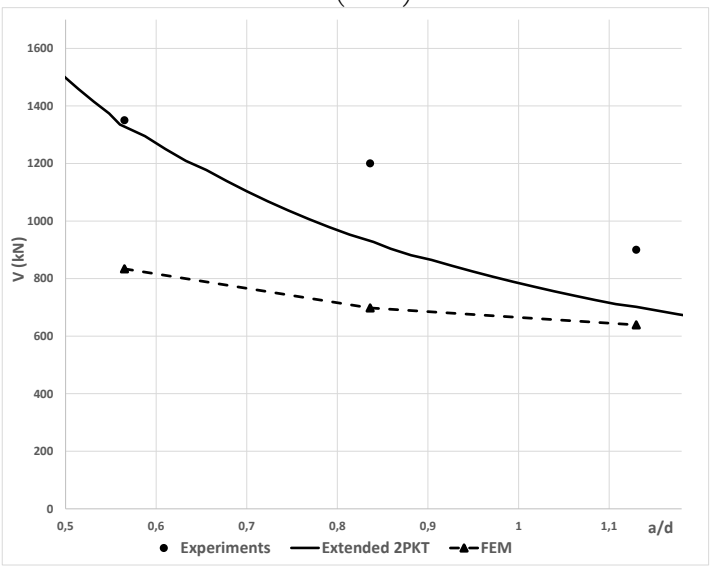

Figure 5.5 – Comparison between FEM and extended 2PKT for h=1000mm for tests by Tan et al. (1999)

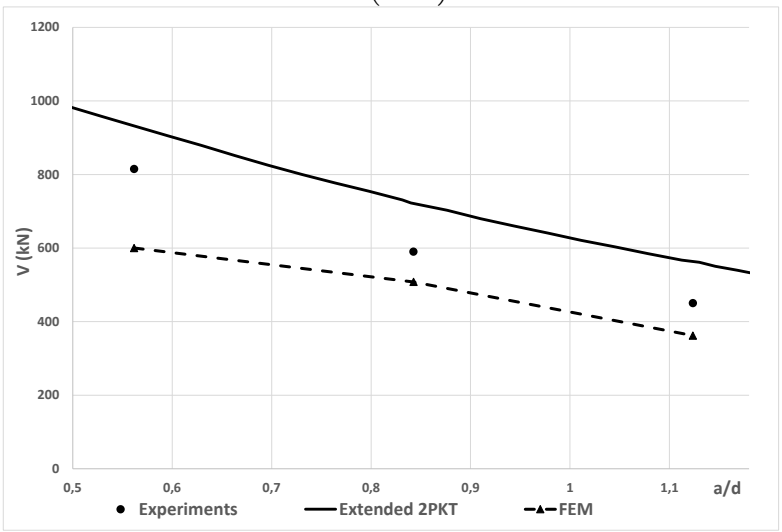

Figure 5.6 – Comparison between FEM and extended 2PKT for h=500mm for tests by Tan et al. (1999)

To conclude, Table 5.1 summarizes the predictions of the finite element model and of the extended 2PKT:

Beam Name	V exp. (kN)	V pred. by extended 2PKT (kN)	V pred. by FEM (kN)	V exp./V pred. by extended 2PKT	V exp./V pred. by FEM	V pred. by extended 2PKT /V pred. by FEM
1P-500/0,50	815	964	600	0,83	1,36	1,64
1P-500/0,75	590	702	508	0,82	1,16	1,42
1P-500/1,00	450	514	362	0,85	1,24	1,47
2P-1000/0,50	1350	1094	834	0,97	1,62	1,67
2P-1000/0,75	1200	824	698	1,29	1,72	1,33
2P-1000/1,00	900	595	639	1,34	1,41	1,05
3P-1400/0,50	1300	1218	1152	1,07	1,13	1,06
3P-1400/0,75	1250	798	1102	1,09	1,13	1,04
3P-1400/1,00	950	693	946	1,01	1,00	0,99
4P-1750/0,50	1100	1330	1492	0,83	0,74	0,89
4P-1750/0,75	1325	1341	1247	0,99	1,06	1,08
4P-1750/1,00	1100	746	1180	0,97	0,93	0,96
			Average	**1,00**	**1.21**	**1.22**
			Coefficient of variation	**16,6%**	**22.2%**	**21.7%**

Table 5.1 – Summary of FEM and extended 2PKT predictions for tests by Tan et al. (1999)

It can be seen that for this test setup the predictions of the extended 2PKT are better than the ones of FEM. Indeed, for most of the specimens, FEM underestimates the failure load while the extended 2PKT produces adequate results except for the smallest specimens where the predictions are unconservative.

5.2.2 Tests by Tan and Mansur (1992)

Figure 5.7 shows the crack pattern predicted by finite element modelling and the crack pattern observed in specimen S43 from the tests conducted by Tan and Mansur (1992).

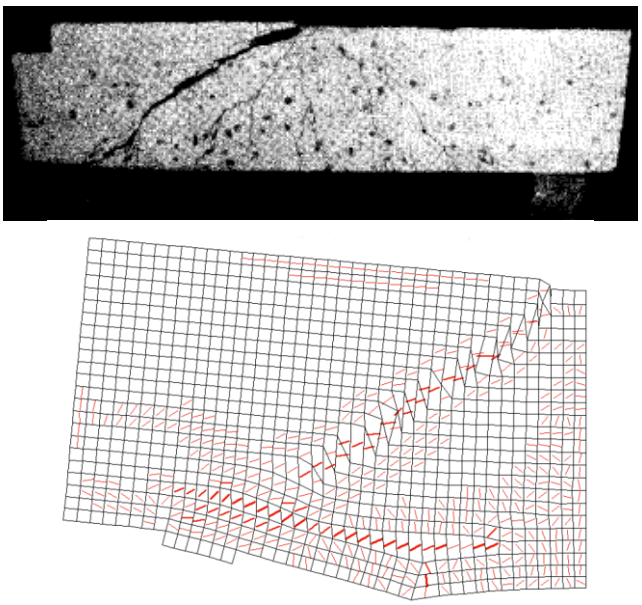

Figure 5.7 – Crack pattern (a) by experiment and (b) by FEM of specimen S43

The predicted failure mode by FEM is a typical diagonal shear crack as it is also the case for the experiment. The failure mode is then well estimated by the software for this specimen. However, for some other specimens, the failure mode doesn't always match with the predictions.

Figures 5.8 and 5.9 show for different values of the shear-span-to-effective-depth ratio a/d the predictions of the finite element modelling and of the extended 2PKT.

For specimens having a/d ratio of 1.5, it can be seen that the predictions of the finite element model are close to the experiments. Compared to the extended 2PKT, FEM predicts better results for the specimens that have a partial prestressing ratio PPR equal to 0.33 and 0.66. For the other specimens, the predictions of extended 2PKT are more accurate. It can be noted that the predictions of FEM seems better for the last specimen (PPR=1). However, this result is due to the fact that average properties for all the four specimens were used to plot the predictions of the extended 2PKT in order to ensure a continuous prediction curve and to avoid noisy results. When, the extended 2PKT is applied to the real properties of the specimen, it predicts better results than the finite element model as it can be seen in Table 5.1.

For specimens having a/d ratio of 2, it can be seen that for the specimens with low partial prestressing ratio, FEM predicts better results than the extended 2PKT while the extended 2PKT predictions are better for the last two specimens that have a partial prestressing ratio of 0.66 and 1. Specially, for the first specimen where no prestressing force is applied, the results of the FEM is much more accurate than the kinematic model for which the ratio between the experimental and predicted results for the shear strength was 0.74.

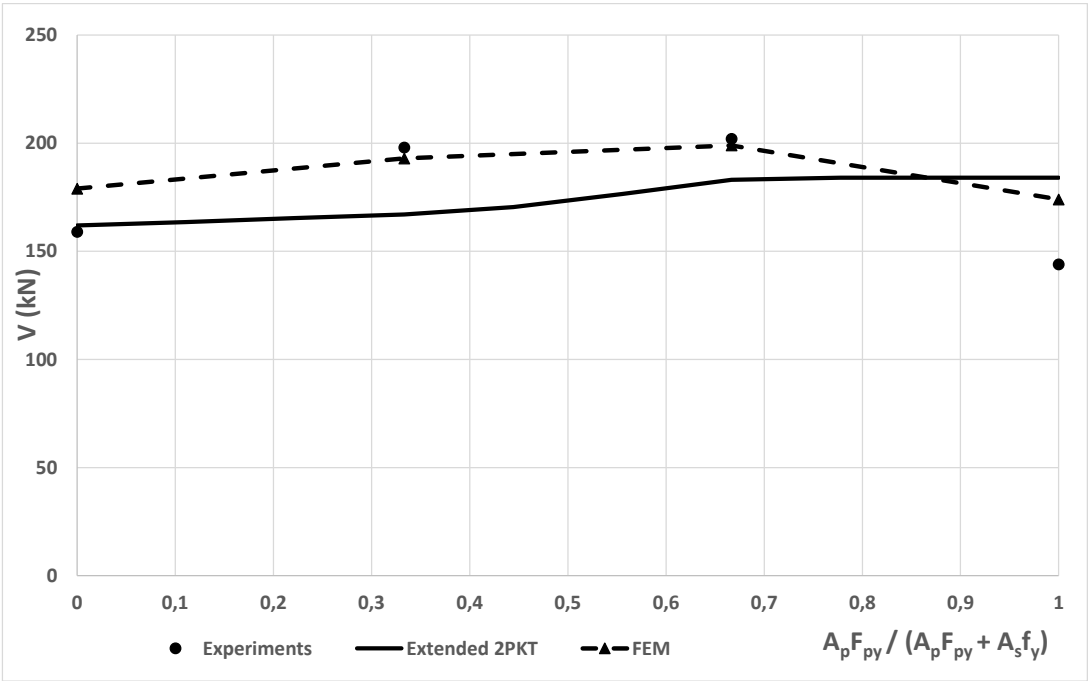

Figure 5.8 – Comparison between FEM and extended 2PKT for a/d=1.5 for tests by Tan and Mansur (1992)

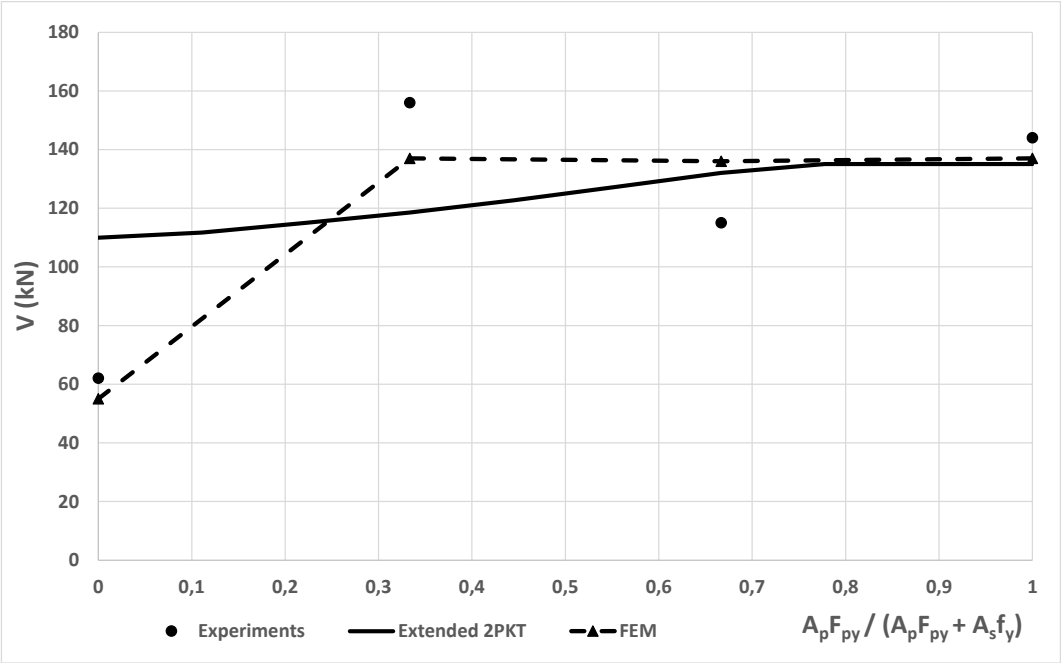

Figure 5.9 – Comparison between FEM and extended 2PKT for a/d=2 for tests by Tan and Mansur (1992)

Table 5.2 presents a summary of the predictions of the finite element model and of the extended 2PKT. It can be seen based on this table that, as opposed to the previous test setup by Tan et al. (1999), the finite element modelling predicts better results than the extended 2PKT. Indeed, the average ratio between experimental and predicted shear strength equals 0.98 and a variation of 11.5% is seen. This variation coefficient is very low compared to the extended 2PKT.

Beam Name	**V exp. (kN)**	**V pred. by extended 2PKT (kN)**	**V pred. by FEM (kN)**	**V exp./V pred. by extended 2PKT**	**V exp./V pred. by FEM**	**V pred. by extended 2PKT / V pred. by FEM**
S13	159	166	179	0,96	0,89	0,93
S23	198	174,2	193	1,14	1,04	0,90
S33	202	183,8	199	1,10	1,03	0,96
S43	144	153,3	174	0,95	0,84	0,89
S14	62	84,1	55	0,74	1,14	1,54
S24	156	116,8	137	1,35	1,14	0,85
S34	115	132,2	136	0,87	0,85	0,98
S44	144	139,6	137	1,03	1,05	1,07
			Average	**1.01**	**0.99**	**1.01**
			Coefficient of variation	**16.8%**	**11.5%**	**20.2%**

Table 5.2 – Summary of FEM and extended 2PKT predictions for tests by Tan and Mansur (1992)

5.2.3 Tests by Teng, Kong and Poh (1998)

Figure 5.10 shows the crack pattern predicted by finite element modelling and the crack pattern observed in specimen P-1b(2) from the tests conducted by Teng, Kong and Poh (1998).

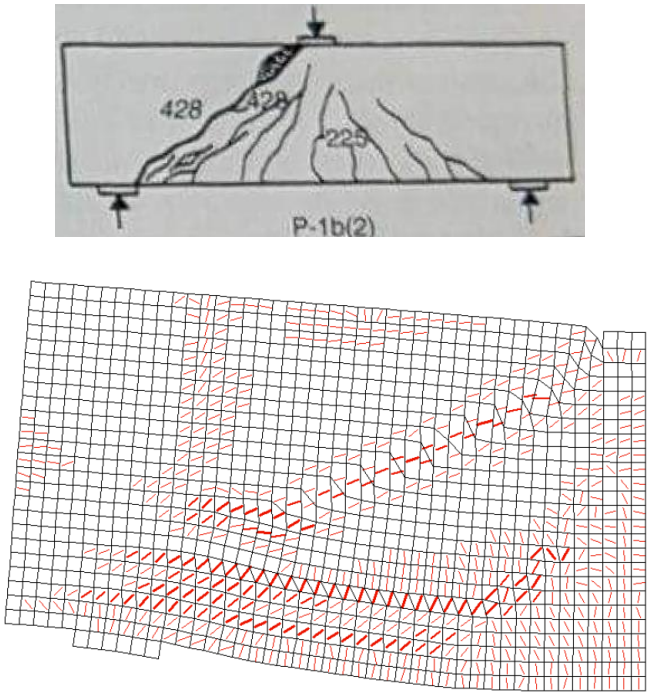

Figure 5.10 – Crack pattern (a) by experiment and (b) by FEM of specimen P-1b(2)

It can be seen that a typical diagonal shear crack develops and propagates from the support plate to the loading plate. The same diagonal crack appears for the experiment where some crushing of concrete also occurred near the loading plate. The failure mode is then well estimated by the software for this specimen. However, as previous test setups, some specimens failed in a different failure mode than the one indicated in the experiment.

Figure 5.11 shows for some specimens the predictions of the finite element modelling and of the extended 2PKT.

For specimens that are not provided with vertical and horizontal web reinforcement, it can be seen that the predictions of the FEM are very close to the predictions of the extended 2PKT and they also seem to follow the same evolution as the extended 2PKT with increasing values of the prestressing force.

For the specimens that are provided with vertical reinforcement, the extended 2PKT predictions are closer to the experiment than the FEM that underestimates the failure load.

Finally, for the specimens that are provided with both vertical and horizontal web reinforcement, FEM predictions are more accurate than the extended 2PKT.

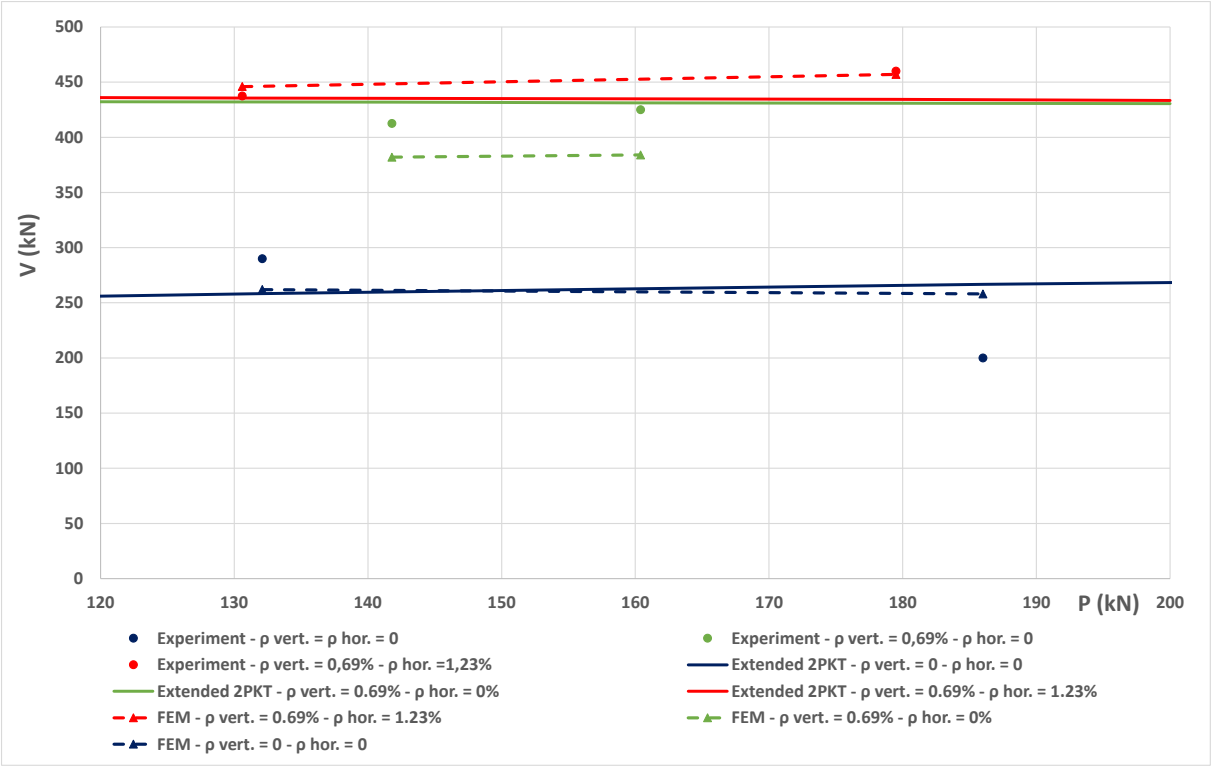

Figure 5.11 – Comparison between FEM and extended 2PKT for specimens from Tan et al. (1999)

The ratios between the experimental failure force and the predicted failure force by the kinematic and by the FEM for each specimen are presented in Fig. 5.12. For most of the specimens, it can be seen that the extended 2PKT predictions are closer to the experiments. It can also be seen that the variation of the predictions is smaller in the extended 2PKT.

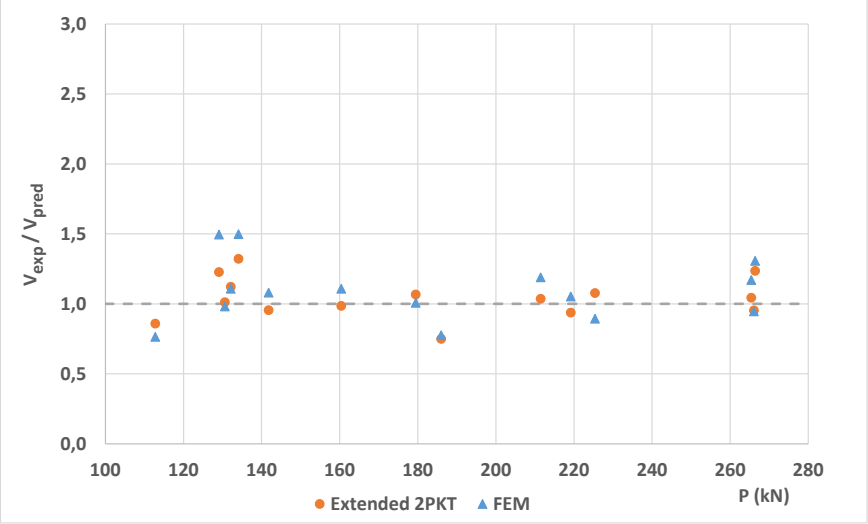

Figure 5.12 – Comparison between Extended 2PKT and FEM predictions for tests by Teng, Kong and Poh (1998)

Finally, Table 5.3 summarizes the predictions of the finite element model and of the extended 2PKT. Again, the predictions listed on the table show that the extended 2PKT is closer to the experiments for most of the specimens. However, the predictions of the FEM are in general very close to the predictions of the extended 2PKT.

Beam Name	V exp. (kN)	V pred. by extended 2PKT (kN)	V pred. by FEM (kN)	V exp./V pred. by extended 2PKT	V exp./V pred. by FEM	V pred. by extended 2PKT / V pred. by FEM
P-1c	275	224	184	1,23	1,49	1,22
P-1a	290	258	262	1,12	1,11	0,98
P-1b	200	267	258	0,75	0,77	1,03
P-2a	413	432	382	0,96	1,08	1,13
P-2b	425	431	384	0,99	1,11	1,12
P-3a	438	433	446	1,01	0,98	0,97
P-3b	460	431	457	1,07	1,01	0,94
P-1b(2)	214	249	280	0,86	0,76	0,88
P-1c(2)	288	218	192	1,32	1,49	1,13
P-1-1,5-WO	370	299	283	1,24	1,31	1,05
P-1-1,5-WV	438	419	374	1,04	1,17	1,12
P-1-1,5-WVH	400	420	423	0,95	0,95	0,99
P-1-1,0-WO	418	446	397	0,94	1,05	1,12
P-1-1,0-WV	538	519	452	1,04	1,19	1,14
P-1-1,0-WVH	560	520	627	1,08	0,89	0,82
			Average	**1,05**	**1,09**	**1.05**
			Coefficient of variation	**13,8%**	**19,5%**	**10.1%**

Table 5.3 – Summary of FEM and extended 2PKT predictions for tests by Teng, Kong and Poh (1998)

5.2.4 Tests by Simionopoulos (1998)

Figure 5.13 shows the crack pattern predicted by finite element modelling and the crack pattern observed in specimen BP25E from the tests conducted by Simionopoulos (1998).

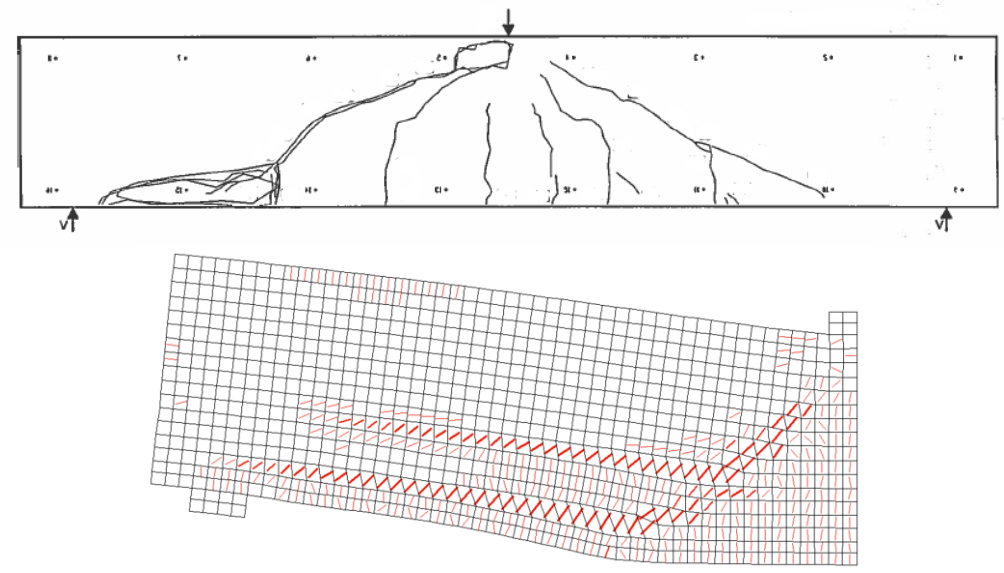

Figure 5.13 – Crack pattern (a) by experiment and (b) by FEM of specimen BP25E

The crack pattern of FEM shows a flexure-shear crack. Indeed, the critical shear crack develops from the flexural crack. An almost horizontal crack develops along the bottom reinforcement towards the support. The crack pattern given by experiment is similar to the one predicted by FEM. For the other specimens of this test setup, FEM predicts also relatively well the failure mode.

Figures 5.14, 5.15 and 5.16 compare the predictions of the FEM and of the extended 2PKT. It can be seen for the smallest specimens that are 250mm high that the predictions of the FEM get closer to the experiments. However, they are still closer to the predictions of the kinematic model than to the experiments. Moreover, they seem to follow the same trend as the extended 2PKT. The same observations can be repeated for the specimens that are 500mm high. For the biggest specimens of the test setup that are 1000mm high, the FEM give almost the same results as the extended 2PKT.

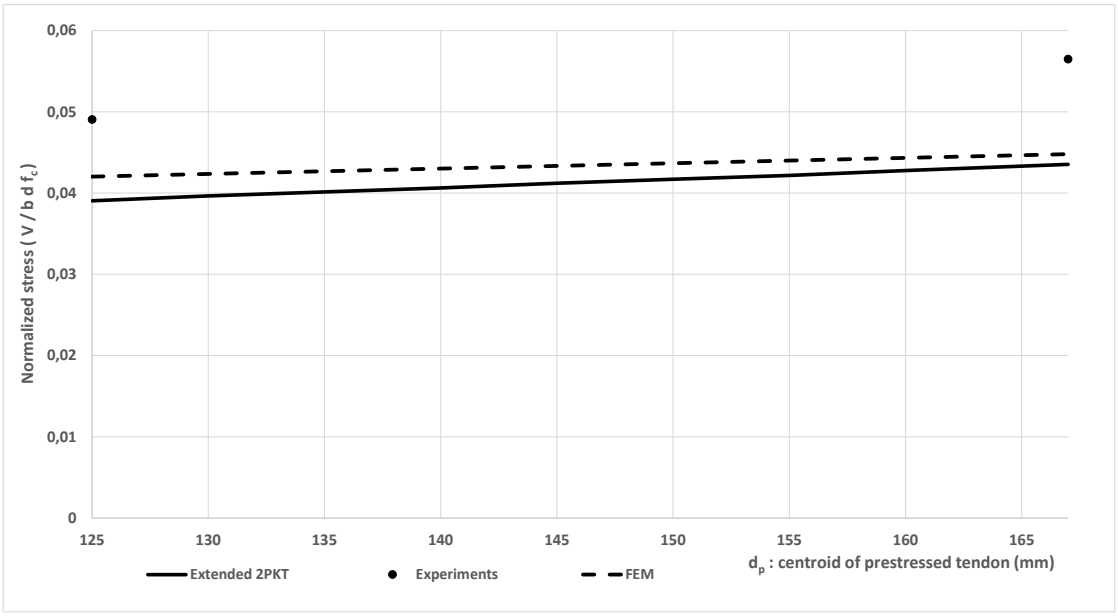

Figure 5.14 – Comparison between FEM and extended 2PKT for specimens of h=250mm from tests by Simionopoulos (1998)

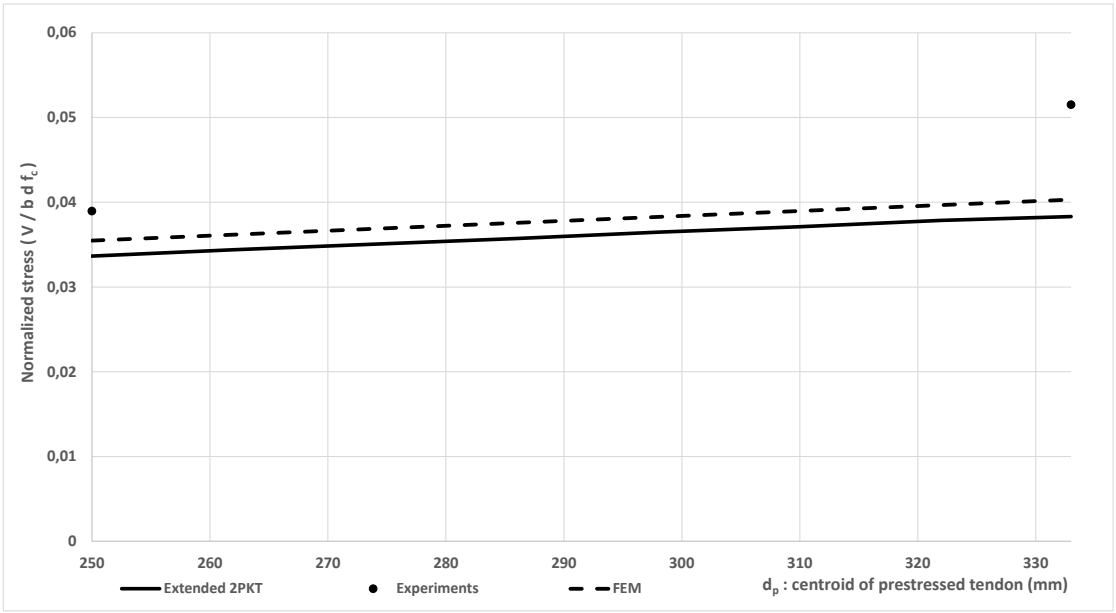

Figure 5.15 – Comparison between FEM and extended 2PKT for specimens of h=500mm from tests by Simionopoulos (1998)

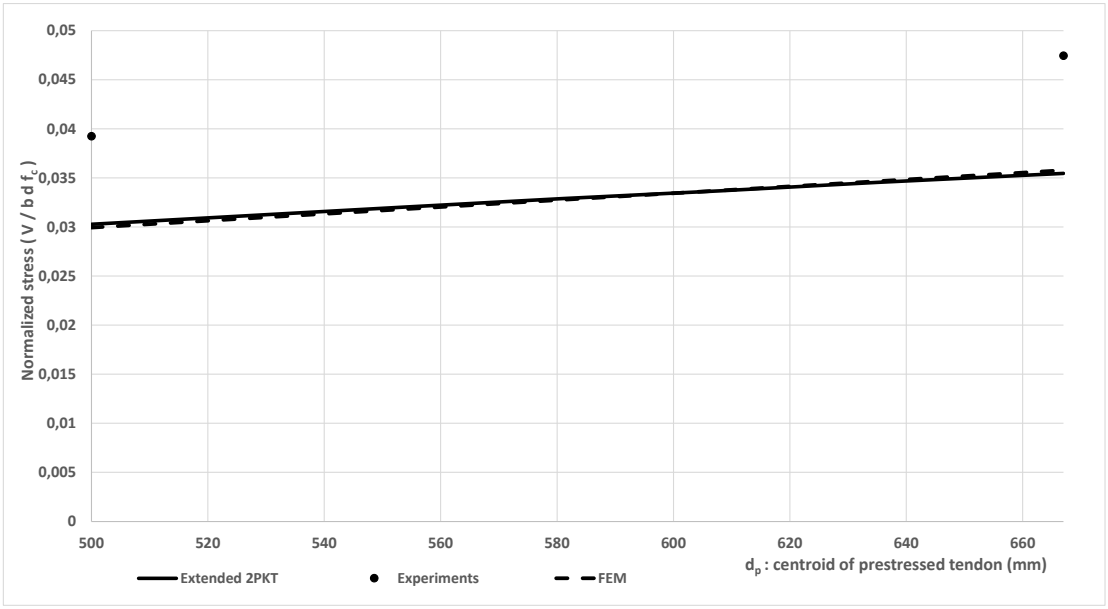

Figure 5.16 – Comparison between FEM and extended 2PKT for specimens of h=1000mm from tests by Simionopoulos (1998)

Finally, Table 5.4 summarizes the predictions of the finite element model and of the extended 2PKT:

Beam Name	**V exp. (kN)**	**V pred. by extended 2PKT (kN)**	**V pred. by FEM (kN)**	**V exp./V pred. by extended 2PKT**	**V exp./V pred. by FEM**	**V pred. by extended 2PKT / V pred. by FEM**
BP100	464	358	354	1,29	1,31	1,01
BP100E	561	419	423	1,33	1,32	0,99
BP50	224	194	204	1,15	1,09	0,94
BP50E	299	222	234	1,34	1,27	0,95
BP25	142,4	113	122	1,25	1,16	0,92
BP25E	164	126	130	1,29	1,26	0,97
Average				1,28	1.24	0.97
Coefficient of variation (%)				4,92%	6.63%	2.92%

Table 5.4 – Summary of FEM and extended 2PKT predictions for tests by Simionopoulos (1998)

5.3 Summary of finite element modelling

Based on the results discussed in the previous sections, some conclusions about the finite element modelling can be drawn. First, the finite element modelling is more complex and more time consuming than the kinematic model. Indeed, for specimens that are higher than 1000mm, the finite element modelling took a significant time to provide the solutions. Consequently, the element size for bigger specimens should be chosen adequately to avoid a large amount of elements in the model.

Also, even if the finite element modelling is a powerful tool when it is adequately used, the failure mode of the specimens does not always correspond to the real failure mode observed in experiments. It is therefore important to keep a critical mind when this kind of models are used to predict failure loads.

Finally, for most of the specimens, it can be seen that the predictions of the finite element models are close to the predictions of the extended 2PKT. Therefore, the predictions of the kinematic model seems to be accurate and consistent. Moreover, it is discovered that for most of the specimens, the predictions of the kinematic model are slightly better than the ones predicted by FEM. Among the four test setups that are studied, the predictions for the tests conducted by Tan and Mansur (1992) and the tests conducted by Simionopoulos are better than the kinematic model. For the other test setups, the extended 2PKT predicts generally slightly better results. For the 27 specimens that failed in shear among the collected specimens, the extended 2PKT produced an average shear strength experimental-to-predicted ratio equal to 1.01 and the coefficient of variation is equal to 16.1%. For comparison, the FEM produced an average shear strength experimental-to-predicted ratio equal to 1.11 and the coefficient of variation is equal to 20.8%. It can be concluded that the extended 2PKT which uses only two degrees of freedom produces better predictions than the complex numerical models with thousands of degrees of freedom.

6. Summary and Conclusions

The first step in this thesis was to collect as many tests performed on prestressed deep beams as possible. However, while many studies and experiments have been conducted on the behaviour of reinforced concrete deep beams, there are relatively few experiments devoted to the effects of prestressing. Taking also into account that this thesis focused on rectangular beams with straight tendons, a total of 41 tests were collected from four experimental studies performed by Tan et al. (1999), Tan and Mansur (1992), Teng, Kong and Poh (1998) and Simionopoulos (1998). All these tests showed clearly that the prestressing increased the ultimate shear strength of deep beams, and therefore this thesis focused on capturing this positive effect.

To capture the effect of prestressing, a Two-Parameter-Kinematic-Theory (2PKT) proposed by Mihaylov et al. (2013) for reinforced concrete deep beams was studied and extended. The original theory is able to predict the ultimate shear strength of reinforced concrete deep beams using only two kinematic parameters (degrees of freedom). This approach was summarized in detailed and was first applied to the tests of prestressed deep beams without modifications. It was shown that the predictions of the original model were reasonably conservative but could be improved. It was identified that the main source of the conservative shear strength predictions was the modelling of the critical loading zones (CLZ). While in the original 2PKT the resistance of the CLZ is independent of the strain in the bottom reinforcement $\varepsilon_{t,avg}$, it became clear that this assumption needed modifications for prestressed members.

The main modification concerning the CLZ was its size. Based on observed crack patterns, the characteristic length of the CLZ was linked to the depth of the flexural compression zone which in turn dependents on strain $\varepsilon_{t,avg}$. This modification led to larger CLZs with higher resistance, where the resistance decreases as the strains in the bottom reinforcement increase.

In addition to the CLZ, two other modifications that were proposed to account for the effect of prestressing. First, the shear force obtained from flexural equilibrium was modified to account for the fact that the prestressing tendons work with high tension from the beginning of loading. This modification lead to increased shear forces derived from flexural equilibrium, and therefore increased shear resistance. An increased resistance was also obtained due to the last modification, namely the inclusion of the dowel action of the prestressing reinforcement.

The extended model was validated against the collected experimental data. The model showed adequate predictions in terms of ultimate shear strength. The trends of the predictions followed well the experiments points as a function of the tests variables. Based on such comparisons with all 27 tests failing in shear, it was found that the average shear strength experimental-to-predicted ratio was 1.01 with a coefficient of variation of 16.1%. In comparison, the original 2PKT produced an average value of 1.24 with a coefficient of variation of 20.1%. These results are considered adequate taking into account the large natural scatter typically observed in deep beam tests

In order to further validate the extended 2PKT, non-linear finite element modelling was performed with program VecTor2 based on the Modified Compression Field Theory (Vecchio and Collins 1986) and Disturbed Stress Field Model (Vecchio 2000). The program implements a 2D plane-stress version of these models and is able to model both monotonic and cyclic loading. The finite element models were built to reflect as accurately as possible the beam properties and boundary conditions used in the tests. The comparisons with the experimental data and earlier results showed that the extended 2PKT method, which uses only two degrees of freedom to capture the deformations in deep beams, produces very similar (or even better) results to those provided by the complex numerical models with thousands of degrees of freedom.

Finally, it is important to note that this study was carried out only for deep beams with straight tendons and rectangular sections. At the same time, it is known that curved tendons will further increase the shear resistance of the member, and therefore the 2PKT requires further modifications in the future. Moreover, I-girders can also be studied as they are very common in practice. The key issue in I-girders will be to study the geometry of the critical loading zone and to evaluate the strength provided by this zone. To conclude, it is important to note that the results from this thesis are promising and the extended model is an easier and faster alternative to non-linear finite element modelling. However, the model cannot be validated against only 27 specimens collected from four different test series. More experimental studies are therefore needed to improve this model and to pave the way for the proposed future investigations.

References

ACI Committee 318, 2011. "Building Code Requirements for Structural Concrete (ACI 318-11) and Commentary", American Concrete Institute, Farmington Hills, MI, 503 pp.

Ahmed, A.H., Khalaf, M.R. [2017] "Behavior of Reinforced Concrete Deep Beams with Large Openings Strengthened by External Post – Tensioning Strands." International Journal of Science and Research (IJSR), Vol. 6 Issue 9, September 2017.

Alshegeir A, Ramirez JA. [1992] "Strut-tie approach of pretensioned deep beam." ACI Structural Journal 1992; 89(3):296_304.

Arthur PD. [1965] "The shear strength of pretensioned I-beams with unreinforced webs." Mag. Concr. Res. 1965; 17(53):199_210.

Kim, T.H., Cheon, J.H., Shin, H.M., [2012] "Evaluation of behavior and strength of prestressed concrete deep beams using nonlinear analysis", Computers and Concrete, Vol. 9, No. 1 (2012) 63-79.

Mihaylov, B. I., Bentz, E. C., Collins, M. P., [2013] "Two-Parameter Kinematic Theory for Shear Behavior of Deep Beams," ACI Structural Journal, Vol. 110, No. 3, pp. 447-455.

Mihaylov, B. I., [2008] "Behavior of Deep Reinforced Concrete Beams under Monotonic and Reversed Cyclic Load," doctoral thesis, European School for Advanced Studies in Reduction of Seismic Risk, Pavia, Italy, 2008, 379 pp.

Mihaylov, B. I., [2015] "Five-Spring Model for Complete Shear Behavior of Deep Beams," Structural Concrete, Vol. 16, No.1, pp. 71-83.

Popovics, S., [1970] "A Review of Stress-Strain Relationships for Concrete," ACI Journal, Vol. 67, No. 3, pp. 243-248.

Ramirez, J.A., [1994] "Strut-tie Design of Pretensioned Concrete Members", ACI Journal Vol. 91, No. 4, pp. 572-578.

Simionopoulos, K. [1998], "Shear Strength of Prestressed Concrete Members of Different Depths", MASc thesis draft, Dept of Civil Engineering, University of Toronto.

Tan KH, Lu HL, Teng S. [1999] "Size effect in large prestressed concrete deep beams." ACI Structural Journal 1999; 96(6):937_46.

Tan, K.H., Mansur M.A., [1992] "Partial Prestressing in Concrete Corbels and Deep Beams," ACI Structural Journal, 89-S24.

Tan KH, Tong K. [1999] "Shear behaviour and analysis of partially prestressed I-girders." The Struct. Eng. 1999; 77(23_24):28_34.

Tan KH, Tong K, Tang CY. [2001] "Direct strut-and-tie model for prestressed deep beams." ASCE J. Struct. Eng. 2001; 127(9):1076_84.

Teng S, Kong FK, Poh SP. [1998] "Shear strength of reinforced and prestressed concrete deep beams." Part II: The supporting evidence. Proc. Inst. Civ. Eng., Struct. Build 1998; 128(2):124_43.

Vecchio, F. J., Collins, M. P. 1997. "The modified compression field theory for reinforced concrete elements subjected to shear", ACI Journal, Vol. 83, No. 2, pp. 219-231.

Vecchio, F. J., Collins, M. P. [2006] "Simplified modified compression field theory for calculating shear strength of reinforced concrete members." ACI Structural Journal, 103(4) :614_624, July-Aug. 2006.

Yoo, T.M., Doh J.H., Guan, H., Fragomeni, S. [2007] "Experimental work on reinforced and prestressed concrete deep beams with various web openings" Griffith University, Innovations in Structural Engineering and Construction.